Polytechnic Institute of New York

AERODYNAMICS LABORATORIES
~
DEPARTMENT OF MECHANICAL and AEROSPACE ENGINEERING

A FINITE-STEP METHOD FOR ESTIMATING THE SPANWISE LIFT DISTRIBUTION OF WINGS IN SYMMETRIC, YAWED, AND ROTARY FLIGHT AT LOW SPEEDS

By A. R. Krenkel

FINAL REPORT

JUNE 1978

Grant Nos. NSG 1107 and 1300

POLY-M/AE Report No. 78-17

A FINITE-STEP METHOD FOR ESTIMATING THE SPANWISE LIFT DISTRIBUTION OF WINGS IN SYMMETRIC, YAWED, AND ROTARY FLIGHT AT LOW SPEEDS

This research was sponsored by the National Aeronautics and Space Administration, Langley Research Center, Hampton, Va., under Grant Nos. NSG 1107 and 1300.

POLYTECHNIC INSTITUTE OF NEW YORK

AERODYNAMICS LABORATORIES

June 1978

POLY-M/AE Report No. 78-17

Acknowledgements

I wish to express my appreciation to the various people who contributed to this effort. Prof. J. Werner contributed much time through technical discussions and is credited for eliminating the low angle of attack numerical instability in the non-linear calculations. Katherine Fahy programmed the computer code and subsequently B. Marianni, G. Homatas and A. Cohen, students, helped with the debugging and production running. Patricia Florence prepared the graphs, and J. Schiavone, student, helped with the preparation of the final report. Typing was done by B. Hein, A. Bianchi, and R. Mohr. I appreciate also the encouragement and support of Prof. M. H. Bloom, Director of the Long Island Center and the Aerodynamics Laboratory.

TABLE OF CONTENTS

A FINITE-STEP METHOD FOR ESTIMATING[†] THE SPANWISE LIFT DISTRIBUTION OF WINGS IN SYMMETRIC, YAWED, AND ROTARY FLIGHT AT LOW SPEEDS

by

A. R. Krenkel[*]

Polytechnic Institute of New York
Aerodynamics Laboratories
Farmingdale, New York

ABSTRACT

The finite-step method has been programmed for computing the span loading and stability derivatives of trapezoidel shaped wings in symmetric, yawed, and rotary flight. Calculations were made for a series of different wing planforms and the results compared with several available methods for estimating these derivatives in the linear angle of attack range. The agreement shown was generally good except in a few cases.

An attempt was made to estimate the nonlinear variation of lift with angle of attack in the high α range by introducing the measured airfoil section data into the finite-step method. The numerical procedure was found to be stable only at low angles of attack.

[†]This research was sponsored by the National Aeronautics and Space Administration, Langley Research Center, Hampton, Va., under Grant Nos. NSG 1107 and 1300.

[*]Associate Professor, Dept. of Mechanical and Aerospace Engineering

I. INTRODUCTION

A large number of linear methods exist for estimating the lift and other force and moment components of arbitrary wing planforms at subsonic speeds. The vortex lattice technique of references 1 and 2 and the distributed singularity methods of references 3 and 4 have demonstrated both versatility and accuracy and have contributed significantly to the design process. However, most of the analytical work done has been limited to the linear or near-linear lift coefficient range and have pertained mainly to symmetric flight. Also, the above-named references are fairly sophisticated and require a significant amount of calculation time on a large computer.

The present study was aimed more specifically to the requirements of General Aviation aircraft, where the sweepback angles are smaller, the airfoil sections conform more towards the NACA series of airfoils, the flow is incompressible, and less computer availability is assumed. It was considered worthwhile also to provide a capability in the subject computer program for estimating the aerodynamic force and moment coefficients and stability derivatives in asymmetric (yawed) flight and in steady maneuvering flight as well as in symmetric equilibrium flight. An attempt was made also to extend the angle of attack range into the nonlinear region near stall.

The finite-step method described in references 5 and 6 is adopted in the subject study. The wing span is divided into a number of segments and a single horseshoe vortex is used to

simulate each of these segments. In this fashion a fewer number of simultaneous equations are required to determine the spanwise distribution of circulation than in those methods, References 1-4, where vortices are distributed in the chordwise direction also. It was assumed that sideslipping motion could be treated by using horseshoe vortices with 'cranked' trailing elements. The trailing elements were assumed to follow the chord lines from the line of quarter chords until the trailing edge of the wing was reached. Following the trailing edge the vortex lines were rotated so that they lie in planes parallel to the (yawed) free stream velocity vector. This assumption was based on the Weissinger method as described in reference 7. It was further assumed that the position and shape of the cranked horseshoe vortices were unaffected by the steady angular velocity of the wing in maneuvering flight.

The nonlinear lift estimation in the stall region was to be accomplished by replacing the estimated linear circulation strength at each spanwise station by the strength corresponding to an airfoil section, as determined experimentally, at the effective angle of attack calculated at the quarter chord. This scheme is essentially that used by Sivells and Neely, reference 8. However, the finite-step method was used instead of lifting-line theory as in reference 8.

Several iterations were made to adjust the span loading after substitution of the (nonlinear) section data. The process was found to be convergent at the lower angles of attack, but

divergent as soon as the effective angle of attack at any spanwise station exceeded the stall angle of the airfoil at that station. Recent papers dealing with this problem, references 9 and 10, have shown similar difficulties and reference 9 indicates a method for obviating them.

A computer program has been prepared, based upon the above analysis, which has the capability of estimating the inviscid incompressible, linear five component aerodynamic coefficients of arbitrary wing planforms at a general angle of attack and sideslip angle, while undergoing steady rotary motion (P, Q, R). The wing geometry was limited to a single trapezoidal shaped panel per side, and includes sweepback, twist, differential twist (left- to right-hand wing panels) and dihedral. The wing can have arbitrary root and tip airfoil sections. However, high lift devices and/or control surface are precluded, as are fuselage and nacelle strut interference, and propulsive slipstream effects.

Numerous computer runs were made on a series of wings of different geometry and the stability derivatives calculated were compared with the available methods for estimating these derivatives in the linear angle of attack range. Very good agreement is shown in all but a few derivatives and these are believed to be of secondary importance.

The computer program should prove most useful for straight and relatively unswept wings ($\Lambda<35^{o}$) of moderate to high aspect ratio ($AR>2$). Low aspect ratio wings and highly swept wings

will introduce separation at the tips and along the leading edges at moderate and high angles of attack, neither of which effect is taken into account in the present method.

II. SYMBOLS

A, AR	Aspect Ratio, b^2/S_{ref}
A	Axial Force
b	wing span measured in x,y plane
c	local chord line
c_T	tip chord
c_R	root chord
c_{MI}	wing chord coincident with left-hand side of wing strip
c_{PL}	wing chord coincident with right-hand side of wing strip
$\bar{c}$	mean aerodynamic chord, $\bar{c}=2\int_o^{b/2} c^2 dy/S_{ref}$, (reference chord)
c_d	section drag coefficient: $D'/q_\infty c$
c_ℓ	section lift coefficient (airfoil lift coefficient): $L'/q_\infty c$
$c_{m_{c/4}}$	section moment coefficient measured about quarter chord point, $(m'/q_\infty c^2)$
C_A	wing axial coefficient: $(A/q_\infty S_{ref})$
C_D	wing drag coefficient: $(D/q_\infty S_{ref})$
C_L	wing lift coefficient: $(L/q_\infty S_{ref})$
C_m	wing moment coefficient: $(m/q_\infty S_{ref}\bar{c})$
C_N	wing normal force coefficient: $(N/q_\infty S_{ref})$
C_Y	side force coefficient: $(Y/q_\infty S_{ref}b)$
C_ℓ	rolling moment coefficient: $(\ell/q_\infty S_{ref}b)$
C_n	yawing moment coefficient: $(n/q_\infty S_{ref}b)$
d	magnitude of a displacement vector, or designation of of a point on c/4
D	total drag force, measured parallel to free stream relative wind vector

F_u, F_v, F_w	influence coefficients used for calculating the induced velocity
$\delta\bar{F}$	elementary force vector
$\bar{F}$	force vector
f,g,h	coordinates of a point measured with respect to the origin of a horseshoe vortex, see figure 6
h_K	normal distance of a point measured to the line of action of a vortex segment
i	an integer used to count horseshoe vortices, from left to right
$\hat{i},\hat{j},\hat{k}$	unit vector triad associated with x,y,z axes
j	an integer used to count wing strips
k_l	factor of proportionality for reducing angle of attack: $0 \leq k_l \leq 1$, see Appendix A
K	an integer used to count the segments of a horseshoe vortex
ℓ	vortex segment length of trailing elements
ℓ_{ref}	general reference length
L	total lift force, measured perpendicular to free stream relative wind vector
m	total pitching moment measured in plane of symmetry
$\bar{M}$	moment vector measured relative to position of the center of gravity
M	Mach number
n	total yawing moment
N	number of spanwise strip (equals horseshoe vortices) considered. Value includes strips on both left- and

right-hand sides of wing

N_F normal force component

$\hat{n}_{1/4}$ unit vector perpendicular to local wing chord plane with components n_4, n_5, n_6 on left, and n_{10}, n_{11}, n_{12} on right-hand sides of wing

$\hat{n}_{3/4}$ unit vector normal to mean camber surface of wing at the 3/4 chord line with components n_1, n_2, n_3 on left, and n_7, n_8, n_9 on right-hand side of wing

P,Q,R rolling rate, pitching rate and yawing rate, respectively, radians per second

$\tilde{P},\tilde{Q},\tilde{R}$ nondimensional rolling rate ($\tilde{P}=\frac{Pb}{2V_\infty}$), pitching rate ($\tilde{Q}=\frac{Q\bar{c}}{2V_\infty}$), and yawing rate ($\tilde{R}=\frac{Rb}{2V_\infty}$), respectively

q_∞ free stream dynamic pressure

$\bar{q}, |\bar{q}|, \hat{q}$ velocity vector, magnitude, and unit vector induced at a point P owing to a single vortex segment

$\hat{r}_{1/4}$ unit vector coincident with line of quarter chords with components r_4, r_5, r_6 on left, and r_{10}, r_{11}, r_{12} on right-hand side of wing

$\hat{r}_{3/4}$ unit vector coincident with line of three-quarter chords with components r_1, r_2, r_3 on left, and r_7, r_8, r_9 on right-hand sides of wing

$\bar{R}_{CG_{c_j}}$ displacement vector from airplane center of gravity to the control point "c_j"

$\bar{R}_1, \bar{R}_3$ displacement vectors from the initial and final ends, respectively, of a vortex segment to the point P

$\hat{r}_2$ unit vector coincident with a vortex segment, positive sign is chosen in agreement with right-hand rule for

	direction of circulation, Γ_i
s	semi-width of wing strip, also semi-span of horseshoe vortex, measured in plane of vortex
S_{ref}	reference wing area, the wing planform area projected on to x,y plane
$\hat{t}_{3/4}$	unit vector tangent to the mean camber surface of wing measured in a chord plane. The components of $\hat{t}_{3/4}$ are t_1, t_2, t_3 on left, and t_7, t_8, t_9 on right-hand side of wing
$\hat{t}_{1/4}$	unit vector coincident with local chord lines with components t_4, t_5, t_6 on left, and t_{10}, t_{11}, t_{12} on right-hand side of wing
u,v,w	induced flow velocity components along the x,y,z axes
$\bar{v}$	induced velocity at point P due to the entire system of horseshoe vortices
U,V,W	total flow velocity components along the x,y,z axes
$\bar{V}$	total relative velocity vector existing at a point P owing to the sum of the free stream, rigid body rotation, and induced velocities
$V_\infty, \bar{V}_\infty$	magnitude and velocity vector of the free stream
x,y,z	orthogonal axes to which wing geometry is referred. The x axis is coincident with the root chord line, the y axis is normal to the plane of symmetry of the wing, positive to the right, and z axis is defined according to the right-hand rule
X,Y,Z	body force components

GREEK SYMBOLS

α	angle of attack
β	angle of sideslip
Γ	dihedral angle, positive for wing tip raised above the xy reference plane.
Γ_i	vortex strength of the i^{th} horseshoe vortex.
$\tilde{\Gamma}_i$	$= \Gamma_i/V_\infty$
δ	angle measured between mean camber line and chord line, positive for positive camber (concave side on bottom of wing).
ϵ	local twist angle
θ	acute angle between $\bar{R}_1$ and $\hat{r}_2$ or obtuse angle between $\bar{R}_3$ and $\hat{r}_2$.
λ	taper ratio of wing ($\lambda = c_T/c_R$)
Λ	angle of sweepback of a constant percent chord line. The quarter chord line is designated without a subscript; other lines are subscripted according to fraction of chord.
ρ	atmospheric density
φ	angle of inclination when viewed from a line parallel to the x axis between bound vortex segment and y axis. Positive for clockwise rotation when looking forward.
ψ	angle of yaw of bound vortex segment. Positive for counter clockwise rotation about z axis when viewed from above.
ω	angular rate of rotation of wing in space, components are P, Q, R.

SUBSCRIPTS

$( )_B$	body axes
$( )_{c_j}$	control points located at 3/4 chord line at midspan of the wing strips.
$( )_{CG}$	center of gravity of airplane.
$( )_{d_j}$	points coincident with origin of horseshoe vortices.
$( )_{\ell_m}$	points located at the 5/8 chord line at the lateral edges of the wing strips.
$( )_i$	denotes the i^{th} horseshoe vortex.
$( )_j$	denotes the j^{th} spanwise strip.
$( )_l$	local value.
$( )_L$	left hand side.
$( )_m$	an integer used to count chordwise vortex segments.
$( )_o$	root chord value
$( )_R$	right hand side.
$( )_{RB}$	rigid body value.
$( )_S$	stability axes.
$( )_T$	tip chord value.
$( )_W$	wind axes.

SUPERSCRIPTS

$\bar{(\ )}$	a vector quantity, (except for $\bar{c}$).
$\hat{(\ )}$	a unit vector.
$( )'$	two dimensional or section value.

ABBREVIATIONS

L.E.	leading edge.
T.E.	trailing edge.

III. ANALYSIS

The various calculations which were required for the preparation of the computer program are presented in this section. These calculations have been broken down into three main categories, namely: (a) the determination of the wing geometrical characteristics as required for determining the "no-flow" boundary conditions, and calculating the effective angle of attack as required in the nonlinear analysis, (b) the finite-step linear analysis, and (c) the modified finite-step method which incorporates the nonlinear airfoil section data.

A. Wing Geometry

Figure 1 presents the planform geometry of the wing and establishes the body axis system used. The x,y plane lies in the plane of the page and hence only the projection of the free stream velocity is shown. The wing shown in figure 1 is planar in that neither twist nor dihedral are indicated.

Figure 2 presents a perspective drawing of the left hand panel of the wing which has been twisted, (zero dihedral case). It has been assumed in this figure: (a) that the root chord lies along the x axis, and (b) that twist is introduced by rotating the tip chord in a plane parallel to the plane of symmetry about the quarter chord point. The tip chord twist angle is defined as ϵ_T, and is subscripted with an L or R which designates the left- or right-hand panels, respectively. The twist angles of the left or right hand panels can have different values in order to study the effect of twist asymmetry. Notice that the twist angle is defined as being positive for the case of washin. This angle will normally

be negative as most wings are washed out. The leading and trailing edges of the wings are assumed to be straight lines, which causes the spanwise variation of the twist angle to be nonlinear if the wing is tapered.

The dihedral angle of the wing is produced by rotating the quarter chord line (and hence the entire left or right hand wing panel) about the x-axis through the angle Γ. The twist and dihedral angles are assumed to be relatively small so that the order in which the rotations take place is inconsequential. In the analysis which follows the twist angle rotation is assumed to occur prior to the dihedral angle rotation.

The purpose of this section is to present the results of an analysis for (a) calculating the spanwise variation of the twist angle, (b) determining the unit tangential and normal vectors required to satisfy the "no-flow" boundary conditions at the three-quarter chord control points, and (c) determining the local angles of attack and sideslip at the quarter chord line. The left hand side of the wing is treated first, and then the right.

Left hand side of wing, $y<0$

The local twist angle of the left hand wing panel, ε_L, at the y station, $(y\leq 0)$, is calculated for a wing without dihedral using the relationship:

$$\tan \varepsilon_L = - \frac{z_{LE}-z_{TE}}{x_{LE}-x_{TE}} \tag{1}$$

Upon determining expressions for the x,z positions of the leading and trailing edges as a function of y, and using the definition for taper ratio, namely that $\lambda = c_T/c_R$, equation 1 can be expressed

as:

$$\tan \varepsilon_L = - \frac{\lambda \left(\sin \varepsilon_{T_L}\right) \frac{y}{b/2}}{1+ \left(1-\lambda \cos \varepsilon_{T_L}\right) \frac{y}{b/2}} \quad ; \quad (y \leq 0) \qquad (2)$$

This equation could serve for the right hand panel also, (with certain sign changes), except that in the general case ε_{T_L} can differ from ε_{T_R}.

The "no flow" boundary condition requires that the (total) flow velocity vector be tangent to the mean camber surface of the wing at the three-quarter chord location of the control points. This boundary condition is prescribed most easily by setting the scalar product of the velocity and local unit normal vector, defined as $\hat{n}_{3/4}$, equal to zero. In order to calculate the unit normal vector, the 3/4 chord line unit vector, $\hat{r}_{3/4}$, and the local unit tangent vector, $\hat{t}_{3/4}$, must be determined. Figure 3 presents a schematic drawing of the vector triad, namely $\hat{r}_{3/4_L}$, $\hat{t}_{3/4_L}$ and $\hat{n}_{3/4_L}$ which is used in the analysis given below.

Figure 4 shows a cambered airfoil section at a typical spanwise station prior to the dihedral angle rotation. The inclination of the mean camber line relative to the chord line is defined as $\delta_{3/4}$ and this angle is assumed to have a linear spanwise variation as given by:

$$\delta_{3/4} = \delta_{3/4_o} - \left[\delta_{3/4_o} - \delta_{3/4_T}\right] \frac{|y|}{b/2} \qquad (3)$$

where $\delta_{3/4_o}$ is the inclination measured at the 3/4 chord station of the root airfoil section and $\delta_{3/4_T}$ is the value measured at the tip airfoil section. Equation 3 is seen to apply to both the left and right hand wing panels. If the zero lift angle of the root

and tip chord airfoil sections are known, these are substituted for $\delta_{3/4_o}$ and $\delta_{3/4_o}$, respectively.

The unit tangential vector, $\hat{t}_{\Gamma=0}$ is rotated about the x axis through the dihedral angle Γ to bring it to its final orientation, namely $\hat{t}_{3/4_L}$. This latter vector is defined as:

$$\hat{t}_{3/4_L} = t_1\hat{i} + t_2\hat{j} + t_3\hat{k}$$

which may be expressed more compactly as:

$$t_{3/4L} = t_1,\ t_2,\ t_3$$

where

$$\begin{aligned} t_1 &= -\cos\ (\epsilon_L+\delta_{3/4}) \\ t_2 &= -\sin\ (\epsilon_L+\delta_{3/4})\sin\ \Gamma \\ t_3 &= \sin\ (\epsilon_L+\delta_{3/4})\cos\ \Gamma\ . \end{aligned} \tag{4}$$

The displacement vector $\bar{R}_{3/4_L}$ is defined as that vector whose tail lies on the 3/4 chord point of the root chord and whose head lies on the 3/4 chord point of the left tip chord. It may be considered as that vector which passes through the locus of control points and its magnitude is given by:

$$d_L = \left[\left(\frac{c_R}{2} - \frac{b}{2}\tan\Lambda - \frac{c_T}{2}\cos\epsilon_{T_L}\right)^2 + \left(\frac{b}{2}\right)^2 + \left(\frac{c_T}{2}\sin\epsilon_{T_L} - \frac{b}{2}\tan\ \Gamma\right)^2\right]^{\frac{1}{2}} \tag{5a}$$

The vector $\hat{r}_{3/4_L}$ is the unit vector associated with the displacement vector $\bar{R}_{3/4_L}$ and is defined as:

$$\hat{r}_{3/4_L} = \frac{\bar{R}_{3/4_L}}{|\bar{R}_{3/4_L}|} = r_1,\ r_2,\ r_3 \tag{5b}$$

where

$$r_1 = \left(\frac{c_R}{2} - \frac{b}{2} \tan \Lambda - \frac{c_T}{2} \cos \epsilon_{T_L} \right) / d_L \tag{5c}$$

$$r_2 = - \frac{b/2}{d_L} \tag{5d}$$

$$r_3 = \left(\frac{c_T}{2} \sin \epsilon_{T_L} - \frac{b}{2} \tan \Gamma \right) / d_L \tag{5e}$$

The unit normal vector, $\hat{n}_{3/4_L}$, is calculated as the vector product of $\hat{r}_{3/4_L}$ and $\hat{t}_{3/4_L}$ and is positive in the upwards direction, (see Figure 3):

$$\hat{n}_{3/4_L} = \hat{r}_{3/4_L} \times \hat{t}_{3/4_L} / |\hat{r}_{3/4_L} \times \hat{t}_{3/4_L}| \tag{6a}$$

and is defined as:

$$\hat{n}_{3/4_L} \equiv n_1, \; n_2, \; n_3 \tag{6b}$$

where

$$n_1 = (r_2 t_3 - r_3 t_2) / d_{3/4_L} \tag{6c}$$

$$n_2 = (r_3 t_1 - r_1 t_3) / d_{3/4_L} \tag{6d}$$

$$n_3 = (r_1 t_2 - r_2 t_1) / d_{3/4_L} \tag{6e}$$

and

$$d_{3/4_L} = [(r_2 t_3 - r_3 t_2)^2 + (r_3 t_1 - r_1 t_3)^2 + (r_1 t_2 - r_2 t_1)^2]^{1/2} \tag{6f}$$

In order to calculate the "effective" angle of attack of this airfoil at the quarter chord point as required by the non-linear analysis, the vector triad associated with the quarter chord point $\hat{r}_{1/4_L}$, $\hat{t}_{1/4_L}$, and $\hat{n}_{1/4_L}$ is calculated. This triad

has the same general orientation as the three-quarter chord triad which is shown in Figure 3. Note that the unit tangent vector, $\hat{t}_{1/4_L}$, is now tangent to the chord line, whereas $\hat{t}_{3/4_L}$ was tangent to the mean camber line. The quarter chord triad is defined as:

$$\hat{r}_{1/4_L} \equiv r_4,\ r_5,\ r_6 \tag{7}$$

$$\hat{t}_{1/4_L} \equiv t_4,\ t_5,\ t_6 \tag{8}$$

$$\hat{n}_{1/4_L} \equiv n_4,\ n_5,\ n_6 \tag{9}$$

where

$$r_4 = -\tan\Lambda/[1+\tan^2\Lambda+\tan^2\Gamma]^{\frac{1}{2}} \tag{10a}$$

$$r_5 = -1/[1+\tan^2\Lambda+\tan^2\Gamma]^{\frac{1}{2}} \tag{10b}$$

$$r_6 = -\tan\Gamma/[1+\tan^2\Lambda+\tan^2\Gamma]^{\frac{1}{2}} \tag{10c}$$

$$t_4 = -\cos\ \varepsilon_L \tag{11}$$

$$t_5 = -\sin\ \varepsilon_L \sin\Gamma \tag{11b}$$

$$t_6 = \sin\ \varepsilon_L \cos\Gamma \tag{11c}$$

$$n_4 = (r_5 t_6 - r_6 t_5)/d_{1/4_L} \tag{12a}$$

$$n_5 = (r_6 t_4 - r_4 t_6)/d_{1/4_L} \tag{12b}$$

$$n_6 = (r_4 t_5 - r_5 t_4)/d_{1/4_L} \tag{12c}$$

and

$$d_{1/4_L} = [(r_5 t_6 - r_6 t_5)^2 + (r_6 t_4 - r_4 t_6)^2 + (r_4 t_5 - r_5 t_4)^2]^{\frac{1}{2}} \tag{12d}$$

Right hand side of wing, $y \geq 0$

The subscript $(\ )_R$ will be used below to designate the right hand panel as indicated earlier. The equations to be given reflect the mirror image of the left and right hand panels except for the fact that the wing tip twist angles can have different values. The development of the equations for the right wing panel parallels the analysis given above.

The local twist angle for the right hand wing panel is given by:

$$\tan \varepsilon_R = \frac{\lambda(\sin \varepsilon_{T_R}) \frac{y}{b/2}}{1-[1-\lambda\cos \varepsilon_{T_R}]\frac{y}{b/2}} \quad ; \ (y \geq 0) \tag{13}$$

which, when compared with equation 2, shows sign and angle changes.

The unit vectors associated with the vector triads located at the three- and one-quarter chord stations follow directly:

$$\hat{t}_{3/4_R} \equiv t_7, \ t_8, \ t_9$$

where

$$t_7 = -\cos (\varepsilon_R + \delta_{3/4}) \tag{14a}$$

$$t_8 = \sin (\varepsilon_R + \delta_{3/4}) \sin \Gamma \tag{14b}$$

$$t_9 = \sin (\varepsilon_R + \delta_{3/4}) \cos \Gamma \tag{14c}$$

The magnitude of the displacement vector $\bar{R}_{3/4_R}$ is given by

$$d_R = \left[\left(\frac{b}{2}\tan\Lambda + \frac{c_T}{2}\cos \varepsilon_{T_R} - \frac{c_R}{2}\right)^2 + \left(\frac{b}{2}\right)^2 + \left(\frac{b}{2}\tan\Gamma - \frac{c_T}{2}\sin \varepsilon_{T_R}\right)^2\right]^{\frac{1}{2}} \tag{15}$$

The unit three-quarter chord vector $\hat{r}_{3/4_R}$ of the right hand panel is defined as:

$$r_{3/4_R} \equiv r_7,\ r_8,\ r_9$$

where

$$r_7 = \left(\frac{c_R}{2} - \frac{b}{2}\tan\Lambda - \frac{c_T}{2}\cos\epsilon_{T_R}\right)/d_R \tag{16a}$$

$$r_8 = \frac{b}{2}/d_R \tag{16b}$$

$$r_9 = \left(\frac{c_T}{2}\sin\epsilon_{T_R} - \frac{b}{2}\tan\Gamma\right)/d_R \tag{16c}$$

From Figure 5 it is seen that:

$$\hat{n}_{3/4_R} = \hat{t}_{3/4_R} \times \hat{r}_{3/4_R} \tag{17a}$$

$$\equiv n_7,\ n_8,\ n_9$$

where

$$n_7 = (t_8 r_9 - t_9 r_8)/d_{3/4_R} \tag{17b}$$

$$n_8 = (t_9 r_7 - t_7 r_9)/d_{3/4_R} \tag{17c}$$

$$n_9 = (t_7 r_8 - t_8 r_7)/d_{3/4_R} \tag{17d}$$

and

$$d_{3/4_R} = [(t_8 r_9 - t_9 r_8)^2 + (t_9 r_7 - t_7 r_9)^2 + (t_7 r_8 - t_8 r_7)^2]^{1/2} \tag{17e}$$

The vector triad associated with the quarter-chord point:

$$\hat{t}_{1/4_R} \equiv t_{10},\ t_{11},\ t_{12}$$

where

$$t_{10} = -\cos\epsilon_R \tag{18a}$$

$$t_{11} = \sin \epsilon_R \sin \Gamma \tag{18b}$$

$$t_{12} = \sin \epsilon_R \cos \Gamma \tag{18c}$$

$$\hat{r}_{1/4_R} \equiv r_{10},\ r_{11},\ r_{12}$$

where

$$r_{10} = r_4 \tag{19a}$$

$$r_{11} = -r_5 \tag{19b}$$

$$r_{12} = r_6 \tag{19c}$$

and

$$\hat{n}_{1/4_R} \equiv n_{10},\ n_{11},\ n_{12} = \hat{t}_{1/4_R} \times \hat{r}_{1/4_R}$$

where

$$n_{10} = (t_{11}r_{12} - t_{12}r_{11})/d_{1/4_R} \tag{20a}$$

$$n_{11} = (t_{12}r_{10} - t_{10}r_{12})/d_{1/4_R} \tag{20b}$$

$$n_{12} = (t_{10}r_{11} - t_{11}r_{10})/d_{1/4_R} \tag{20c}$$

$$d_{1/4_R} = [(t_{11}r_{12}-t_{12}r_{11})^2+(t_{12}r_{10}-t_{10}r_{12})^2 + (t_{10}r_{11}-t_{11}r_{10})^2]^{\frac{1}{2}} \tag{20d}$$

Sufficient geometric information has been determined so that the finite-step method and its subsequent non-linear modification can be applied.

B. Finite-Step Method, Linear Case

The spanwise variation of circulation along a wing is estimated in the Finite-Step Method using a set of single horseshoe vortices in the chordwise direction and N such sets of vortices distributed in the spanwise direction. A reasonable number for N is 40, which corresponds to 20 vortices per side of the wing. The finite-step calculation used here is similar to that presented by Campbell (reference 5) and Blackwell (reference 6).

The horseshoe vortex elements considered herein have bound elements which are both swept and inclined to the x,y plane as those of Margason and Lamar (reference 1), but lie in the plane of the wing rather than being centered in the x,y plane of the wing as assumed in reference (1). The trailing legs of the horseshoe vortices follow the chord lines initially and then have a crank at the trailing edge of the wing, see Figure 6. Those segments which are located downstream of the trailing edge lie more nearly in the free stream direction. In the case of sideslip these segments have a deflection angle β with respect to the plane of symmetry, so they are streamwise with respect to the sideslip variation. In the case of angle of attack the trailing segments have a deflection which is proportional to the angle of attack in order to simulate the Kutta-Joukowski condition at the trailing edge. (It has been suggested that the constant of proportionality be one-half in reference 2.) However, the constant of proportionality, k_1, can be varied at the option

of the user.*

Figure 6 presents the plan view of the wing and illustrates the spanwise distribution of the horseshoe vortices and shows a typical wing segment. The semi-width of the horseshoe vortex is defined as s, where s is calculated:

$$s = \frac{b}{2N\cos\Gamma} \tag{21}$$

Referring to this figure, it can be seen that the point x_i, y_i, z_i is the origin of the i^{th} vortex. This vortex has a spanwise or bound segment which is coincident with the line of quarter chords of the wing and is therefore displaced vertically from the horizontal reference plane, the x,y plane. The axes of the i^{th} vortex, namely, f,g,h, are parallel to the x,y,z axes but are displaced by the distances x_i, y_i, z_i. The chordwise segments are assumed to be parallel to the x axis, and hence the twist angle is not simulated exactly. The maximum twist angle of the typical wing is less than 5^o everywhere, so that the physical displacement of the horseshoe vortex and wing segment should not be significant. The boundary condition on the j^{th} segment at the control point x_{c_j}, y_{c_j}, z_{c_j} has been moved to the plane of the vortex. (The inclination of the unit vector $\hat{n}_{3/4}$, which defines the normal direction to the mean camber surface of the wing, has been calculated in the preceding section. The

*The value k_1 equals zero causes the downstream segments to lie in the plane of the wing, and the value k_1 equals unity causes these segments to be parallel to the free-stream velocity vector. Further details are given in Appendix A.

components of $\hat{n}_{3/4}$ are determined at the control point which is designated with the subscript $(\ )_c$.

The velocity induced at the j^{th} control point due to the i^{th} horseshoe vortex is calculated according to an algorithm which is presented in Appendix A. The general horseshoe vortex is considered in this Appendix to have five straight-line segments: a bound or spanwise segment which was previously described as lying along the quarter-chord line of the wing, two chordwise segments which lie on, (or near, if the wing has twist), the left and right-hand edges of each segment, and two segments which extend downstream from the trailing edge to a distance of approximately one-thousand root chords, which approximates infinity. These five segments are designated K=1→5 where the segments are counted clockwise when viewed from above. They will be referred to as the bound, chordwise, or trailing segments in the discussions which follow.

The velocity induced at the point P by the i^{th} horseshoe vortex can be expressed functionally in the form:

$$\bar{v}_{P(f,g,h)} = \frac{\Gamma_i}{4\pi}\left[F_{u_{i,(P)}}\hat{i}+F_{v_{i,(P)}}\hat{j}+F_{w_{i,(P)}}\hat{k}\right]$$

where the influence coefficients are defined as F_u, F_v, and F_w. These influence coefficients can, in turn, be expressed in functional form:

$$F=F(f,g,h,s,\psi,\varphi,\alpha,\beta,k_1,c_{MI},c_{PL})$$

The analytical expressions of these functions will be exceedingly lengthy and while impressive, have no particular virtue in themselves. Therefore the velocity induced by each vortex segment

is calculated separately and then summed by the computer for K=1,5. For the special case of β=0 and k_1=0, the calculations agree with results obtained using the influence coefficient formulas given in references (1), (5) and (6).

The spanwise variation of circulation is determined by calculating the induced velocity at a control point, "c_j", for the N system of horseshoe vortices where each of these vortices has an assigned but unknown strength Γ_i. This velocity is then added to the sum of the free stream velocity and the velocity produced by the angular rotation vector $\bar{\omega}$ at c_j. The boundary condition requires that the total velocity vector is tangent to the mean camber surface at the control point. The control point is located at the midspan, three-quarter-chord line of each wing strip. The simultaneous matching of the flow tangency requirement at the N control points leads to a set of N linear algebraic equations which are solved for the vortex strength values. The Kutta-Joukowski theorem is applied to calculate the incremental forces which act on the bound and chordwise segments of the horseshoe vortices. Incremental moments due to these elementary forces are determined also using the center of gravity as reference center. The incremental forces and moments are integrated over the entire wing in order to determine the force and moment coefficients desired for both body and stability axes.

1. Calculation of the Induced Velocity, $\bar{v}_{c_j}$

The location of the origin of the i^{th} vortex, counting from i=1 on the left wing tip to i=N on the right wing tip, is given

by the following equations:

$$y_i = -\frac{b}{2} + (2i-1)s\cos\Gamma \;;\; i=1 \text{ to } N$$
$$x_i = -|y_i|\tan\Lambda \qquad (22)$$
$$z_i = -|y_i|\tan\Gamma$$

The location of the j^{th} control point, "c_j", is given by the following equations:

$$y_{c_j} = -\frac{b}{2} + (2j-1)s\cos\Gamma \;;\; j=1 \text{ to } N$$
$$x_{c_j} = -|y_{c_j}|\tan\Lambda - \frac{1}{2}c_R\left\{1 - \frac{1-\lambda}{b/2}|y_{c_j}|\right\} \qquad (23)$$
$$z_{c_j} = -|y_{c_j}|\tan\Gamma$$

The displacement distances are calculated as:

$$f = x_{c_j} - x_i$$
$$g = y_{c_j} - y_i \qquad (24)$$
$$h = z_{c_j} - z_i$$

The induced velocity at the control point, "c_j", owing to the system of i=1 to N vortices distributed evenly over the wing span is calculated as:

$$\bar{v}_{c_j} = u_{c_j}, v_{c_j}, w_{c_j} \qquad (25)$$

where

$$u_{c_j} = \sum_{i=1}^{N} \frac{\Gamma_i}{4\pi} F_{u_{ij}}$$

$$v_{c_j} = \sum_{i=1}^{N} \frac{\Gamma_i}{4\pi} F_{v_{ij}}$$

$$w_{c_j} = \sum_{i=1}^{N} \frac{\Gamma_i}{4\pi} F_{w_{ij}} \tag{26}$$

The influence coefficients are given by equations (A24), (A25), and (A26), which are presented in Appendix A.

2. Determination of Spanwise Variation of Circulation

The unit normal vectors located at the j^{th} control point have been calculated in the geometry section as:

$$\hat{n}_{3/4_L} = (n_1, n_2, n_3) \qquad Y_{c_j} < 0$$

$$\hat{n}_{3/4_R} = (n_7, n_8, n_9) \qquad Y_{c_j} > 0 \tag{27}$$

The velocity at the control point will be tangent to the wing surface when the scalar products of the unit normal vectors and the total velocity vectors are zero:

$$\bar{V}_{c_j} \cdot \hat{n}_{3/4} = 0 \tag{28}$$

where the total velocity vector $\bar{V}_{c_j}$ is the sum of the free stream relative velocity vector, $(\bar{V}_\infty)$, the relative velocity produced by the angular rate of rotation $(-\bar{\omega}x\bar{R}_{CG_{c_j}})$, and the induced velocity $(\bar{v}_{c_j})$:

$$\bar{V}_{c_j} = \bar{V}_\infty - \bar{\omega}x\bar{R}_{CG_{c_j}} + \bar{v}_{c_j} \tag{29}$$

The boundary condition, equation (28), becomes, after substitution of equation (29) and rearranging:

$$\bar{v}_{c_j} \cdot \hat{n}_{3/4} = (-\bar{V}_\infty + \bar{\omega}x\bar{R}_{CG_{c_j}}) \cdot \hat{n}_{3/4} \tag{30}$$

The left-hand side of equation (30) contains the unknowns Γ_i, i=1 to N, while the right-hand side is known. The velocity on the right-hand side of equation (30) is recognized as the rigid body velocity at the control point and for simplicity the terms are combined:

$$\bar{V}_{RB_{c_j}} \equiv - \bar{V}_\infty + \bar{\omega} x \bar{R}_{CG_{c_j}} \tag{31}$$

where

$$\bar{V}_\infty = -V_\infty (\cos\beta\cos\alpha\, \hat{i} + \sin\beta\, \hat{j} + \cos\beta\sin\alpha\, \hat{k}) \tag{32a}$$

$$\bar{\omega} = P,\ Q,\ R \tag{32b}$$

$$\bar{R}_{CG_{c_j}} = (x_{c_j} - x_{CG})\hat{i} + (y_{c_j} - y_{CG})\hat{j} + (z_{c_j} - z_{CG})\hat{k} \tag{33}$$

Equations (29) to (33) are normalized by division of the magnitude of the free stream velocity vector. The nondimensional rolling, pitching and yawing rates $\tilde{P}$, $\tilde{Q}$, and $\tilde{R}$ are introduced also where:

$$\tilde{P} = \frac{Pb}{2V_\infty} \ ; \ \tilde{Q} = \frac{Q\bar{c}}{2V_\infty} \ ; \ \tilde{R} = \frac{Rb}{2V_\infty} \tag{34}$$

The nondimensional rigid body velocity components become:

$$\frac{U_{RB_{c_j}}}{V_\infty} = \cos\beta\cos\alpha + \tilde{Q}\left(\frac{z_{c_j} - z_{CG}}{\bar{c}/2}\right) - \tilde{R}\left(\frac{y_{c_j} - y_{CG}}{b/2}\right)$$

$$\frac{V_{RB_{c_j}}}{V_\infty} = \sin\beta + \tilde{R}\left(\frac{x_{c_j} - x_{CG}}{b/2}\right) - \tilde{P}\left(\frac{z_{c_j} - z_{CG}}{b/2}\right) \tag{35}$$

$$\frac{W_{RB_{c_j}}}{V_\infty} = \cos\beta\sin\alpha + \tilde{P}\left(\frac{y_{c_j} - y_{CG}}{b/2}\right) - \tilde{Q}\left(\frac{x_{c_j} - x_{CG}}{\bar{c}/2}\right)$$

The left-hand side of equation (30), divided by V_∞, for the left-hand wing panel can be written as:

$$\frac{\bar{v}_{c_j}}{V_\infty} \cdot \hat{n}_{3/4_{L_j}} = \frac{1}{4\pi} \sum_{i=1}^{N} \frac{\Gamma_i}{V_\infty}(n_{1_j}F_{u_{ij}}+n_{2_j}F_{v_{ij}}+n_{3_j}F_{w_{ij}}), \quad j=1 \text{ to } \frac{N}{2} \tag{36}$$

The simultaneous equations for Γ_i, i=1 to N are obtained by substitution of equations (35) and (36) into equations (30):

$$\sum_{i=1}^{N} (\frac{\Gamma_i}{V_\infty}) (n_{1_j}F_{u_{ij}}+n_{2_j}F_{v_{ij}}+n_{3_j}F_{w_{ij}})$$

$$= 4\pi\left[\frac{U_{RB_{c_j}}}{V_\infty} n_{1_j} + \frac{V_{RB_{c_j}}}{V_\infty} n_{2_j} + \frac{W_{RB_{c_j}}}{V_\infty} n_{3_j}\right] \tag{37a}$$

$$\text{for } j=1 \text{ to } \frac{N}{2}$$

$$\sum_{i=1}^{N} (\frac{\Gamma_i}{V_\infty}) (n_{7_j}F_{u_{ij}}+n_{8_j}F_{v_{ij}}+n_{9_j}F_{w_{ij}})$$

$$= 4\pi\left[\frac{U_{RB_{c_j}}}{V_\infty} n_{7_j} + \frac{V_{RB_{c_j}}}{V_\infty} n_{8_j} + \frac{W_{RB_{c_j}}}{V_\infty} n_{9_j}\right] \tag{37b}$$

$$\text{for } j=\frac{N}{2}+1 \text{ to } N$$

Equations (37) represents N linear, algebraic equations which are used to determine the N values of (Γ_i/V_∞). For simplicity $\tilde{\Gamma}_i$ is defined as the ratio of Γ_i to V_∞, and this variable will be used subsequently.

3. Calculation of Linear Force and Moment Coefficients

The elementary force produced by a vortex filament of length ℓ immersed in a flow is calculated using the Kutta-Joukowski Theorem, as applied by Prandtl:

$$\delta\bar{F} = \rho\bar{V}_{\ell} x \bar{\Gamma}_{\ell} \tag{38}$$

where $\bar{V}_{\ell}$ is the local velocity vector determined at the mid-point of the vortex segment under consideration. Equation (38) will be used to calculate the forces acting on the chordwise and bound segments separately, in that order.

a) Chordwise segments

There are N+1 chordwise segments and the subscript m will be used to number these segments, see Figure 7. The right-hand chordwise segment on the j^{th} wing strip is coincident with the left-hand chordwise segment on the $(j^{th}+1)$ strip. The force on the combined segment will be calculated using the net circulation acting. The first and last segments, on the left and right-hand wing tips, respectively, will have a circulation which corresponds to the value existing on the horseshoe vortices located at the respective wing tips. The chordwise vortex segments are counted using the integer variable m, where m varies from 1 to N+1, and the counting again proceeds from left to right beginning at the left wing tip chord. The net vortex strength acting on the m^{th} segment are calculated according to the equations given in the table:

Value of m	$\Gamma(m)$	Value of i
1	$\Gamma_{m=1}=\Gamma_{i=1}$	i=m=1
m, m=2 → N	$\Gamma_m=\Gamma_i-\Gamma_{i-1}$	i=m
N+1	$\Gamma_{m=N+1}=\Gamma_{i=N}$	i=N

(39)

The midpoint of the chordwise segments are subscripted $(\ )_{\epsilon_m}$ and the induced velocity at these points are calculated using the method described in Appendix A. The induced velocity due to a (single) segment at a point which lies anywhere on that segment, or on the straight line extension of that segment is equal to zero. A test is provided by calculating the perpendicular distance between every line segment and the point in question. If the perpendicular distance is zero (the practical criterion used is $\Delta\ell \leq 0.1s$), the induced velocity from that segment is not calculated, which avoids the indeterminate form which would result were the computer to evaluate the equations for the induced velocity at that point.

The position of the points ϵ_m are calculated:

$$y_{\epsilon_m} = -\frac{b}{2} + 2(m-1)s\cos\Gamma, \quad m=1 \text{ to } (N+1)$$

$$x_{\epsilon_m} = -\frac{3}{8}c_R - |y_{\epsilon_m}|\tan\Lambda_{5/8} \tag{40}$$

$$z_{\epsilon_m} = -|y_{\epsilon_m}|\tan\Gamma$$

where

$$\tan\Lambda_{5/8} = \tan\Lambda - \frac{3}{2A}\left(\frac{1-\lambda}{1+\lambda}\right) . \tag{41}$$

The induced velocity at the point ϵ_m is calculated:

$$\frac{\bar{v}_{\epsilon_m}}{V_\infty} = \frac{1}{4\pi}\sum_{i=1}^{N} \tilde{\Gamma}_i [F_u\hat{i} + F_v\hat{j} + F_w\hat{k}] \tag{42}$$

using:

$$f = x_{\epsilon_m} - x_i$$

$$g = y_{\epsilon_m} - y_i \tag{43}$$

$$h = z_{\epsilon_m} - z_i$$

where $\tilde{\Gamma}_i$ are those values obtained by the solution of equation (37). The influence coefficients are again those defined by equations (A24), (A25), and (A26).

The vector $\bar{\Gamma}_m$ is determined using the magnitudes Γ_m as per equation (39) and the unit vectors $\hat{r}_{2_{K=2}} = \hat{i}$ which correspond to the left-hand chordwise vortex segments (K=2) as defined in Appendix A, except for the right-hand wing tip segment (m=N+1) where the negative of the $\hat{i}$ unit vector is used:

$$\bar{\Gamma}_m = \Gamma_m \hat{i}, \qquad m = 1 \text{ to } N$$

and (44)

$$\bar{\Gamma}_{N+1} = -\Gamma_{N+1} \hat{i}, \qquad m = N + 1 .$$

The lengths of the chordwise segments are calculated

$$\ell_m = \frac{3}{4} c_{MI_j} \qquad m = 1 \text{ to } N, \quad m = j$$

and (45)

$$\ell_{N+1} = \frac{3}{4} (c_{PL})_N = \frac{3}{4} c_T$$

The total velocity is calculated at the points ϵ_m:

$$\bar{V}_{\epsilon_m} = \bar{v}_{\epsilon_m} - \bar{V}_{RB_{\epsilon_m}}, \qquad m = 1 \text{ to } N + 1 \tag{46}$$

where $\bar{V}_{RB_{\epsilon_m}}$ is defined by equation (31) except that the point of determination is now ϵ_m rather than c_j as in that equation. The terms or components of $\bar{V}_{RB_{\epsilon_m}}/V_\infty$ are given by equation (35) upon replacing the values x_{c_i}, y_{c_i}, z_{c_i} with x_{ϵ_m}, y_{ϵ_m}, z_{ϵ_m}.

The incremental forces on the chordwise segments are calculated by substitution of the results of equations (39), (44), (45) and (46) into equation (38), to wit:

$$\left(\frac{\delta\bar{F}}{\rho}\right)_m = \bar{V}_{\epsilon_m} \times (\Gamma_m \hat{i}) \left(\frac{3}{4} c_{MI}\right)_m ; \quad m=1 \text{ to } N \tag{47a}$$

and

$$\left(\frac{\delta\bar{F}}{\rho}\right)_{N+1} = - \bar{V}_{\epsilon_{N+1}} \times (\Gamma_N \hat{i}) \frac{3}{4} c_T ; \quad m=N+1 \tag{47b}$$

These expressions may be nondimensionalized by division of both sides of the equation by $\frac{1}{2} V_\infty^2 S_{ref}$. Defining the free-stream dynamic pressure, $q_\infty = \frac{1}{2} \rho V_\infty^2$, the nondimensional incremental force equation becomes:

$$\left(\frac{\delta\bar{F}}{q_\infty S_{ref}}\right)_m = \frac{2}{S_{ref}} \left(\frac{3}{4} c_{MI}\right)_m \left(\tilde{\Gamma}_m\right) \frac{\bar{V}_{\epsilon_m}}{V_\infty} \times \hat{i} ; \quad m=1 \text{ to } N \tag{48a}$$

and

$$\left(\frac{\delta\bar{F}}{q_\infty S_{ref}}\right)_{N+1} = - \frac{2}{S_{ref}} \left(\frac{3}{4} c_T\right) \left(\tilde{\Gamma}_N\right) \frac{\bar{V}_{\epsilon_{N+1}}}{V_\infty} \times \hat{i} ; \quad m=N+1 \tag{48b}$$

The total force produced by the chordwise segments is:

$$\left(\frac{\bar{F}}{q_\infty S_{ref}}\right)_{CH} = \left(\frac{\delta\bar{F}}{q_\infty S_{ref}}\right)_{N+1} + \sum_{m=1}^{N} \left(\frac{\delta\bar{F}}{q_\infty S_{ref}}\right) \tag{48c}$$

The resolution of the body axes force components along stability axes is given following the derivation of the bound segment force vectors.

The incremental moments, referenced to the center of gravity, produced by the chordwise segment is:

$$\delta\bar{M}_m = \bar{R}_{CG_{\epsilon_m}} \times \delta\bar{F}_m \tag{49a}$$

The body axes moment coefficients are defined by the equation:

$$\bar{M} = C_{\ell_B} S_{ref} q_\infty b \hat{i} + C_{m_B} S_{ref} q_\infty c_{ref} \hat{j} + C_{n_B} S_{ref} q_\infty b \hat{k} \tag{49b}$$

The moment is nondimensionalized by the factor $q_\infty S_{ref} \ell_{ref}$ and is calculated using equations (48c) and (49):

$$\left(\frac{\bar{M}}{q_\infty S_{ref} \ell_{ref}}\right)_{CH} = \left[\frac{\bar{R}_{CG_{\epsilon_{N+1}}}}{\ell_{ref}} \times \left(\frac{\delta\bar{F}_{N+1}}{q_\infty S_{ref}}\right)\right] + \sum_{m=1}^{N} \frac{\bar{R}_{CG_{\epsilon_m}}}{\ell_{ref}} \times \left(\frac{\delta\bar{F}_m}{q_\infty S_{ref}}\right) . \tag{50}$$

b) Bound vortex segments

There are elemental forces on the N bound vortex segments which must be summed in order to find their contributions to the overall forces and moments. The increment forces are obtained using equation (38), where the local velocity is again evaluated at the midpoint of the segment, which in this case is the origin of the horseshoe vortices. This point is defined as point d, and the coordinates of d are given by equation (22). For the sake of completeness, the displacements and the induced velocity at the point d are written:

$$\begin{aligned} f &= x_{d_j} - x_i \\ g &= y_{d_j} - y_i \\ h &= z_{d_j} - z_i \end{aligned} \tag{51a}$$

where

$$\begin{aligned} y_{d_j} &= -\frac{b}{2} + (2j-1)s\cos\Gamma \quad , \quad y_i = -\frac{b}{2} + (2i-1)s\cos\Gamma \\ x_{d_j} &= -|y_{d_j}|\tan\Lambda \quad , \quad x_i = -|y_i|\tan\Lambda \\ z_{d_j} &= -|y_{d_j}|\tan\Gamma \quad , \quad z_i = -|y_i|\tan\Gamma \end{aligned} \tag{51b}$$

$j=1$ to N $\qquad$ $i=1$ to N

and the induced velocity is calculated:

$$\frac{\bar{v}_{d_j}}{V_\infty} = \frac{1}{4\pi} \sum_{i=1}^{N} \tilde{\Gamma}_i [F_u \hat{i} + F_v \hat{j} + F_w \hat{k}] \tag{51c}$$

where F_u, F_v, F_w are summed over K as shown in equations (A24), (A25), and (A26), except the terms K=3 are omitted, since the point d_j lies on bound vortex segments. The total velocity is calculated at the point d_j:

$$\bar{V}_{d_j} = \bar{v}_{d_j} - \bar{V}_{RB_{d_j}} \tag{52}$$

where $\bar{V}_{RB_{d_j}}$ is defined by equation (31) except that the point of determination is now d_j rather than c_j as in that equation. The components of $\bar{V}_{RB_{d_j}}/V_\infty$ are given by equation (35) upon replacing the values $(x,y,z)_{c_j}$ with $(x,y,z)_{d_j}$ as given by equation (51b).

The length of the spanwise segments, and their circulation strengths are given by:

$$\ell = 2s[1+\cos^2\Gamma\tan^2\Lambda]^{\frac{1}{2}} \tag{53}$$

$$\bar{\Gamma}_j = \Gamma_i \hat{r}_{z_j,K=3} \; ; \quad i=j \tag{54}$$

These results, equations (52), (53), and (54), are substituted into (38).and the increment force on the j^{th} bound vortex segment is calculated:

$$\left(\frac{\delta\bar{F}_j}{\rho}\right)_{BND} = \bar{V}_{d_j} \times \bar{\Gamma}_j (2s[1+\cos^2\Gamma\tan^2\Lambda]^{\frac{1}{2}}) \; ; \; j=1 \text{ to } N$$

Division by $\frac{1}{2} V_\infty^2 S_{ref}$ leads to the nondimensional equation:

$$\left(\frac{\delta\bar{F}_j}{q_\infty S_{ref}}\right)_{BND} = \frac{4s}{S_{ref}} \left[1+\cos^2\Gamma\tan^2\Lambda\right]^{\frac{1}{2}} \left(\tilde{\Gamma}_{j=i}\right) \frac{\bar{V}_{d_j}}{V_\infty} \times \hat{r}_{a_{j,K=3}} \; ;$$

$$j=1 \text{ to } N \qquad (55)$$

The total force on the bound segments is given by:

$$\left(\frac{\bar{F}}{q_\infty S_{ref}}\right)_{BND} = \sum_{j=1}^{N} \left(\frac{\delta\bar{F}}{q_\infty S_{ref}}\right)_j \quad , \quad j=i \qquad (56)$$

The incremental moment coefficient, measured about the c.g. of the j^{th} bound segment is:

$$\left(\frac{\delta\bar{M}_j}{q_\infty S_{ref} \ell_{ref}}\right)_{BND} = \frac{\bar{R}_{CG_{d_j}}}{\ell_{ref}} \times \left(\frac{\delta\bar{F}_j}{q_\infty S_{ref}}\right)_{BND} \qquad (57)$$

The total moment is obtained by summing equation (57):

$$\left(\frac{\bar{M}}{q_\infty S_{ref} \ell_{ref}}\right)_{BND} = \sum_{j=1}^{N} \left(\frac{\delta\bar{M}_j}{q_\infty S_{ref} \ell_{ref}}\right)_{BND} \qquad (58)$$

Finally we sum the force and moment coefficients on the chordwise and bound segments using the results given by (48c) and (56), and (50) and (58), respectively:

$$\left(\frac{\bar{F}}{q_\infty S_{ref}}\right)_T = \left(\frac{\bar{F}}{q_\infty S_{ref}}\right)_{BND} + \left(\frac{\bar{F}}{q_\infty S_{ref}}\right)_{CH} \qquad (59a)$$

$$\left(\frac{\bar{M}}{q_\infty S_{ref} \ell_{ref}}\right)_T = \left(\frac{\bar{M}}{q_\infty S_{ref} \ell_{ref}}\right)_{BND} + \left(\frac{\bar{M}}{q_\infty S_{ref} \ell_{ref}}\right)_{CH} \qquad (59b)$$

The total force is defined using body axes components

$$\bar{F}_T = X\hat{i} + Y\hat{j} + Z\hat{k}$$

where X is the negative of the conventional axial force (X=-A).

The component X is positive in the forward direction (thrust); Y is the side force, positive to the right; Z is the negative of the conventional normal force ($Z=-N_F$). The component Z is positive in the downwards direction.

The body axes force coefficients are determined:

$$C_x = \frac{X}{q_\infty S_{ref}} \quad , \quad C_y = \frac{Y}{q_\infty S_{ref}} \quad , \quad \& \quad C_z = \frac{Z}{q_\infty S_{ref}} \tag{60}$$

The moment coefficients are likewise defined:

$$C_{\ell_B} = \frac{M_x}{q_\infty S_{ref} \ell_{ref}} \left(\frac{\ell_{ref}}{b}\right); \quad C_{m_B} = \frac{M_y}{q_\infty S_{ref} \ell_{ref}} \left(\frac{\ell_{ref}}{\bar{c}}\right);$$

$$C_{n_B} = \frac{M_z}{q_\infty S_{ref} \ell_{ref}} \left(\frac{\ell_{ref}}{b}\right) \tag{61}$$

The lift, drag and side force coefficients are calculated relative to stability axes:

$$\begin{aligned} C_L &= C_x \sin\alpha - C_z \cos\alpha \\ C_Y &= C_y \\ C_D &= - (C_x \cos\alpha + C_z \sin\alpha) \end{aligned} \tag{62}$$

and the moment coefficients are obtained:

$$\begin{aligned} C_{\ell_S} &= C_{\ell_B} \cos\alpha + C_{n_B} \sin\alpha \\ C_{m_S} &= C_{m_B} \\ C_{n_S} &= - C_{\ell_B} \sin\alpha + C_{n_B} \cos\alpha \end{aligned} \tag{63}$$

which completes the linear analysis.

The above analysis has been programmed, see Appendix B, and values for $\tilde{\Gamma}_i$ for i=1 to N appear as output data as well as the force and moment coefficients listed above in equations (60), (61), (62), and (63).

C. Modified Finite-Step Method: Nonlinear Case

The analysis of the previous section resulted in a procedure for calculating the span loading and integrated wing force and moment coefficients which correspond to the linear case. (Actually the results were not strictly linear since trigonometric terms involving angle of attack and sideslip were not replaced by the usual small angle approximations). The linear analysis, however, does not predict the stall characteristics of the wing, i.e. it leads to an over-estimation of the lift and an under-estimation of the drag at angles of attack above ~10°. It seems reasonable to expect that a more realistic estimation of the wing coefficients could be achieved by replacing the thin-airfoil-theory section characteristics, ($\alpha_o = 2\pi$ 1/rad), with the section aerodynamic characteristics as determined from wind tunnel measurements, references 11 or 12, or as predicted by some of the more advanced airfoil theories which take into account the viscous forces in the boundary layer, see references 13 and 14. While this calculation appears to be straightforward, it has not been possible to achieve the desired results.

The idea of replacing the theoretical airfoil section characteristics with experimental values is not particularily new, (see Reference 12, p. 20). Sivells and Neely, reference 8, have adopted

this procedure using lifting line theory, and it seemed that such a procedure would also be adaptable to the Finite-Step Method.

The procedure adopted for estimating the nonlinear aerodynamic coefficients of the wing is basically that of using finite-step calculations to estimate the span loading of the wing initially. The effective angle of attack at the quarter chord is calculated from the span loading as in lifting-line theory. These effective angles are used to determine the local lift coefficients from test data of airfoils. A new span loading can be determined using this airfoil lift data and the effective angles of attack re-estimated in an iterative fashion.

The procedure used in the computer program is amplified below, and the difficulties encountered are described.

1. The effective angle of attack at each wing segment is calculated using the following equation:

$$\tan \alpha_j = \frac{(\bar{V}_{dj}/V_\infty) \cdot \hat{n}_{\frac{1}{4}j}}{(\bar{V}_{dj}/V_\infty) \cdot \hat{t}_{\frac{1}{4}j}} \tag{64}$$

where the values of $\bar{V}_{d_j}$ are determined from the linear analysis. This equation is similar to the effective angle of attack calculated in Prandtl's lifting line theory:

$$\alpha_{eff_j} = \alpha_{geom.} - w_j/V_\infty \tag{65}$$

2. The airfoil section data c_ℓ, c_d, $c_m = f(\alpha)$ are determined at each segment using the value of α_j determined from equation 64. Data for the tip and root airfoil sections are interpolated linearly from root to tip to account for the spanwise variation of airfoil section. The spanwise distribution of circulation is computed from these local lift coefficients using:

$$\tilde{\Gamma}_{original}\ (y) = c_{\ell_j}\ c_j/2$$

Values of $\tilde{\Gamma}_{original}$ appear as output from the computer program. It was intended that the values of $\tilde{\Gamma}$ as computed in this step be used to replace the linear finite-step values used in (1) and these steps repeated until no further significant changes in the loading occurred. However, values of $\tilde{\Gamma}_{orig}$ near the wing tips induced numerical instabilities which necessitated the addition steps which are described next. A fuller explanation of the difficulties is given below.

3. The values of $\tilde{\Gamma}_{orig}$, as computed in step 2 above for those segments which are located in a region of approximately one chord inboard from each of the wing tips, are discarded. The finite-step method is then employed to calculate replacement values. The procedure used is similar to that used in the linear finite-step analysis except that the values of the circulation in the central portion of the wing are held fixed and equal to $\tilde{\Gamma}_{original}$. This is equivalent to replacing lifting-line theory values near the wing tips with lifting surface theory values. The results of this calculation are labelled $\tilde{\Gamma}_{SIMQ}$ and also appear in the computer output.

4. It was necessary to "fair" the values of $\tilde{\Gamma}_{SIMQ}$ calculated in the tip regions in step 3 into the central wing values determined in step 2 and a polynomial curve fitting technique was employed to accomplish this. The central wing values of $\tilde{\Gamma}_{SIMQ}$, since they were determined from lifting-line theory which is known to overestimate the lift, were reduced using Jones' edge correction factor obtained from reference 15. This correction is:

$$\tilde{\Gamma}_{SIMQ} = \frac{\tilde{\Gamma}_{orig}}{E} \quad ; \quad (-\frac{b}{2} + c_T) < y < (\frac{b}{2} - c_T)$$

where E is the complete elliptical integral with modulus k, i.e.:

$$E = \int_0^{\pi/2} \sqrt{1 - k^2 \sin^2 \bar{\Phi}}\, d\bar{\Phi} = E(k, \pi/2) \geq 1$$

and

$$k = \sqrt{1 - (\frac{4}{\pi A})^2}$$

After application of the Jones' factor, the level of $\tilde{\Gamma}$, from the finite-step calculations, joined the central wing values and the overall distribution could be faired using the subroutine MARIAN. The faired circulation values were labelled $\tilde{\Gamma}_{MARIAN}$. The values also appear in the computer output.

These stratagems were partially successful in overcoming the inherent instabilities which exist in the nonlinear calculation.

The first instability was uncovered at low angles of attack where the lift coefficient angle of attack relationship is linear. The net downwash at the quarter chord of any wing segment, the term w_j/V_∞ in equation (65), can be regarded as the algebraic sum of the downwash produced by the segment on itself plus the upwash contributed by every other segment, assuming they are all lifting segments. Suppose that, for some reason, the circulation at one particular wing segment is unduly large compared with its neighboring segments. When the effective angle of attack is calculated on the next iteration, this segment will have a downwash contribution on itself which is too large and α_{eff} will be too low. The segments which are adjacent to this segment will experience a large upwash and their effective angles of attack and lift coefficients will be too large. As a result, it can be seen that the high lift on the first segment will start an oscillation of effective angle of attack with attendant changes in section lift and circulation upon itself, and that this oscillation will spread laterally to the adjacent segments. This oscillation will continue to propagate spanwise with each new iteration. This first instability arose because of the difficulty of calculating downwash near the wing tips as described in step 2 above.

Prof. J. Werner suggested that it would be possible to suppress this oscillation by using the finite-step method to calculate the wing tip loading while retaining the use of section data to determine the loading on the central portion of the wing. The polynomial approximation used to "fair" the loading in the tip and central regions served to eliminate the instability.

The second instability occurred at the higher angles of attack, once the airfoil section lift slope became negative. The second instability can be visualized by assuming that one wing segment, presumably the one with the highest effective angle of attack and the lowest stall angle on the wing, reaches an angle where its section lift curve slope is negative. On the next iteration the effective angle of attack of this segment will be increased because the downwash due its own circulation will decrease, which in turn will produce a decrease in lift coefficient. The process is unstable and continues until the lift curve slope of this segment becomes positive again above the stall angle of attack. The work described in references 9 and 10 shows similar results in the steady flow calculation. It is indicated in these references that is necessary to go to unsteady flow theory in order to achieve even the qualitative behavior of the wing lift in the stalled region.

Figure 8 presents the variation of wing lift coefficient with angle of attack for an unswept wing of aspect ratio 8.04. The experimentally determined pitch characteristic of this wing, compared with the results of nonlinear lifting-line theory, are presented in reference 16. Both the linear and nonlinear finite-step method computer results for five iterations are also shown. The linear results as expected, are seen to over-estimate the lift coefficient

by a substantial margin above an angle of attack of 12^{o}. Since the linear curve values are used in the first step of the non-linear calculation, and they will clearly lead to downwash angles which are too large; curve #1 is seen to fall below the test data by a substantial margin. On the second iteration, the under-estimated local lift coefficients can result in high effective angles of attack some of which, at the higher geometric angles of attack, exceed the local stall angles. Thereafter the stall propagates across the wing with the result that the lift coefficients are larger than the test data below above $\alpha = 14^{o}$ (they approach the linear theory results), but rapidly drop at the higher angles. The lift coefficient on the second iteration at $\alpha = 22^{o}$ is off scale as are the values at the lower angles as the number of iterations increases.

IV. DISCUSSION OF RESULTS

A parametric study was conducted with the program described in the previous sections in order to validate the accuracy of the methods used. The lift, lift curve slope, and longitudinal and directional stability derivatives of a series of wings were computed. The aspect ratios considered varied between $A = 2$ and $A = 7$. Sweepback angles of $\Lambda = 0$ and 45° and taper ratios of $\lambda = 0.25$, 0.50 and 1.00 were used. Computer runs were made for only select combinations of these variables in order to make direct comparisons with the theoretical and/or experimental results available.

Figures 9, 10 and 11 compare the present results for the computation of lift curve slope, static margin, and induced drag factor with the vortex-lattice results presented in reference 1. It can be seen from these comparisons that the results obtained compare quite well with the vortex lattice method results. The results should compare exactly for the vortex lattice method using one chordwise vortex, ($\overline{N}_c = 1$), except for the fact that the vortex lattice method uses streamwise vortices in the Treffetz plane and moves the "no-flow" boundary condition to this plane also. The present method places the vortices on the wing plane. Also, the downstream trailing legs lie one-half way between the wing chord plane and the free stream velocity direction, as recommended by Ruppert, reference 2. The largest discrepancy occurs in Figure 11 for the swept wings of taper ratio equal to one-half, but percentage-wise the difference is small.

Figures 12 and 13 present the variation of the pitch damping derivatives C_{L_q} and C_{m_q} with aspect ratio for two sweep angles, 0 and 45°, and two taper ratios, λ = 1.0 and 0.5*. The computer results are compared with the theoretical results obtained from reference 17. The agreement between these methods is satisfactory except for some differences noted for the high aspect ratio swept wings.

Figures 14 to 17 present the static lateral-directional stability derivatives, C_{ℓ_β}, C_{n_β} and C_{Y_β}, estimated by the computer program with the theoretical and experimental results available from various NACA/NASA reports, references 7, 18 and 19.

Figure 14 presents the variation of C_{ℓ_β}/C_L with aspect ratio. The results obtained using the present method have been compared with three different analytical methods, see Figures 14a and 14b. The present method agrees best with the method of reference 7 for the unswept wings, which is not surprising since the computer program is based upon the vortex modelling system suggested therein. The calculations for the swept and tapered wings, see Figure 14b, agree more closely with the results of reference 19, however. Figure 14c presents the variation of C_{ℓ_β}/C_L with taper ratio for the swept and unswept wings of aspect ratio 7, which illustrates the better agreement between theory and computer results for the highly swept wings.

A detailed examination of the computer output revealed the ob-

*The standard NASA stability derivatives are used in this section of the report and in the figures.

vious: that the rolling moments contributed by the vortices located near the wing tips were the most significant and that the integrated values of the rolling moment was the difference in the bending moments at the wing root of the left- and right-hand wing panels. Thus the value of C_{ℓ_β}/C_L calculated for the straight wing is equal to the difference of two large numbers of nearly identical magnitude. The actual value of C_{ℓ_β}/C_L for large aspect ratio straight wings therefore is sensitive to the minor asymmetry of the span loading due to sideslip angle. In the case of the low aspect ratio and/or swept wing the differences become more pronounced and hence better agreement with theory is achieved.

Separation of the flow from the leeward wing tip due to the greater amount of spanwise flow of the boundary layer might cause the tip chordwise vortex segment to leave the wing panel and trail streamwise rather than chordwise as assumed in the present calculations. This effect would produce a significant loading distribution change at the leeward tip and alter both the rolling and yawing moments due to sideslip angle appreciably. This effect has not been investigated numerically.

Figure 15 presents a comparison of the results obtained with the present method with those from references 18 and 20 for estimating the effect of wing dihedral angle upon C_{ℓ_β}. It can be seen that better agreement is reached with the data and theory (Weissinger) presented in reference 20.

Figure 16 presents the estimated directional stability derivatives for the wings compared with the values obtained from reference 18. As pointed out from this reference, the directional stability derivative is very difficult to predict and so the dis-

agreement shown between the two sources is not unexpected. (It should also be pointed out that there is a much more recent and advanced source of information concerning the estimation of stability derivatives, namely reference 22, and that it is realized that all of the derivatives presented herein should be compared with this source. However the methods of reference 22 are necessarily longer and more tedious and the line had to be drawn somewhere).

Figure 17 presents the estimated values of C_{Y_β} with those obtained using reference 17. The zero sweepback values compare fairly well but there is considerable disagreement between the swept wing values. Reference 18 suggests that the theory of reference 17 is probably not too suitable for estimating C_{Y_β} of the wing. The possibility remains that the present method values are reasonable.

Figure 18 presents the damp-in-roll derivative, C_{ℓ_p}. Computed values are shown for $\alpha = 0^\circ$ and 10°. It is seen that the values of C_{ℓ_p} increase slightly with angle of attack. This effect is not taken into account in the method presented in reference 18 and deserves further verification.

Figure 19 presents the variation of the yaw-due-to roll derivative, $(\Delta C_{n_p})_1/C_L$ which contains only the contribution due to wing lift and induced drag forces. There is another contribution due to the variation of profile drag with angle of attack which of course is not taken into account by the present method, linear case. Reference 18 indicates that the theoretical values presented therein are in agreement with the experimental data, all taper ratios, which suggests that further work is required on the present

method.

Figure 20 presents the variation of the side force-due-to roll derivative and fairly good agreement is shown. On the basis of the results shown in Figure 19 this agreement might be fortuitous, and further study may be warranted here too.

Figures 21, 22, and 23 present the yaw rate derivatives C_{ℓ_r}/C_L, $(\Delta C_{n_r})_I/C_L^2$, and C_{y_r}/C_L^2. Figure 21 shows that the roll-due-to-yaw derivative has a variation with aspect ratio which runs counter to the theoretical values given in reference 18. However, as indicated in this reference, certain empirical corrections are required to adjust the theoretical values of C_{ℓ_r}/C_L in order to agree with wind tunnel measured values. On this basis the present method results remain questionable and further verification is required.

The yaw damping derivative, $(\Delta C_{n_r})_I/C_L^2$, presented in Figure 22 has the proper variation with aspect ratio but the agreement with the level of the theoretical curves is poor for the straight wings and is worse for the swept wings. Further investigation here is suggested also.

Figure 23 presents the side force-due-to-yaw derivative and good agreement is shown for the straight wing cases while the swept wing cases differ by several orders of magnitude. Reference 18 indicates that experimental data show that the theory (obtained from reference 17) is inadequate. Thus the "good" agreement shown for the straight wing cases is suspect.

V. CONCLUSION

The linear finite-step method results for estimating the force and moment coefficients in symmetric, sideslipping, and rotary flight has been shown to predict values which are, for the most part, reasonable. However, it would appear that further refinement in the estimation of the lateral-directional rotary derivatives is required.

The nonlinear finite-step method at low angles of attack converges to a solution which is reasonable but does not agree too well with the experimental data. At angles of attack above the stall the steady flow numerical procedure becomes unstable and is unusable in its present form.

VI. REFERENCES

1. Margason, R.J. and Lamar, John E.: "Vortex-Lattice Fortran Program for Estimating Subsonic Aerodynamic Characteristics of Complex Planforms". NASA D-6142 Feb., 1971.

2. Rubbert, Paul E.: "Theoretical Characteristics of Arbitrary Wings by a Non-Planar Vortex Lattice Method". Doc. No. D6-9244, Boeing Co., Feb., 1964.

3. Goldhammer, M.L., Lopez, M.L., Shen C. C.: "Methods for Predicting the Aerodynamic and Stability and Control Characteristics of STOL Aircraft. Vol. I Basic Theoretical Methods". AFFDL-73-146-Vol. I, Dec., 1973.

4. Hess, John L.: "Calculation of Potential Flow about Arbitrary Three-Dimensional Lifting Bodies". McDonnell Douglas Rept. No. MDC J5679-01, Oct., 1972.

5. Campbell, George S.: "A Finite-Step Method for the Calculation of Span Loadings of Unusual Plan Forms. NACA RML50L13, 1951.

6. Blackwell, James A., Jr.: "A Finite-Step Method for Calculation of Theoretical Load Distributions for Arbitrary Lifting - Surface Arrangements at Subsonic Speeds". NASA TN D5335, July, 1969.

7. Queijo, M. J.: "Theoretical Span Load Distributions and Rolling Moments for Sideslipping Wings of Arbitrary Plan Form in Incompressible Flow". NACA TR 1269, 1956.

8. Sivells, J.C., and Neely, R.H.: "Method of Calculating Wing Characteristics by Lifting-line Theory using Nonlinear Section Data". NACA TN 1269, 1947.

9. Levinsky, E. S.: "Theory of Wing Span Loading Instabilities Near Stall". Paper #25, AGARD Conference Proceedings No. 204, Sept. 1976.

10. Kroeger, R. A., and Feistel, T.W.: "Reduction of Stall-Spin Entry Tendencies Through Aerodynamic Design". SAE Paper 760481, April 1976.

11. Abbott, I. H. and von Doenhoff, A.E., Stivers, L.S., Jr.: "Summary of Airfoil Data". NACA TR824, March, 1945.

12. Abbott, I. H. and von Doenhoff, A. E.: "Theory of Wing Sections". Dover Publications, Inc. New York.

13. Stevens, W. A., Goradia, S. H. and Braden, J. A.: "Mathematical Model for Two-Dimensional Multicomponent Airfoils in Viscous Flow". NASA CR-1843, 1971.

14. Bhateley, Ishwar, C. and McWhirter, Jack W.: "Development of Theoretical Method for Two-Dimensional Multi-Element Airfoil Analysis and Design". AFFDL-TR-72-96, August, 1972.

15. Jones, R.T.: "Correction of the Lifting-Line Theory for the Effect of the Chord". NACA TN 817, 1941.

16. Neely, R. H. et al: "Experimental and Calculated Characteristics of Several NACA 44- Series Wings with Aspect Ratios of 8, 10, and 12 and Taper Ratios of 2.5 and 3.5". NACA TN 1270, 1946.

17. Toll, T. A., Queijo, M. J.: "Approximate Relations and Charts for Low-Speed Stability Derivatives of Swept Wings". NACA TN1581, May 1978.

18. Campbell, J. P., McKinney, M. O.: "Summary of Method for Calculating Dynamic Lateral Stability and Response and for Estimating Lateral Stability Derivatives". NACA TR 1098, 1952.

19. Polhamus, E. C., Sleeman, W. C., Jr.: "The Rolling Moment due to Sideslip of Swept Wings at Subsonic and Transonic Speeds". NASA TN D-209, February 1960.

20. Bird, J. D.: "Some Theoretical Low-Speed Span Loading Characteristics of Swept Wings in Roll and Sideslip". NACA TR 969, 1950.

21. Goodman, A., Fisher, L.R.: "Investigation at Low Speeds of the Effect of Aspect Ratio and Sweep on Rolling Stability Derivatives of Untapered Wings". NACA TR 968, 1950.

22. Hoak, D., et al.: "USAF Stability and Control DATCOM". USAFFDL Report Oct. 1960, Revised February 1972.

APPENDIX A: Calculation of the Induced Velocity Influence Coefficents

The velocity induced at a general point, P, by a horseshoe vortex having a bound segment with both sweepback and dihedral, and trailing legs which are cranked, is developed in this appendix. The planview and a sectional view of a horseshoe vortex is shown in Figure A-1, included at the end of this appendix.

The bound segment, bc, lies on the line of quarter chords of the appropriate wing panel, see Figure A-1. The bound segment thus has the sweepback and dihedral angles of this line, and is displaced vertically from the xy reference plane for a wing with non-zero dihedral. The chordwise segments, ab and cd, are parallel to the x axis. The trailing segments, $\infty_1 a$, and $d\infty_2$ are inclined at the angle β with respect to the plane of symmetry and their projection in the plane of symmetry is inclined at the angle $k_1\alpha$ with respect to the x axis. For k_1 equal to unity the trailing segments are parallel to the free stream velocity vector, while for k_1 equal to zero these vortices lie in the chord plane of the wing with the twist angle removed. The structure of these vortices is described further below.

The wing twist angle has not been simulated by the horseshoe vortices, because if it were, the chordwise segments of a typical horseshoe vortex would not be parallel for a wing with twist. What has been done is to assume that all the bound and chordwise segments on each side of the wing lie in a common

plane which contains the quarter chord line and the root chord. These planes (one on the left and another on the right sides of the wings) are inclined at the angles Γ with respect to the xy reference plane. In order to simulate twist more accurately it would have been necessary to introduce a twist angle rotation of the chordwise segments and this was considered an unnecessary complication. However the wing twist angle is accounted for properly when calculating the "no flow" condition at the control points.

The velocity induced at a general point P by the K^{th} rectilinear vortex segment, with strength Γ_i, is derived with the aid of Figure A-2. The vectors $\bar{R}_{1_K}$ and $\bar{R}_{3_K}$ are displacement vectors from the beginning and end, respectively, of the K^{th} segment to the point P. The unit vector $\hat{r}_{2_K}$ serves to define the direction cosines of the segment and is positive according to the right hand rule for the assumed direction of Γ_i. The magnitude of the velocity induced at P is given by:

$$|\bar{q}_K| = \frac{\Gamma_i}{4\pi h_K}\left(\cos\ \theta_{1_K} + \cos\ \theta_{3_K}\right) \qquad \text{(A-1)}.$$

where

$$h_K = |\bar{R}_{3_K} \times \hat{r}_{2_K}| = |\bar{R}_{3_K}| \sin\ \theta_{3_K} \qquad \text{(A-2)}.$$

$$\cos\ \theta_{1_K} = \bar{R}_{1_K} \cdot \hat{r}_{2_K} / |\bar{R}_{1_K}| \qquad \text{(A-3)}.$$

$$\cos \theta_{3_K} = -\bar{R}_{3_K} \cdot \hat{r}_{2_K} / |\bar{R}_{3_K}| \qquad \text{(A-4)}.$$

The velocity at P is calculated:

$$\bar{q}_K = |\bar{q}_K| \, \hat{q}_K \qquad \text{(A-5)}.$$

where

$$\hat{q}_K = \frac{\hat{r}_{2_K} \times \bar{R}_{1_K}}{|\hat{r}_{2_K} \times \bar{R}_{1_K}|} = \frac{\hat{r}_{2_K} \times \bar{R}_{1_K}}{h_K} = \frac{\hat{r}_{2_K} \times \bar{R}_{3_K}}{h_K} \qquad \text{(A-6)}.$$

hence

$$\bar{q}_K = \frac{\Gamma_i}{4\pi h_K^2}\left(\cos \theta_{1_K} + \cos \theta_{3_K}\right)\left(\hat{r}_{2_K} \times \bar{R}_{3_K}\right) \qquad \text{(A-7)}.$$

The u_K, v_K, w_k components of $\bar{q}_k$ are found:

$$u_k = \bar{q}_K \cdot \hat{i} \,, \quad v_K = \bar{q}_K \cdot \hat{j} \,, \quad w_K = \bar{q}_K \cdot \hat{k} \qquad \text{(A-8)}.$$

The vectors $\bar{R}_{1_K}$, $\hat{r}_{2_K}$, and $\bar{R}_{3_K}$ are defined in terms of their components

$$\left.\begin{aligned} \bar{R}_{1_K} &= R_{1_{1_K}}, R_{1_{2_K}}, R_{1_{3_K}} \\ \hat{r}_{2_K} &= R_{2_{1_K}}, R_{2_{2_K}}, R_{2_{3_K}} \\ \bar{R}_{3_K} &= R_{3_{1_K}}, R_{3_{2_K}}, R_{3_{3_K}} \end{aligned}\right\} \quad K = 1,2,3,4,5 \qquad \text{(A-9)}.$$

The unit vectors $\hat{r}_{2_K}$ can be expresses in terms of the geometry presented in Figure A-1. Their components are given in the following table:

TABLE A-1 Components of $\hat{f}_{2_K}$ for K= 1→5

	K=1	K=2	K=3	K=4	K=5
$R_{2_{1_K}}$	$\cos\beta \cos k_1\alpha$	1	$\cos\phi\tan\Psi/\sqrt{1+\cos^2\phi\tan^2\Psi}$	-1	$-R_{2_{1_1}}$
$R_{2_{2_K}}$	$\sin\beta$	0	$\cos\phi/\sqrt{1+\cos^2\phi\tan^2\Psi}$	0	$-R_{2_{2_1}}$
$R_{2_{3_K}}$	$\cos\beta \sin k_1\alpha$	0	$\sin\phi/\sqrt{1+\cos^2\phi\tan^2\Psi}$	0	$-R_{2_{3_1}}$

Where:

$\Psi = \Lambda$, $\Phi = \Gamma$, for $y_i<0$

$\Psi = -\Lambda$, $\Phi = -\Gamma$ for $y_i>0$

The vector $\bar{R}_3$ for a particular value of K becomes the vector $\bar{R}_1$ for the next higher value of K, e.g., $\bar{R}_{3_{K=2}} = \bar{R}_{3_{K=3}}$, and this simplifies the calculation somewhat. There are basically only six vectors which need to be considered and these are the vectors which mark the ends or corners of the cranked horseshoe vortices, namely: $\bar{R}_{\infty 1}$, $\bar{R}_a$, $\bar{R}_b$, $\bar{R}_c$, $\bar{R}_d$, and $\bar{R}_{\infty 2}$. It is noted that the ends of the trailing legs are not taken to be located at infinity but rather at approximately 1000 root chords downstream for ease of computation. The value cos θ_1 for K_1, and cos θ_3 for K=5, are nearly equal to unity at such a great distance downstream. The aerodynamic influence of the trailing legs at a distance beyond 1000 c_R is negligible. The components of $\bar{R}_{1_K}$ and $\bar{R}_{3_K}$ for K=1→5 are given in Table A-2. Notice that x,y,z have been replaced with f,g,h, respectively in this table since the latter variables

will be the ones used in the formulation given in the main body of the report, see equation 24.

Table A–2 Components of $\bar{R}_{1_K}$ and $\bar{R}_{3_K}$ for K –1–5

K	$\bar{R}_{1_K}$			$\bar{R}_{3_K}$		
	$R_{1_{1_K}}$	$R_{1_{2_K}}$	$R_{1_{3_K}}$	$R_{3_{1_K}}$	$R_{3_{2_K}}$	$R_{3_{3_K}}$
K=1	$1000c_R\cos\beta\cdot\cos(k_1\alpha)+s\cdot\cos\phi\tan\Psi+{}^3/_4 c_{MI}+f$	$1000c_R\sin\beta+s\cos\phi+g$	$1000c_R\cos\beta\cdot\sin(k_1\alpha)+s\sin\phi+h$	$s\cos\phi\tan\Psi+{}^3/_4 c_{MI}+f$	$s\cos\phi+g$	$s\sin\phi+h$
K=2	$=R_{3_{1_1}}$	$R_{3_{2_1}}$	$R_{3_{3_1}}$	$s\cos\phi\tan\Psi+f$	$s\cos\phi+g$	$s\sin\phi+h$
K=3	$R_{3_{1_2}}$	$R_{3_{2_2}}$	$R_{3_{3_2}}$	$-s\cos\phi\tan\Psi+f$	$s\cos\phi+g$	$-s\sin\phi+h$
K=4	$R_{3_{1_3}}$	$R_{3_{2_3}}$	$R_{3_{3_3}}$	$-s\cos\phi\cdot\tan\Psi+{}^3/_4 c_{PL}+f$	$-s\cos\phi+g$	$-s\sin\phi+h$
K=5	$R_{3_{1_4}}$	$R_{3_{2_4}}$	$R_{3_{3_4}}$	$1000c_R\cos\beta\cdot\cos(k_1\alpha)-s\cos\phi\tan\Psi+{}^3/_4 c_{PL}+f$	$1000c_R\sin\beta-s\cos\phi+g$	$1000c_R\cos\beta\cdot\sin(k_1\alpha)-s\sin\phi+h$

The induced velocity components given by equation A-8 are found by performing the steps indicated in equations A-2, A-3, A-4, and A-7. For the sake of completeness the amplified equations used are given below.

$$h_K^2 = (R_{2_{2_K}} R_{3_{3_K}} - R_{2_{3_K}} R_{3_{2_K}})^2 + (R_{2_{3_K}} R_{3_{1_K}} - R_{2_{1_K}} R_{3_{3_K}})^2 + (R_{2_{1_K}} R_{3_{2_K}} - R_{2_{2_K}} R_{3_{1_K}})^2 \quad \text{(A-10}$$

$$R_{1_K} = |\overline{R}_{1_K}| = \left[R_{1_{1_K}}^2 + R_{1_{2_K}}^2 + R_{1_{3_K}}^2\right]^{\frac{1}{2}} \quad \text{(A-11)}$$

$$R_{3_K} = |\overline{R}_{3_K}| = \left[R_{3_{1_K}}^2 + R_{3_{2_K}}^2 + R_{3_{3_K}}^2\right]^{\frac{1}{2}} \quad \text{(A-12)}$$

$$\cos\theta_{1_K} = \left[R_{1_{1_K}} R_{2_{1_K}} + R_{1_{2_K}} R_{2_{2_K}} + R_{1_{3_K}} R_{2_{3_K}}\right] / R_{1_K} \quad \text{(A-13)}$$

$$\cos\theta_{3_K} = -\left[R_{1_{1_K}} R_{2_{1_K}} + R_{3_{2_K}} R_{2_{2_K}} + R_{3_{3_K}} R_{2_{3_K}}\right] / R_{3_K} \quad \text{(A-14)}$$

$$u_K = \frac{\Gamma_i}{4\pi}\left(\frac{\cos\theta_{1_K} + \cos\theta_{3_K}}{h_K^2}\right)(R_{2_{2_K}} R_{3_{3_K}} - R_{2_{3_K}} R_{3_{2_K}}) \quad \text{(A-15)}$$

$$v_K = \frac{\Gamma_i}{4\pi}\left(\frac{\cos\theta_{1_K} + \cos\theta_{3_K}}{h_K^2}\right)(R_{2_{3_K}} R_{3_{1_K}} - R_{2_{1_K}} R_{3_{3_K}}) \quad \text{(A-16)}$$

$$w_K = \frac{\Gamma_i}{4\pi}\frac{\cos\theta_{1_K} + \cos\theta_{3_K}}{h_K^2}(R_{2_{1_K}} R_{3_{2_K}} - R_{2_{2_K}} R_{3_{1_K}}) \quad \text{(A-17)}$$

$$u_j = \sum_{K=1}^{5} u_K \quad \text{(A-18)}$$

$$v_j = \sum_{K=1}^{5} v_K \quad \text{(A-19)}$$

$$w_j = \sum_{K=1}^{5} w_K \quad \text{(A-20)}$$

The influence coefficents are defined:

$$u_j = \frac{\Gamma_i}{4\pi} Fu_{ij} \tag{A-21}$$

$$v_j = \frac{\Gamma_i}{4\pi} Fv_{ij} \tag{A-22}$$

$$w_j = \frac{\Gamma_i}{4\pi} Fw_{ij} \tag{A-23}$$

hence

$$Fu_{ij} = \sum_{K=1}^{5} \frac{\cos \theta_{1_K} + \cos \theta_{3_K}}{h_K^2} \left(R_{2_{2_K}} R_{3_{3_K}} - R_{2_{3_K}} R_{3_{2_K}} \right) \tag{A-24}$$

$$Fv_{ij} = \sum_{K=1}^{5} \frac{\cos \theta_{1_K} + \cos \theta_{3_K}}{h_K^2} \left(R_{2_{3_K}} R_{3_{1_K}} - R_{2_{1_K}} R_{3_{3_K}} \right) \tag{A-25}$$

$$Fw_{ij} = \sum_{K=1}^{5} \frac{\cos \theta_{1_K} + \cos \theta_{3_K}}{h_K^2} \left(R_{2_{1_K}} R_{3_{2_K}} - R_{2_{2_K}} R_{3_{1_K}} \right) \tag{A-26}$$

In the calculation of the influence coefficents, equations A-24, A-25, and A-26, for the case where the general point P corresponds to the point d_j (which lies on the bound vortex segment, see Section III.B.3.b.) it is necessary to omit the terms for K=3 when i=j. In this case and others where the numerical evaluation of the influence coefficents may have become difficult owing to the fact that $\theta_1 \rightarrow 0$, i.e., the point P approaches the line upon which the segment lies and equation A-1 becomes indeterminate, the computer omits the induced velocity of that segment. A general test is made and the computer omits the induced velocity components of any vortex segment when the value h_K becomes less than 0.1s.

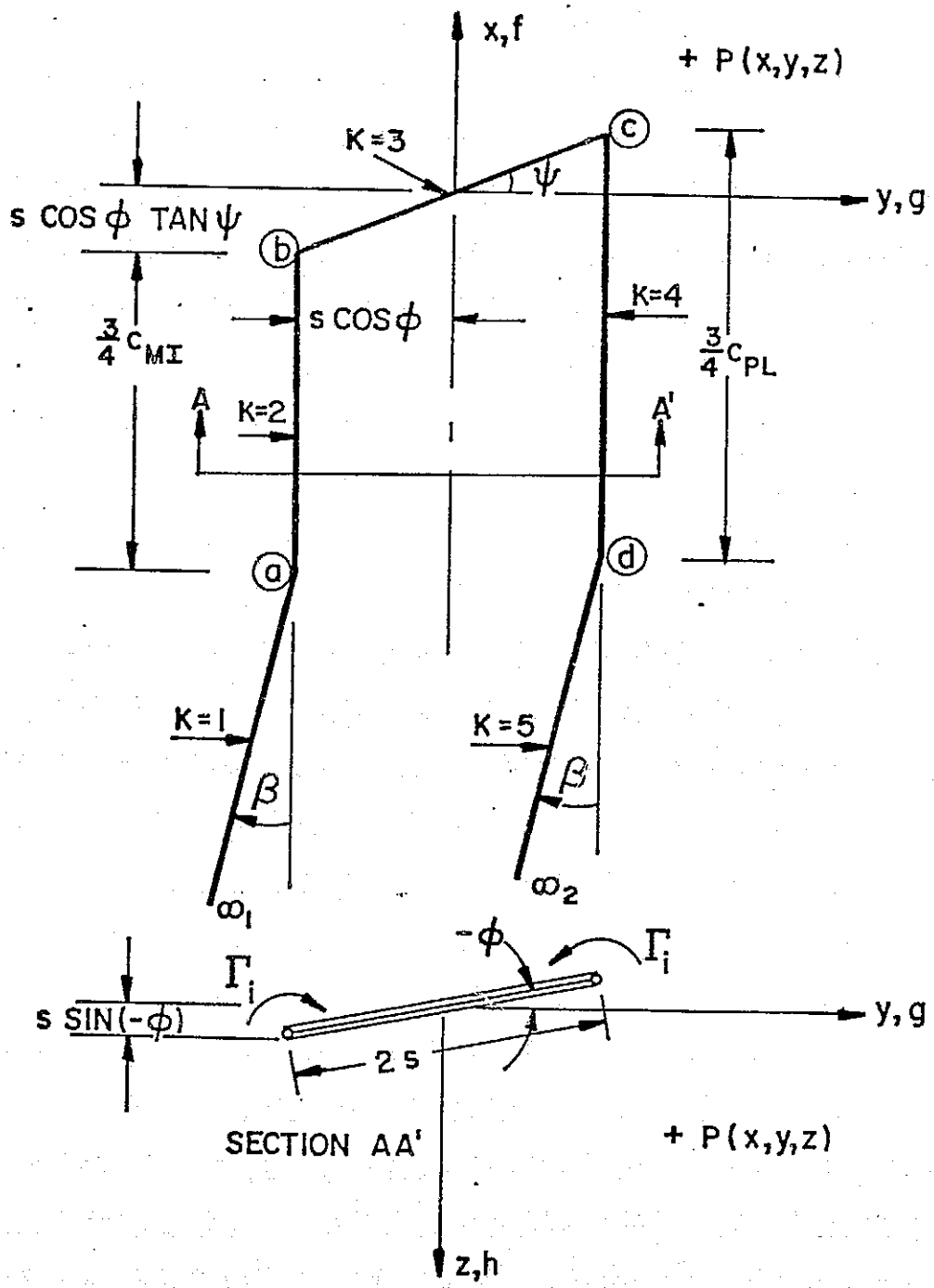

FIG. A-1 PLAN AND SECTIONAL VIEW OF A TYPICAL HORSESHOE VORTEX

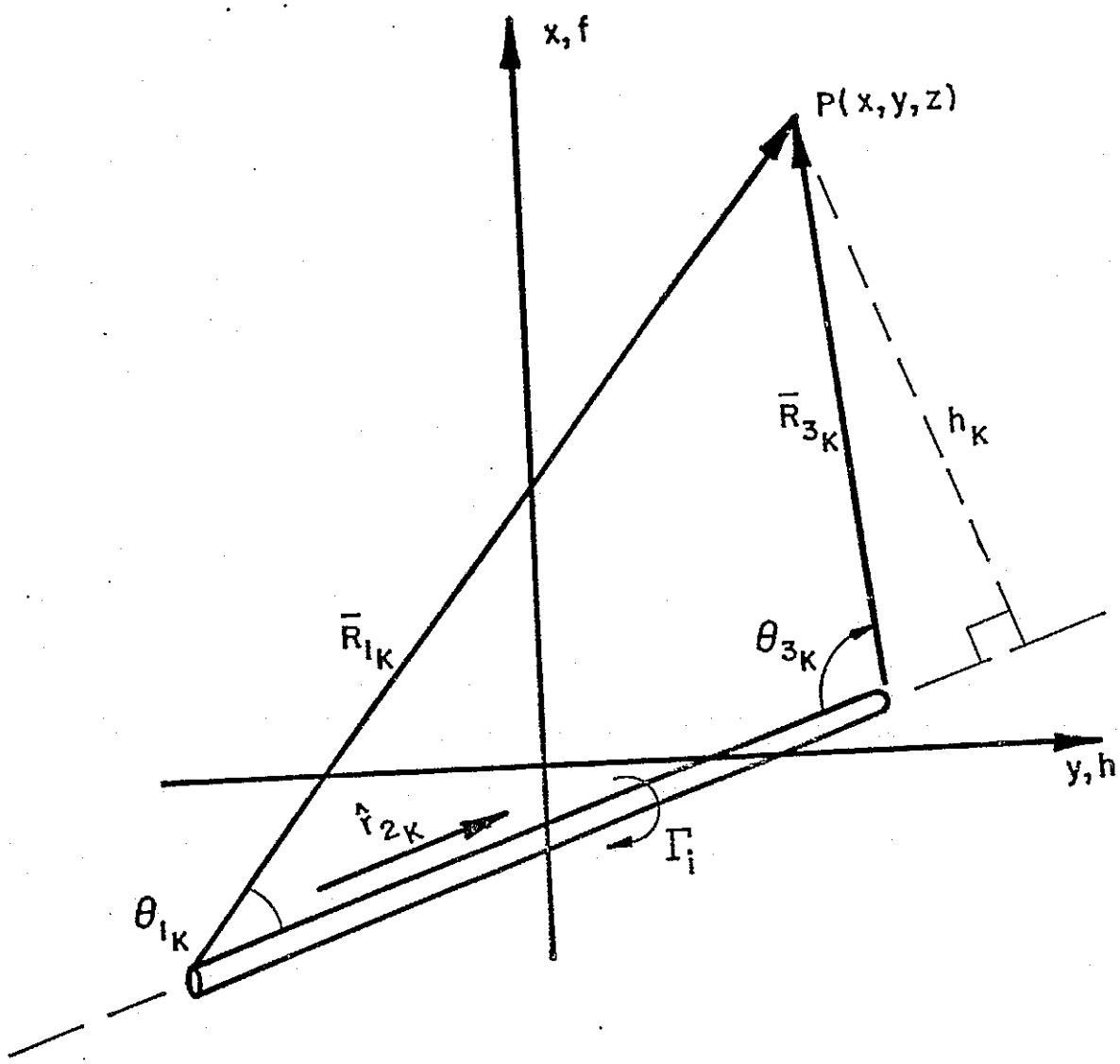

FIG. A-2 VECTOR DIAGRAM FOR CALCULATING VELOCITY INDUCED BY A VORTEX SEGMENT

Appendix B: Instructions for Operating the Computer Program

1. Program Description

The program computes the spanwise distribution of circulation, $\tilde{\Gamma}(y) = \Gamma_i/V_\infty$, and the linear force and moment coefficients for a wing alone in a steady, incompressible inviscid fluid flow using the finite-step method. Provisions are included for studying variations of angle of attack, angle of sideslip, and the angular rates of rotation P, Q, and R.

The wing geometry is limited to a single trapezoidal panel per side and left-to-right geometric symmetry is assumed, except that differential wing twist is considered in order to permit the study of manufacturing anomalies. The wing is divided into an even number, N, of segments of equal spanwise dimensions. The number chosen for N can be varied between twenty and one hundred in the program. The segments are numbered 1 to N, from left to right, beginning on the left wing tip. The program solves N equations for the spanwise distribution of circulation in every case. Advantage could have been taken of aerodynamic symmetry for those cases dealing with symmetric flight only, and N/2 equations solved instead. The program is inefficient to this extent.

A provision has also been made for the calculation of the

nonlinear aerodynamic coefficients of the wing but this part of the program is not working satisfactorily as described previously. This calculation may be deleted as described in section 3 below. There are also some minor variations provided for preparing the input data concerned with wing geometry.

2. Operating Information

Core and Time Requirements:

Computer: CDC 6600

Core : 77 K_8 to load

70 K_8 to execute

Time : Approximately 4 minutes

3. Input Data

There are two options for loading the basic wing geometry. In the first option, the span and root and tip chord dimensions are given and the planform area, aspect ratio. and taper ratio are computed. In the second option, the area, aspect ratio and taper ratio are loaded directly. The root chord is assumed equal to unity in the second option.

The angles of attack and sideslip and the angular rates P, Q, R are varied in the following manner. Five DØ LØØPs are nested from the outermost variable R, to the innermost variable β, in the order R, Q, P, α, β. The calculations proceed by selecting the

first set of values, namely, R_1, Q_1, P_1, α_1, and varies β from β_1 to β_{IB}. Upon completion of this calculation, the next α is chosen holding R_1, Q_1, P_1 fixed and calculations are made for the various β values. After calculations have been made for all the angle of attack values considered, the computer then repeats these calculations for the different roll rates. Subsequently, all the preceding calculations are repeated for the different pitch rates and then the different yaw rates in that order. It is more efficient usually to use different cases to consider separately the effects of these variables than to use the nesting provided in the program.

Multiple cases can be run consecutively by repeating the information required for a single case, see description given for card (1) below.

Card No.	Variable	Format	Description
(1)	NØCASE	15	Number of cases to be run. The program is presently arranged so that only cards (2) to (5a) or (5b) can be modified. Changes to cards (6), etc., requires a complete reloading of the input.
(2)	CRF	8F10.0	c_{ref} mean aerodynamic chord, or

Card No.	Variable	Format	Description
(2)	(Contd.)		reference chord length. (m/ft.)
	CLD	8F10.0	Sweepback angle of quarter chord line, Λ, degrees, positive for sweepback.
	CGD	"	Dihedral angle of quarter chord line, Γ, degrees. positive for tip chord elevated above root chord.
	ETLD	"	Twist angle of the left wing tip chord, ϵ_{T_R}, degrees, positive for washin (negative for washout).
	ETRD	"	Twist angle of the right wing tip chord, ϵ_{T_R}, degrees, positive for washin.
	D34ØD	"	The angle the mean camber line makes with the chord line at the wing root (y=0), $(\delta_{3/4})_0$, degrees, positive for positive camber, see Figure 4. This value is equal to the geometric value for the linear case only, and should equal the negative of $(\alpha_{L_0})_0$, approximately when the airfoil aero-

Card No.	Variable	Format	Description
			dynamic data is known.
(2)	D34TD	8F10.0	The same as D34ØD , except that this value pertains to the wing tip rather than the wing root.
	XCG	"	The longitudinal position of the center of gravity, measured from the quarter chord point of the root chord, x_{CG}, (m/ft.), positive for the CG ahead of the ¼ C_R point, see Figure 1.
(3)	YCG	"	The lateral displacement of the CG from the plane of symmetry, y_{CG}, (m/ft.), positive for a displacement to the right.
	ZCG	"	The vertical displacement of the CG from the x,y reference plane, z_{CG}, (m/ft.), positive for a displacement below the reference plane, see Figure 2.
	RK1	"	The value, k_1, where k_1 is the fractional value of the displacement angle of the wing wake above the wing chord plane; when k_1=0, the wake trails

Card No.	Variable	Format	Description
(3)	(Contd.)		in the wing chord plane and when $k_1=1$, the wake trails parallel to V_∞. Nominal value is $k_1=\frac{1}{2}$.
	ALORD	8F10.0	Angle of zero lift of the root chord, $(\alpha_{L_0})_0$, degrees, obtained from airfoil section data. Value should be negative for a positive camber.
	ALOTD	"	Angle of zero lift of the tip chord, $(\alpha_{L_0})_0$, degrees, from airfoil section data.
(4)	N	10I5	Number of wing segments, $20 < N < 100$, $N_{nominal} = 40$.
	ITA	"	Number of angles of attack used in the table of airfoil section characteristics, see card (6) below. The maximum value for ITA is 20.
	LAS	"	Option for loading planform geometry, LAS < 0 calls for card (5a) whereon span, root and tip chord, and air speed are placed. For LAS > 0, card (5b) is used instead, wheron reference

Card No.	Variable	Format	Description
(4)	(Contd.)		area, aspect ratio, taper ratio and air speed are placed.
	IA	10I5	The number of angles of attack to be considered are indicated by the variable IA, IA_{max} = 25.
	IB	"	The number of angles of sideslip to be considered are indicated by the variable IB, IB_{max} = 5.
	IP	"	The number of roll rates, pitch rates, and yaw rates to be considered are indicated by the variables IP,
	IQ	"	IQ and IR, respectively. A maximum
	IR	"	of five values of each may be considered.
	LIN	"	The variable LIN exercises the option to calculate the linear aerodynamic results only, LIN = +1.; or the combined linear and nonlinear results, LIN = -1. In the linear only case, it is unnecessary to load cards (6) to (25).

The following card is an optional card, but either it or card (5b) must be used. In order for (5a) to be used,

LAS < 0, see card (4).

Card No.	Variable	Format	Description
(5a)	B	8F10.0	Wing span, b, (m/ft.)
	CT	"	Tip chord, C_T, (m/ft.)
	CR	"	Root chord, C_R, (m/ft.)
	VI	"	Air speed, V_∞, (m/sec. or ft./sec.)
(5b)	SR	"	Wing planform area, S_{ref}, (m^2/ft^2)
	A	"	Aspect ratio, A, nondim.
	SL	"	Taper ratio, λ, nondim.
	VI	"	Air speed, V_∞, (m/sec. or ft./sec.)

The airfoil section characteristics are placed on the next group of cards which are ITA in number. The root chord values are listed first, followed by the tip values. If LIN > 0, omit these cards.

(6)	TA(I)	7F10.4	Angle of attack, α, degrees
	CLR(I)	"	Root section lift coefficient, c_ℓ, nondim.
	CDR(I)	"	Root section drag coefficient, c_d, nondim.

Card No.	Variable	Format	Description
(6)	CMR(I)	7F10.4	Root section pitching moment coefficient, $c_{m_{c/4}}$, nondim.
	CLT(I)	"	Tip section lift coefficient, c_{ℓ}, nondim.
	CDT(I)	"	Tip section drag coefficient, c_{d}, nondim.
	CMT(I)	"	Tip section pitching moment coefficient, $c_{m_{c/4}}$, nondim.
(7)			
(25)			

The next group of cards list the values of the angle(s) of attack, angle(s) of sideslip, roll rates, pitch rates, and yaw rates for which calculations are to be made.

(26)	AL(1)	8F10.0	Value(s) of the angle(s) of attack, α, degrees for which calculations are to be made. A maximum of 25 values may be considered.
(29)	AL(IA)	"	

Card No.	Variable	Format	Description
(30)	BE(1) ↓ BE(IB)	8F10.0	Value(s) of the angle(s) of sideslip, β, degrees. A maximum of 5 values may be considered.
(31)	P(1) ↓ P(IP)	"	Value(s) of the roll rate(s), P, rads./sec. A maximum of 5 values may be considered.
(32)	Q(1) ↓ Q(IQ)	"	Value(s) of the pitch rate(s), Q, rads./sec. A maximum of 5 values may be considered.
(33)	R(1) ↓ R(IR)	"	Value(s) of the yaw rate(s), R, rad./sec. A maximum of 5 values may be considered.

Additional cases may be listed by repeating the input cards listed above from 2 to 5a or 5b . Table B-1 presents the general arrangement of the input cards.

4. Output Data

The output will be described for the case where the combined linear/nonlinear option has been chosen. (In linear case only, the nonlinear output will, of course, not appear.)

The output is arranged in four basic groupings:

a. The wing geometric variables are listed together with

some input constants which serve to identify the case: CREF = $c_{ref} = \bar{c}$, ETL = $\epsilon^{o}_{T_L}$, (DELTA 3/4)0 = $(\delta_{3/4})^{o}_{o}$, XCG = x_{CG}, ZCG = z_{CG}, GAMMA = Γ^{o}, ETR = $\epsilon^{o}_{T_R}$, (DELTA 3/4)T = $(\delta_{3/4})^{o}_{T}$, YCG = y_{CG}, K1 = k_1, LAMBDA = $\Lambda^{o} = \Lambda^{o}_{c/4}$, ALPHA = $\alpha^{o}_{L_o}$, V INF = V_∞ (ft./sec. or m/sec.), CT = c_T, B = b, CR = c_R (or alternatively SREF = S_{ref}, A = A., LAMBDA = λ), E = E. These values are not repeated anywhere in the run.

b. The angular velocity components R, Q, P (rads./sec.) and the angle of attack and angle of sideslip are listed on the next line.

c. The linear data is listed in the following manner:

1. The linear-analysis spanwise values of the circulation $\tilde{\Gamma}_i = (\Gamma_i/V_\infty)$ is listed left to right, for the N segments, beginning of course with the value I = 1, continuing to I = N. (I = 1 corresponds to the segment on left wing tip and I = N corresponds to the segment on the right wing tip.)

2. The linear, integrated, force coefficients C_x, C_y, C_z and the moment coefficients: CLB = C_{ℓ_B}, CMB = C_{m_B}, and CNB = C_{n_B} for the body axes are printed on the next line. A title appears in the preceding line.

3. The above data is transferred to stability axes,

labelled as such, and printed on a single line. The force coefficients are CL = C_L, CY = C_Y, and CD = $C_{D_{induced}}$; the moment coefficients are CLS = C_{ℓ_s}, CMS = C_{m_s}, and CNS = C_{n_s}.

d. The nonlinear data is listed in the following manner:

1. The N values of $\tilde{\Gamma}_{original}$ are printed for the wing segments, beginning with the left tip value and ending with the right tip value, from left to right across the page. These values correspond to the first iteration.

2. In a similar fashion, the values $\tilde{\Gamma}_{Simq}$ are printed, followed by the values of $\tilde{\Gamma}_{Marian}$.

3. The N values of the pairs of number TCLJ(J) = $2\tilde{\Gamma}_i/c_j$ and CLJ(J) = c_{ℓ_j} are printed side-by-side. The value TCLJ(J) is the "theoretical" section lift coefficient at the j^{th} segment corresponding to the value of the circulation (at that segment) determined by linear theory, while CLJ(J) is the section lift coefficient at the j^{th} segment determined from the wind tunnel data tabulations corresponding to the computed value of α_j.

4. The effective angle of attack, α_j, is printed for

each of the N segments.

5. The integrated nonlinear force and moment coefficients for the body and stability axes, as was done for the linear calculation, are printed next.

6. Four more iterations follow the first before the angle of attack or angle of sideslip change (or P, Q, R change) to the next value.

5. Programming Information

Purpose of Subroutines:

EEL2 — Computes the complete elliptical integral $E(k, \pi/2)$ where $k=\sqrt{1-(b/a)^2}$ and $a/b=\pi A/4$, for correcting lifting-line theory according to R.T. Jones: $c_\ell=2\pi\alpha_{eff}/E$.

SIMQ — Solution of simultaneous linear algebraic equations used primarily for the determination of the $\tilde{\Gamma}$ vector which satisfies the no-flow boundary condition in the linear calculation, but also used in the nonlinear calculation for determining the lifting surface value of the circulation in a region one tip chord in length located at the wing tips.

FUVW — Calculates the induced-flow velocity influence coefficients.

MARIAN — A seventh order polynomial curve-fitting procedure which smooths the spanwise distribution of circulation, joining the section values in-board to the lifting-surface theory values near the tips.

There is no interdependence of these subroutines.

TABLE B1

Card	1–5	6	7–10	11–20	21–30	31–40	41–50	51–60	61–72	73–80
①	NOCASE →									
②	C_{REF}			Λ°	Γ°	ϵ_{TL}°	ϵ_{TR}°	$(\delta_{3/4})_L^\circ$	$(\delta_{3/4})_T^\circ$	
③	y_{CG}			z_{CG}	h_1	$(\alpha_{LR})_R^\circ$	$(\alpha_{LR})_T^\circ$	T	T	X_{CG}
④	N		ITA	LAS	IA	IB	IP	IQ	IR	LIN	T	T	T
⑤a	b			C_T	C_R	V_∞	T	T	T	T
⑤b	S_{REF}			A	λ	V_∞	T	T	T	T
⑥	α			$C_{l\,ROOT}$	$C_{d\,ROOT}$	$C_{m\,c/4\,ROOT}$	$C_{l\,TIP}$	$C_{d\,TIP}$	$C_{m\,c/4\,TIP}$	T
	↓			↓	↓	↓	↓	↓	↓	T
㉕										T
㉖	α_1			α_2	α_3	α_4	α_5	α_6	α_7	T
㉗	α_9			α_{10}	α_{11}	α_{12}	α_{13}	α_{14}	α_{15}	α_8
㉘	α_{17}			α_{18}	α_{19}	α_{20}	α_{21}	α_{22}	α_{23}	α_{16}
㉙	α_{25}			T	T	T	T	T	T	α_{24}
㉚	β_1			β_2	β_3	β_4	β_5	T	T	T
㉛	P_1			P_2	P_3	P_4	P_5	T	T	T
㉜	Q_1			Q_2	Q_3	Q_4	Q_5	T	T	T
㉝	R_1			R_2	R_3	R_4	R_5	T	T	T

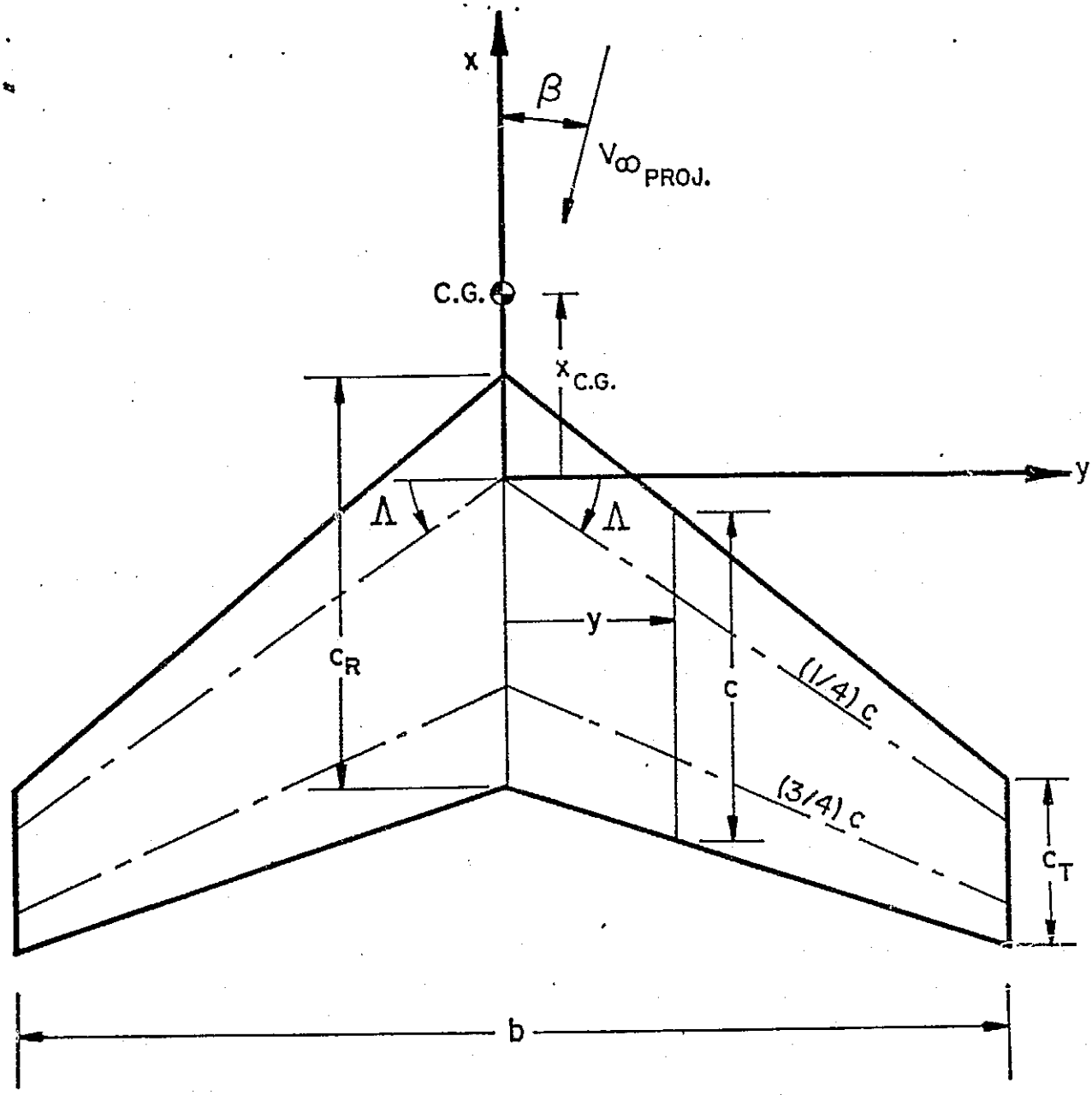

FIG. 1 WING GEOMETRY

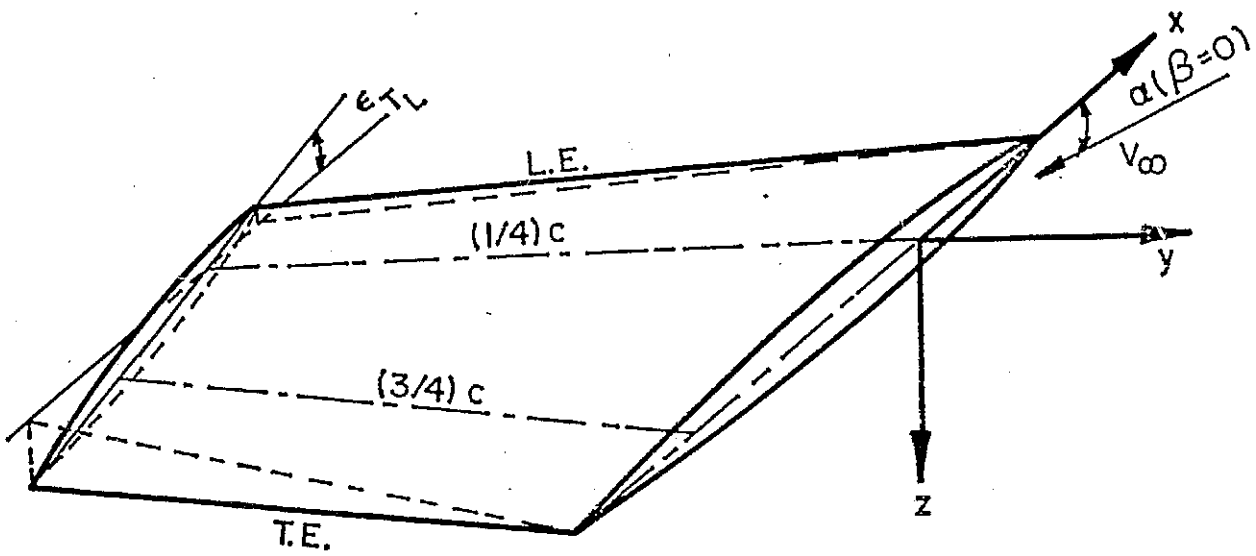

FIG. 2 LEFT HAND WING PANEL DEFINING TWIST ANGLE (ZERO DIHEDRAL CASE)

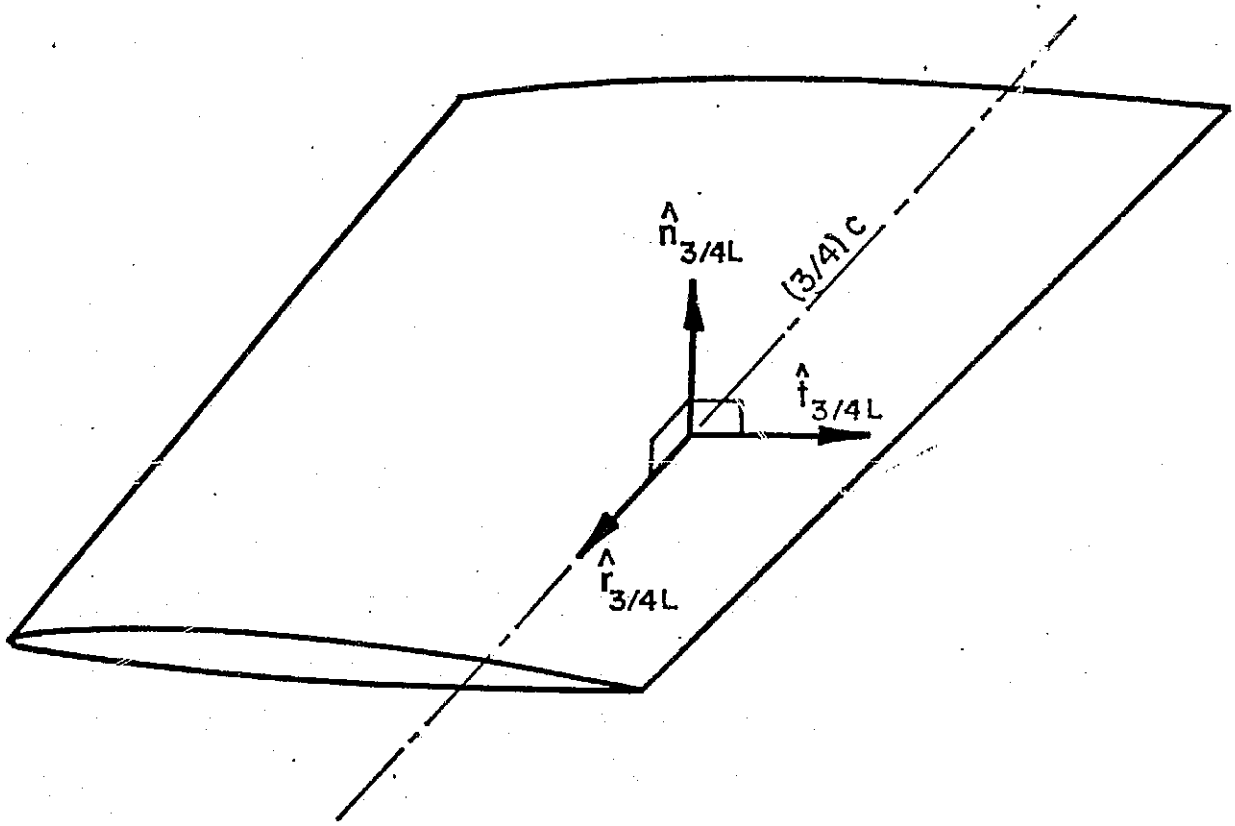

FIG. 3 LEFT HAND WING PANEL DEFINING UNIT TANGENT AND NORMAL VECTORS ALONG THREE-QUARTER CHORD LINE

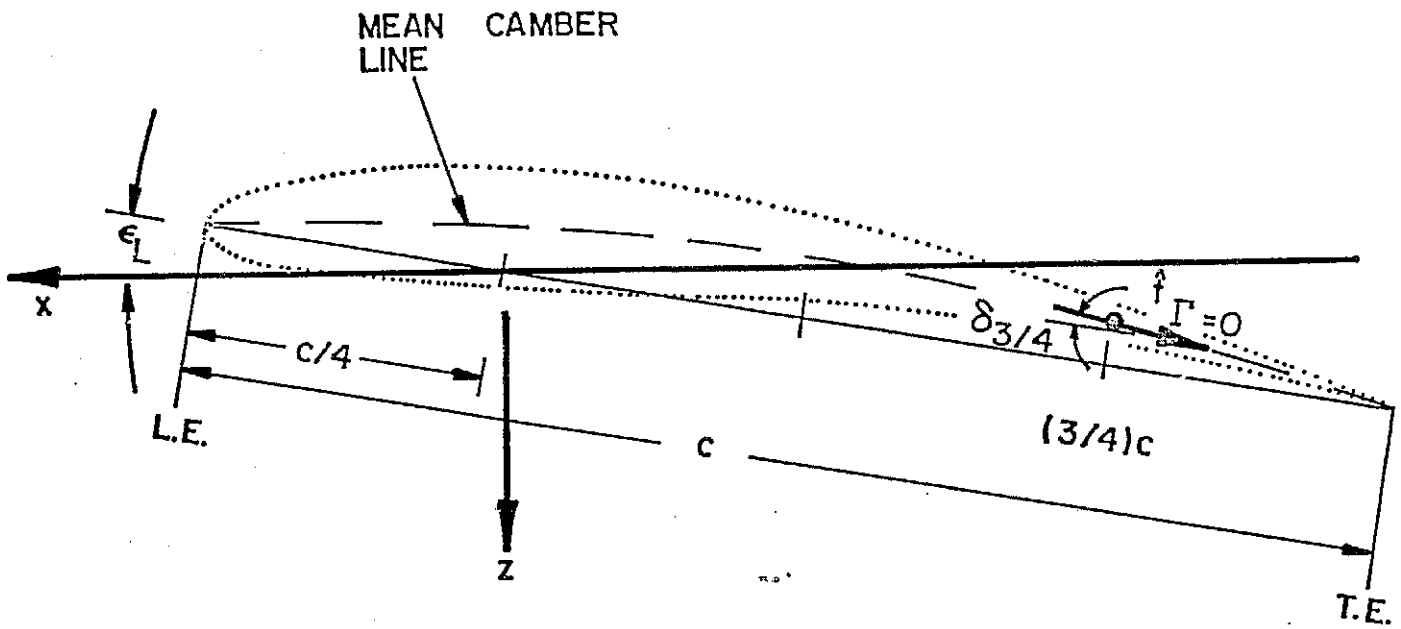

FIG. 4 TYPICAL CHORD PLANE DEFINING BOUNDARY CONDITION AT THREE-QUARTER CHORD POINT

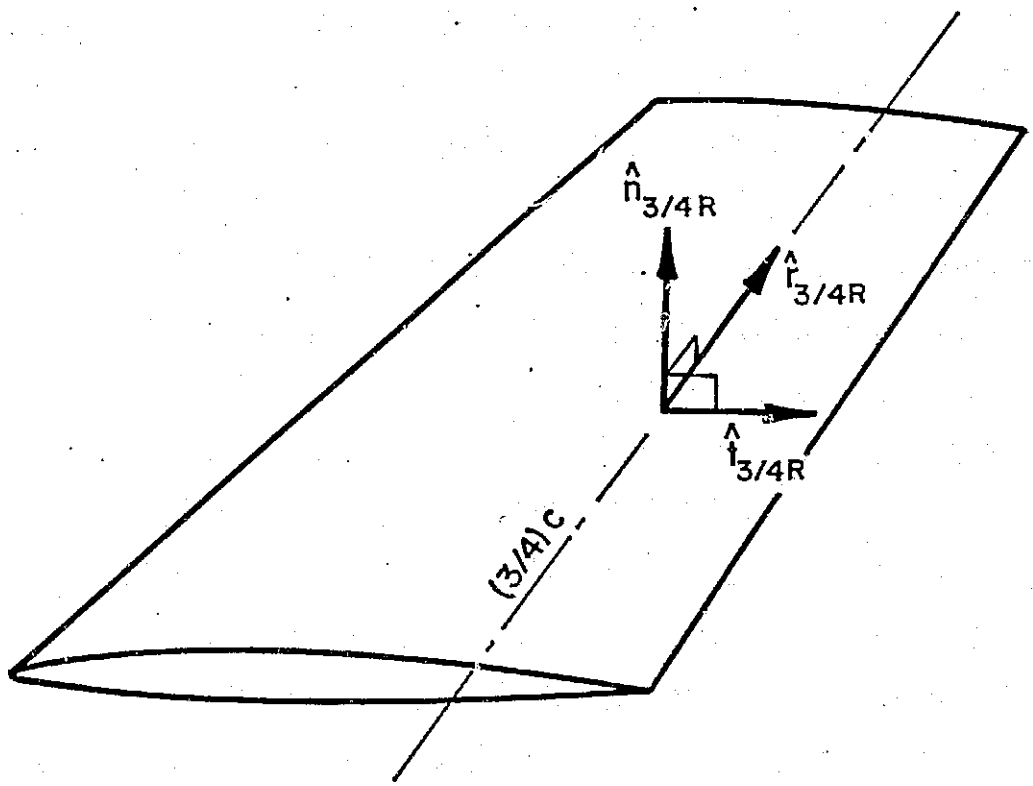

FIG. 5 RIGHT HAND WING PANEL DEFINING UNIT TANGENT AND NORMAL VECTORS ALONG THREE-QUARTER CHORD LINE

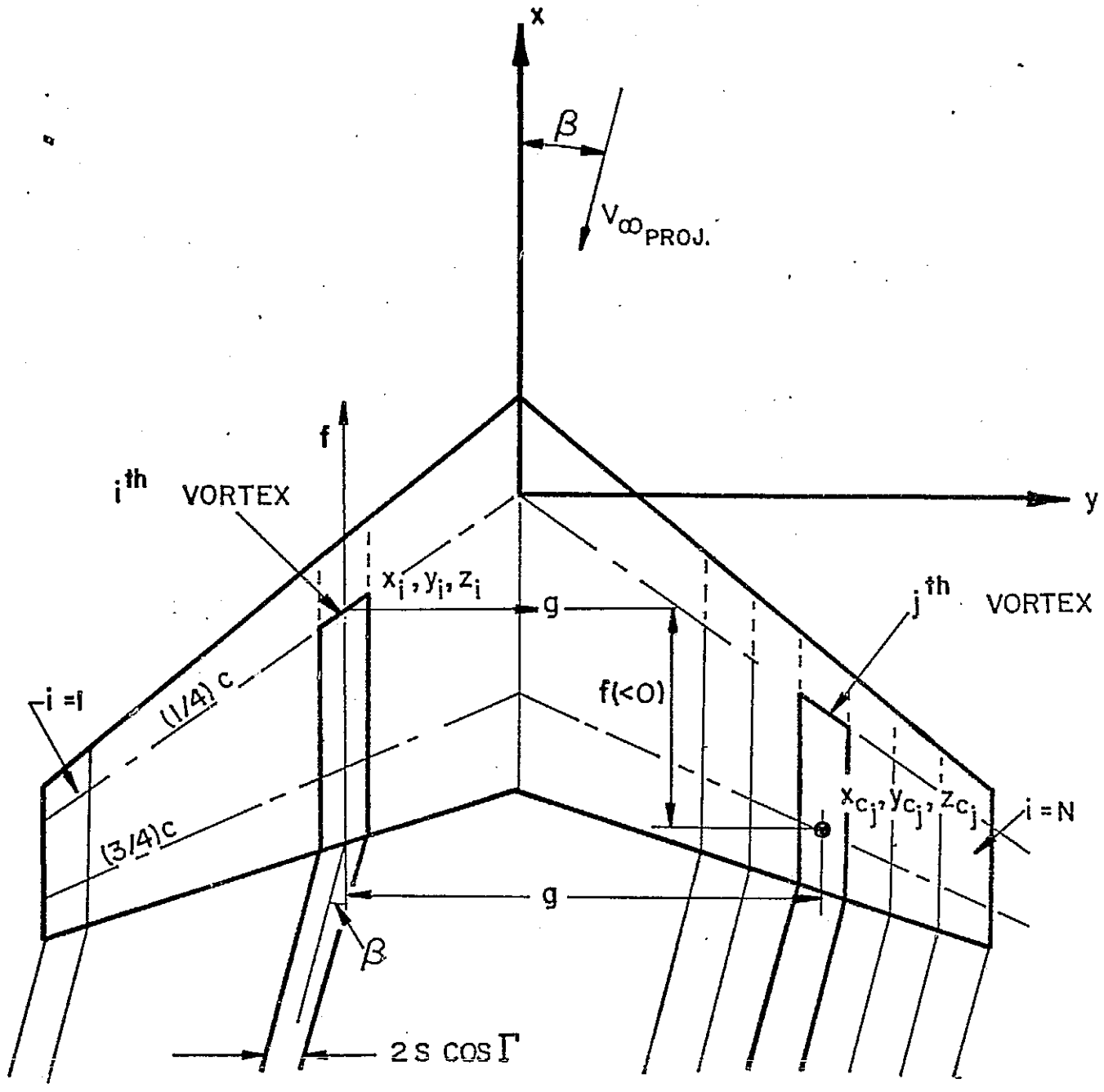

FIG. 6 PLANFORM GEOMETRY SHOWING HORSESHOE VORTEX ELEMENTS

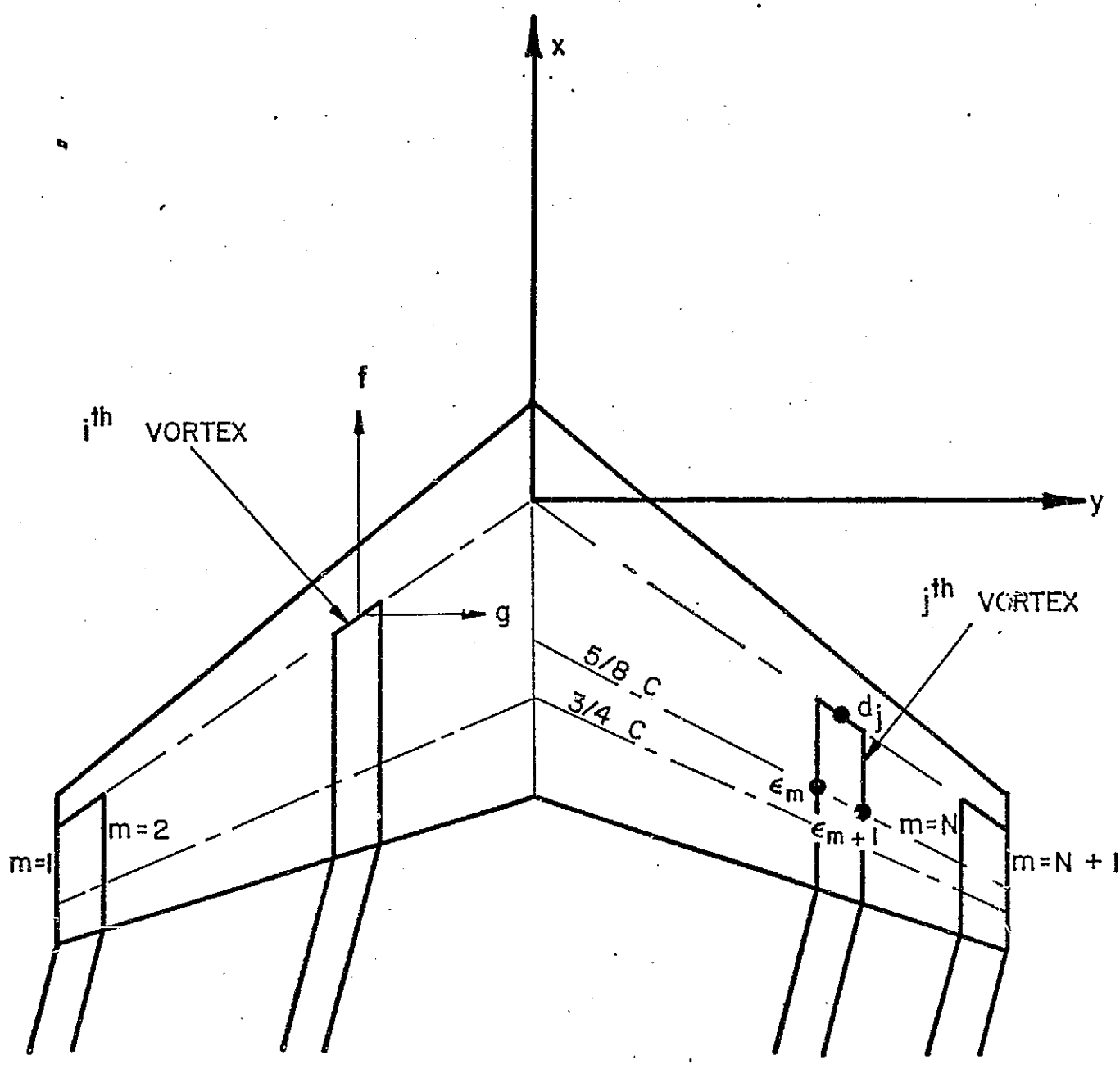

FIG. 7 SCHEMATIC DRAWING ILLUSTRATING BOUND AND CHORDWISE VORTEX SEGMENTS FOR CALCULATING FORCES AND MOMENTS

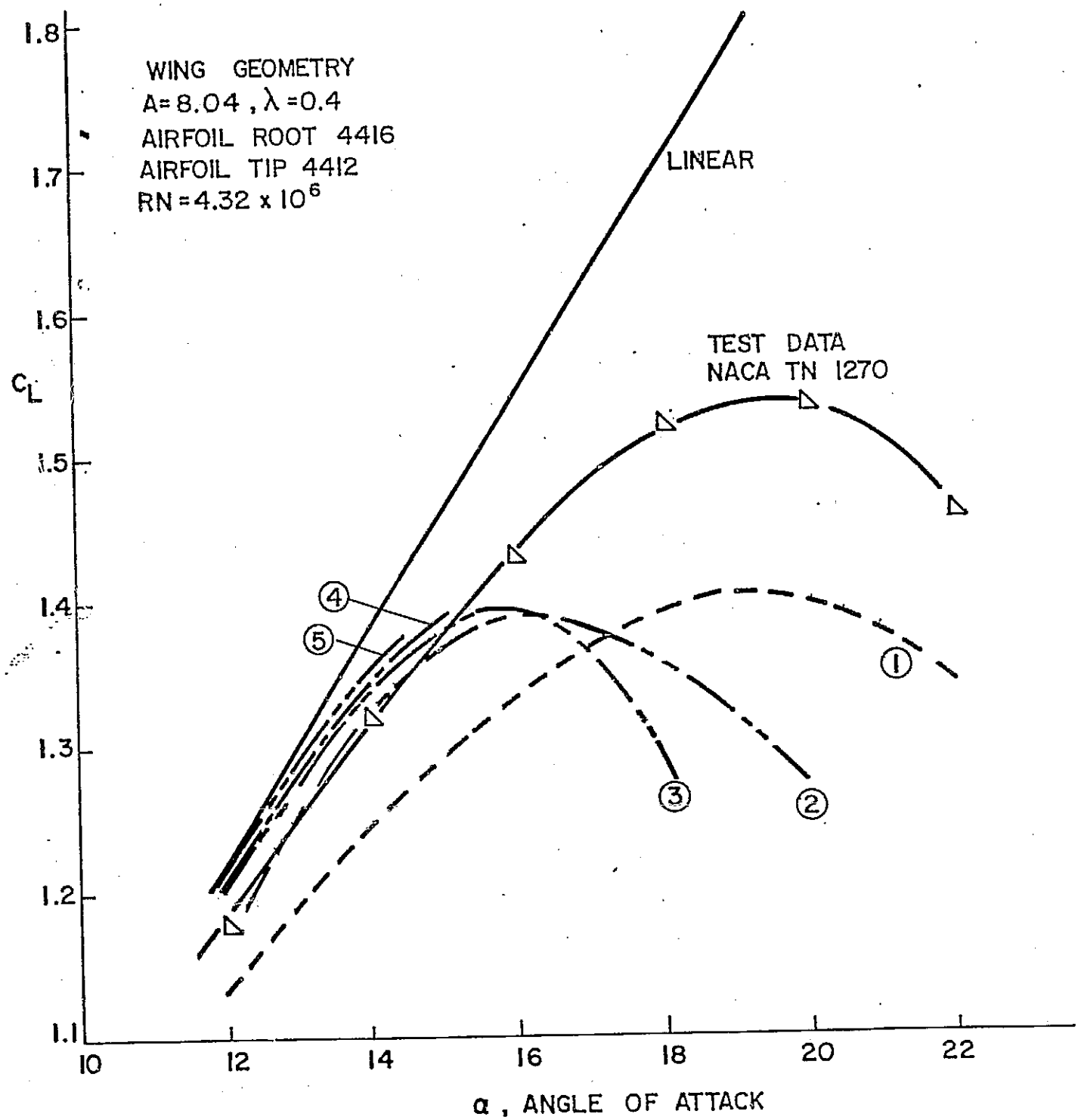

FIG. 8 VARIATION OF LIFT COEFFICIENT WITH ANGLE OF ATTACK - NONLINEAR THEORY

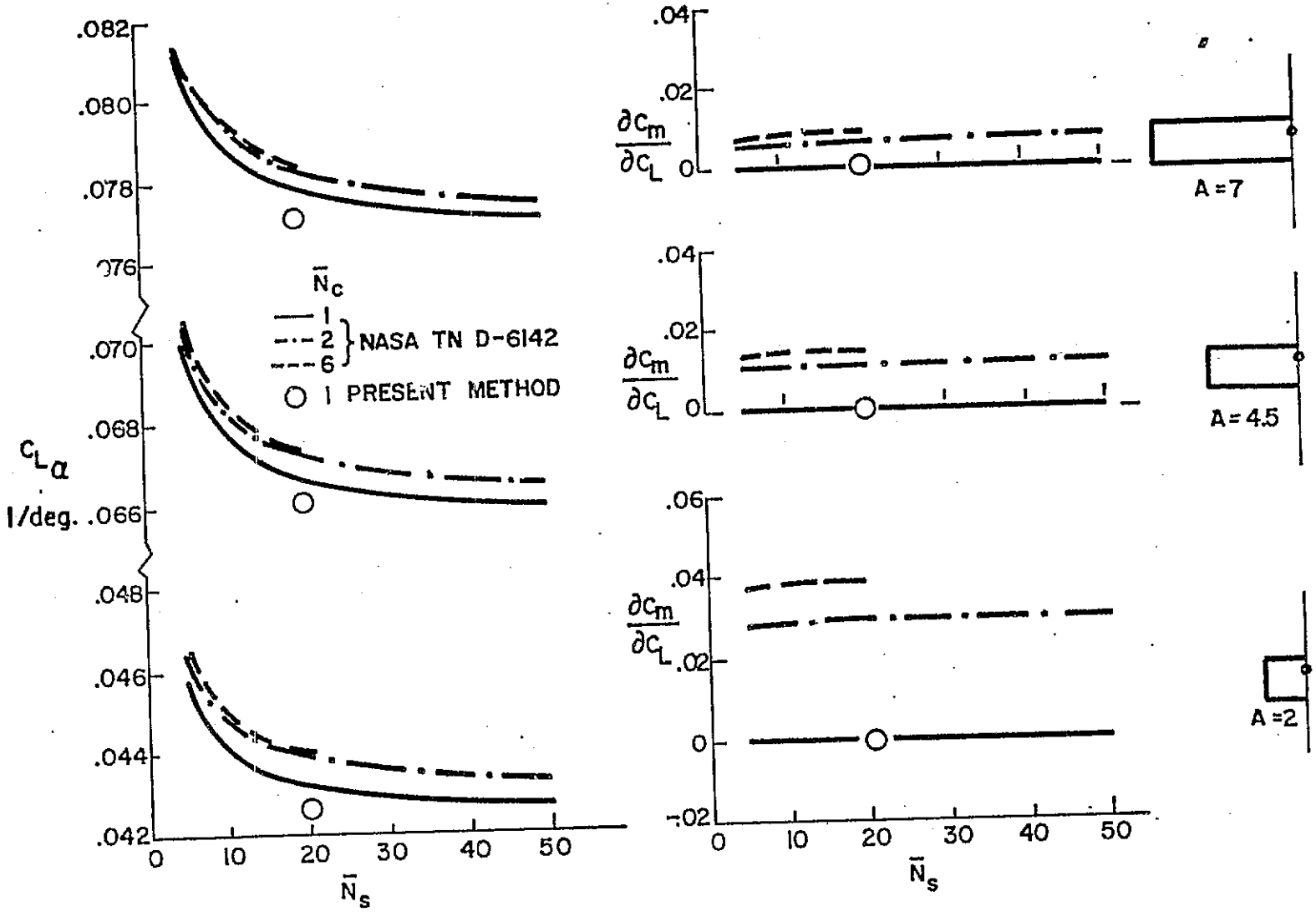

FIG. 9 COMPARISON OF PRESENT CALCULATIONS WITH VORTEX LATTICE METHOD – STRAIGHT WINGS

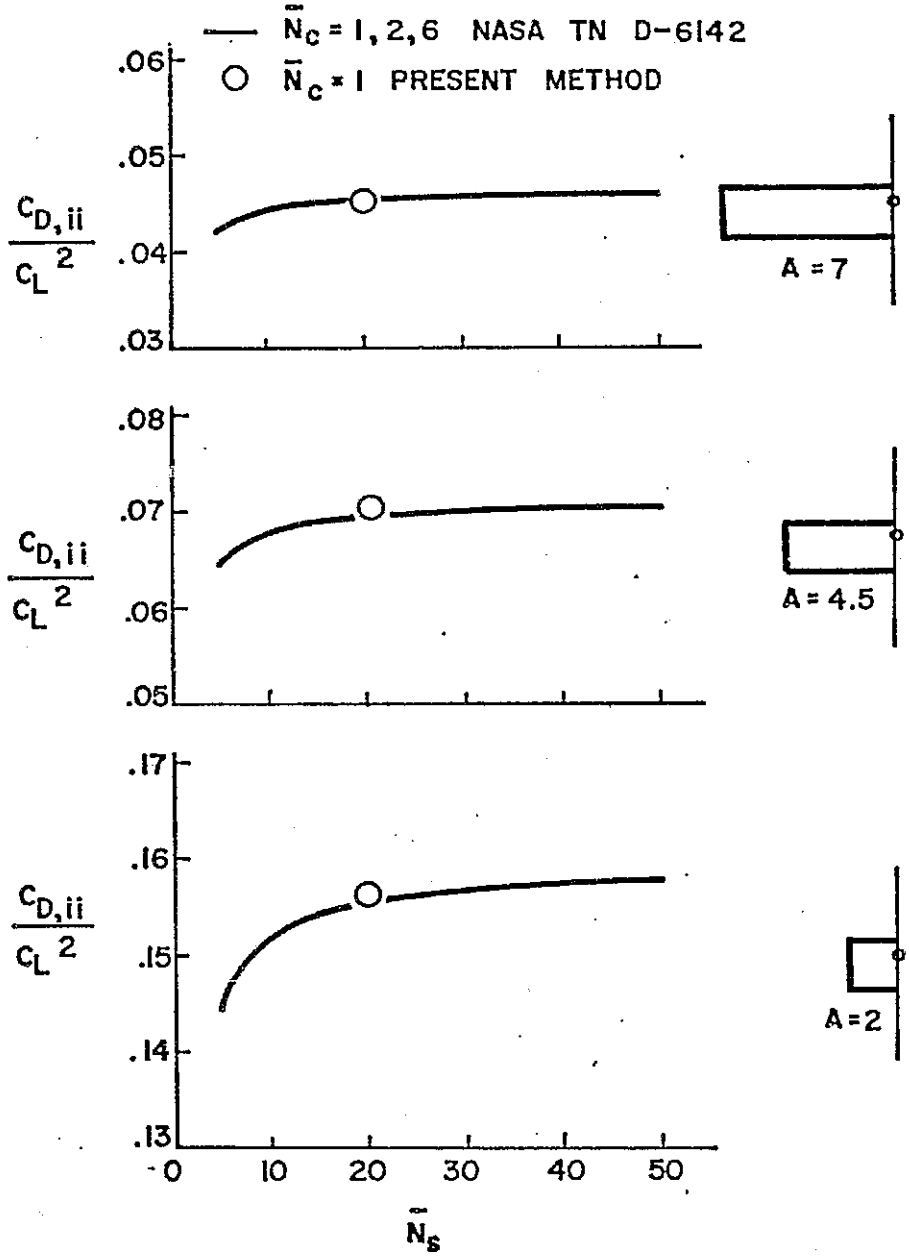

FIG. 5 CONCLUDED

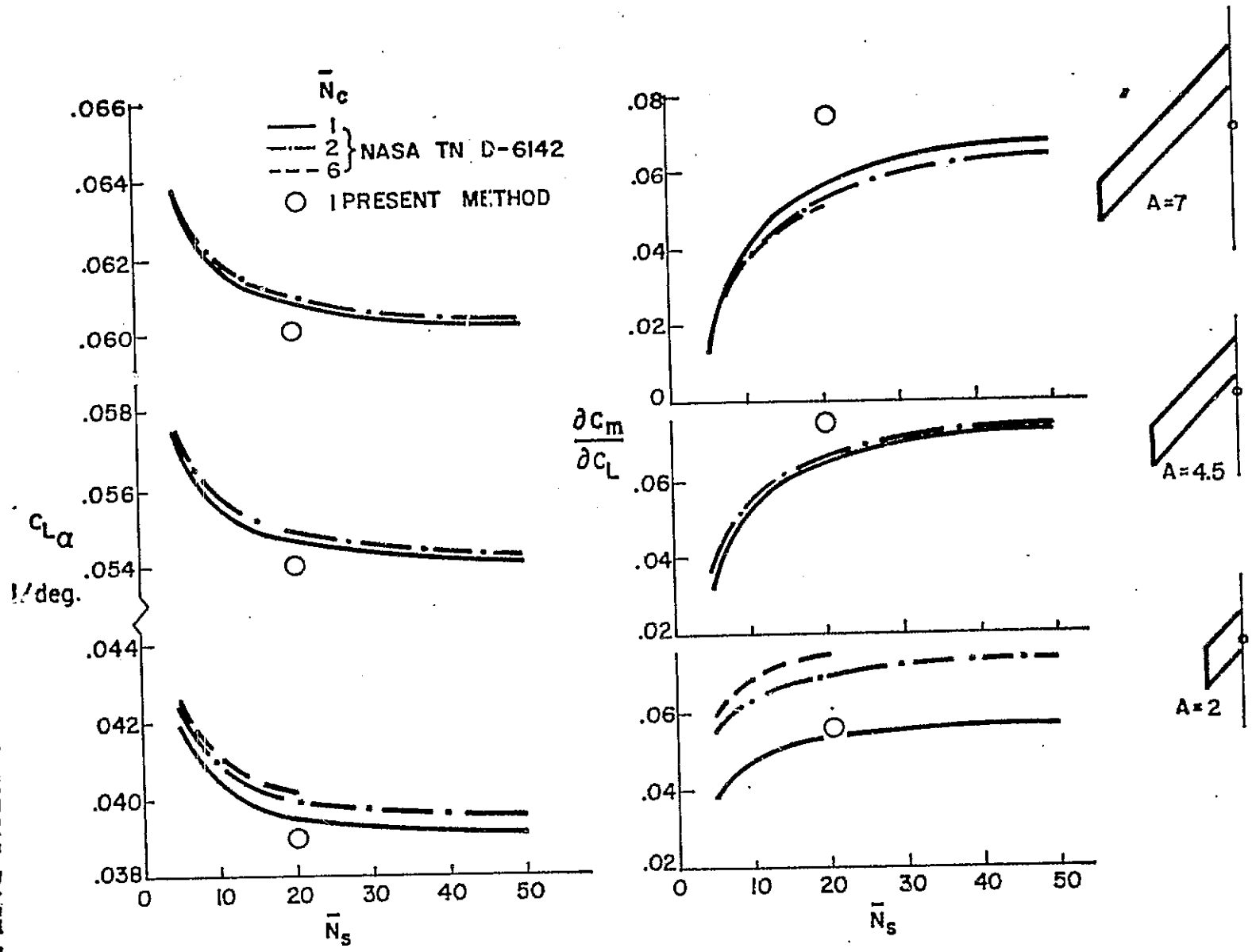

FIG. 10 COMPARISON OF PRESENT CALCULATIONS WITH VORTEX LATTICE METHOD, SWEPT (Λ=45°), UNTAPERED WINGS

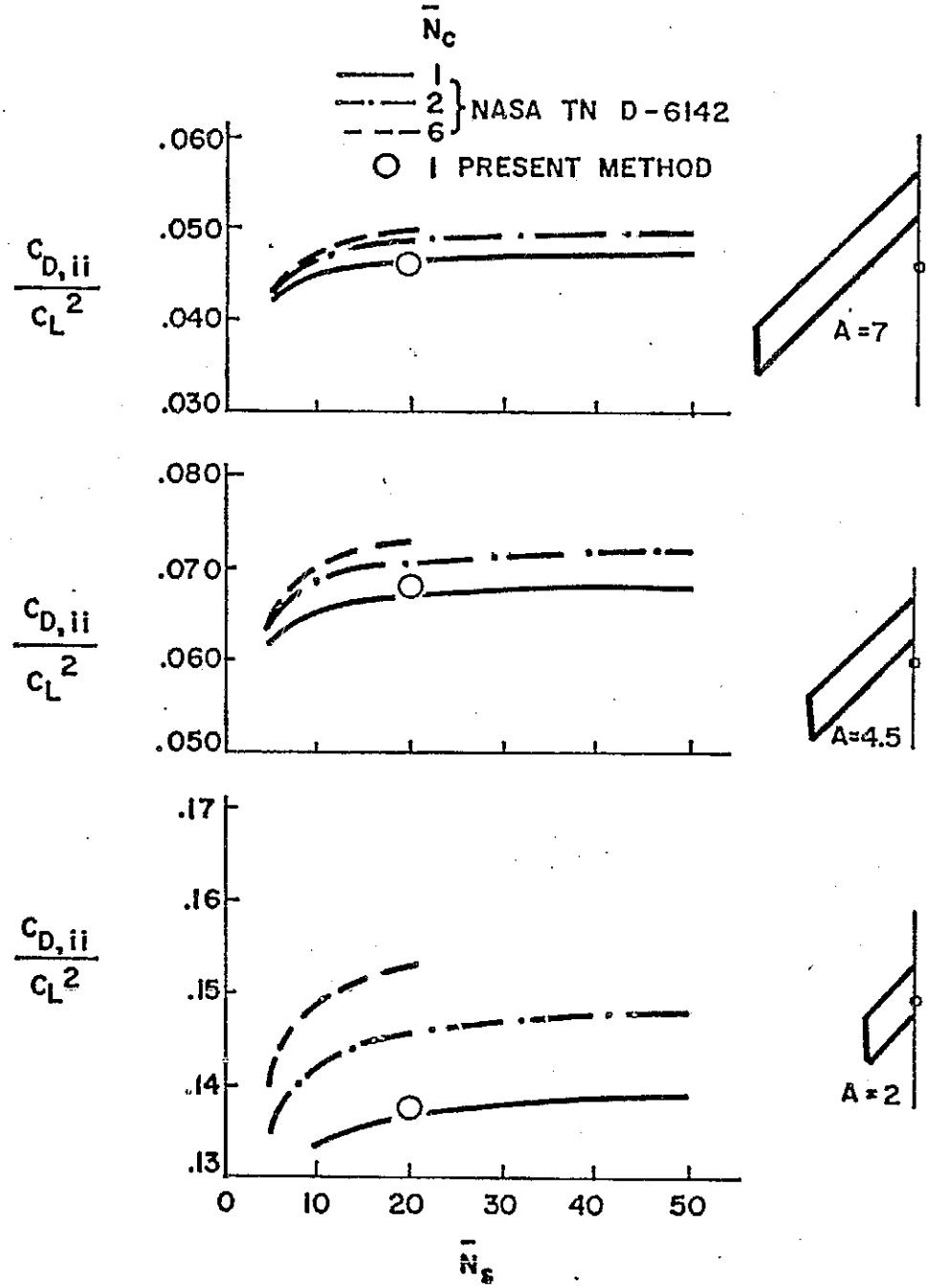

FIG. 10 CONCLUDED

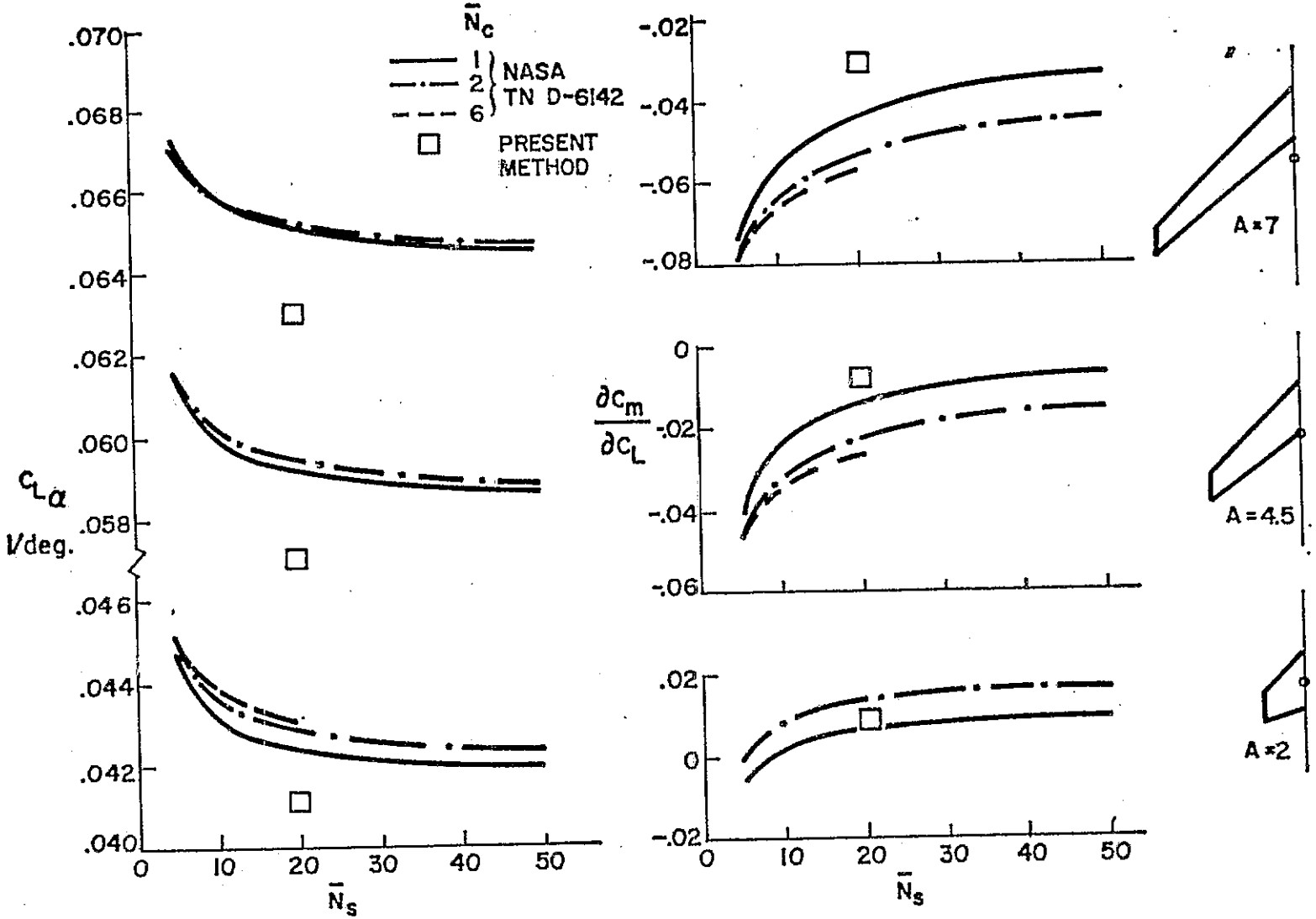

FIG. 11 COMPARISON OF PRESENT CALCULATIONS WITH VORTEX LATTICE METHOD, SWEPT ($\Lambda = 45°$), TAPERED ($\lambda = 0.5$) WINGS

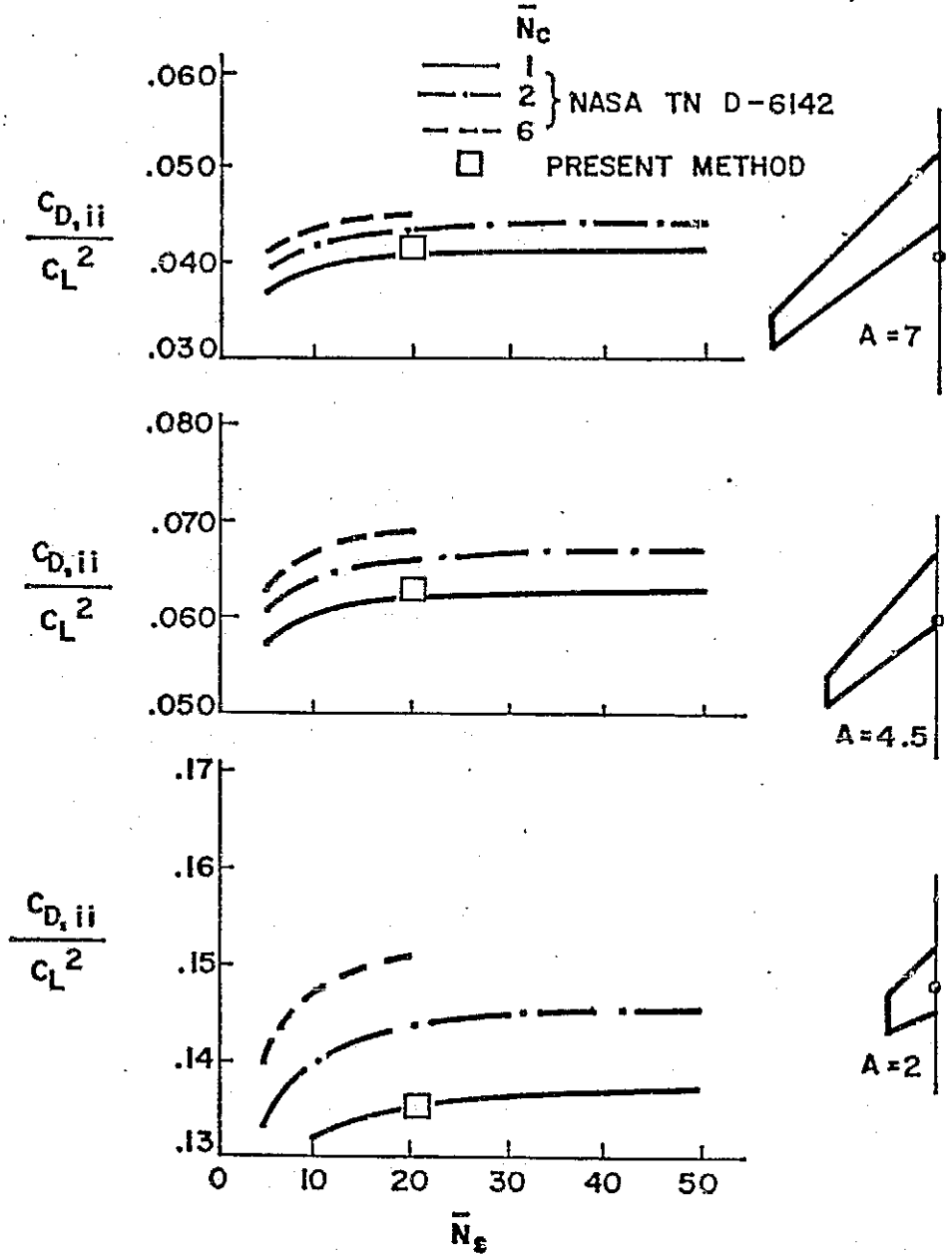

FIG. 11 CONCLUDED

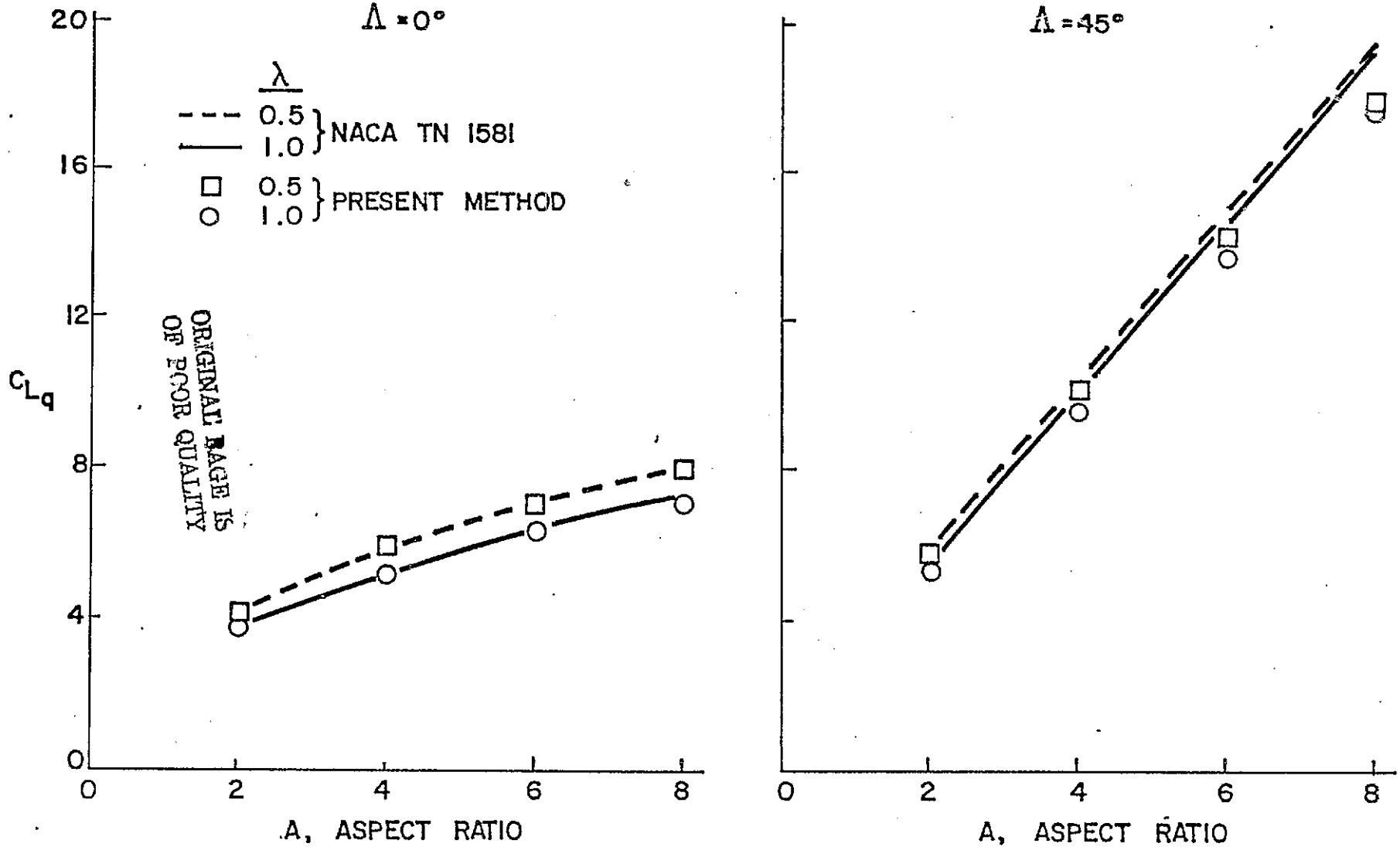

FIG. 12 COMPARISON OF PITCH DAMPING DERIVATIVES, C_{L_q} VS A

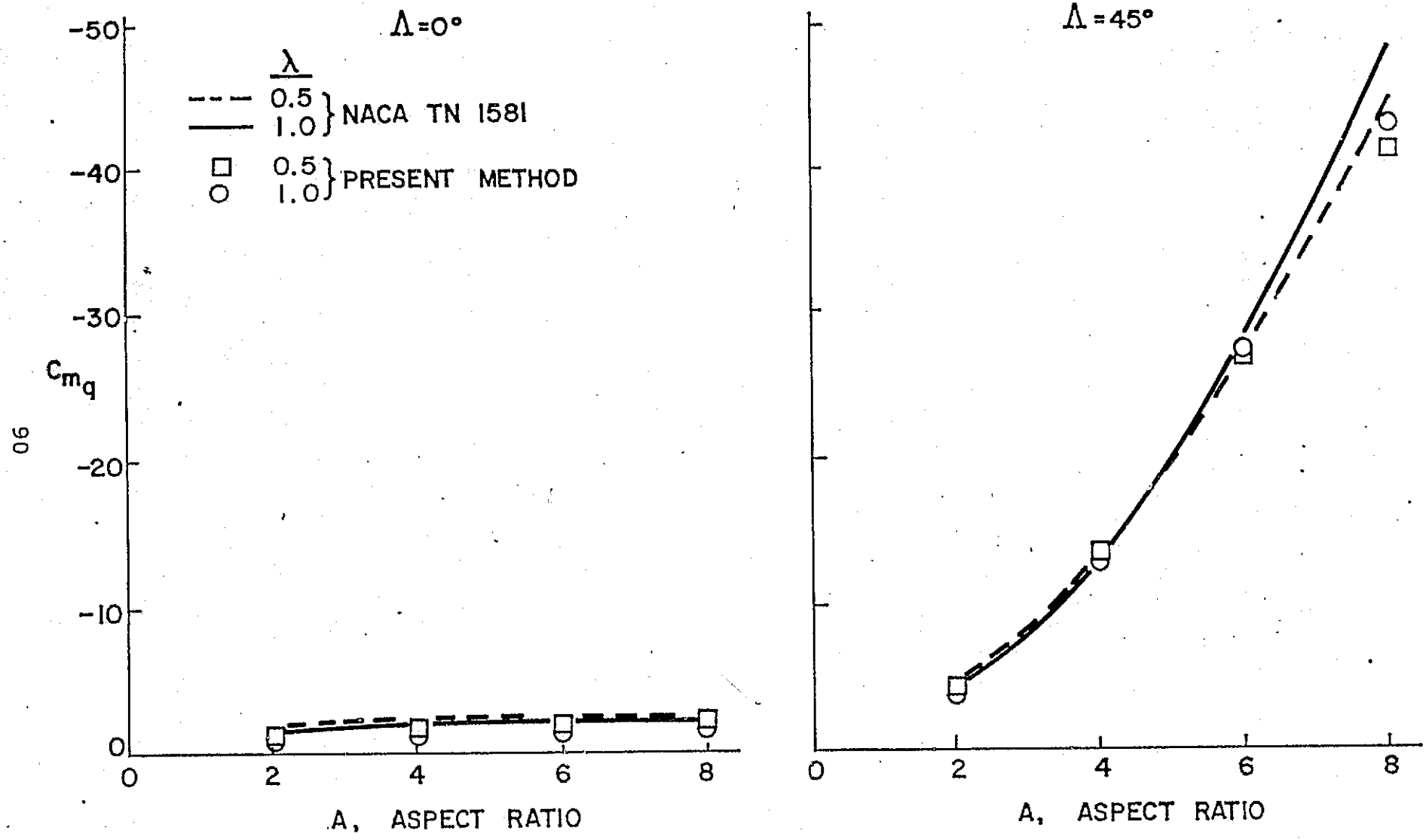

FIG 13 COMPARISON OF PITCH DAMPING DERIVATIVES, C_{m_q} VS A

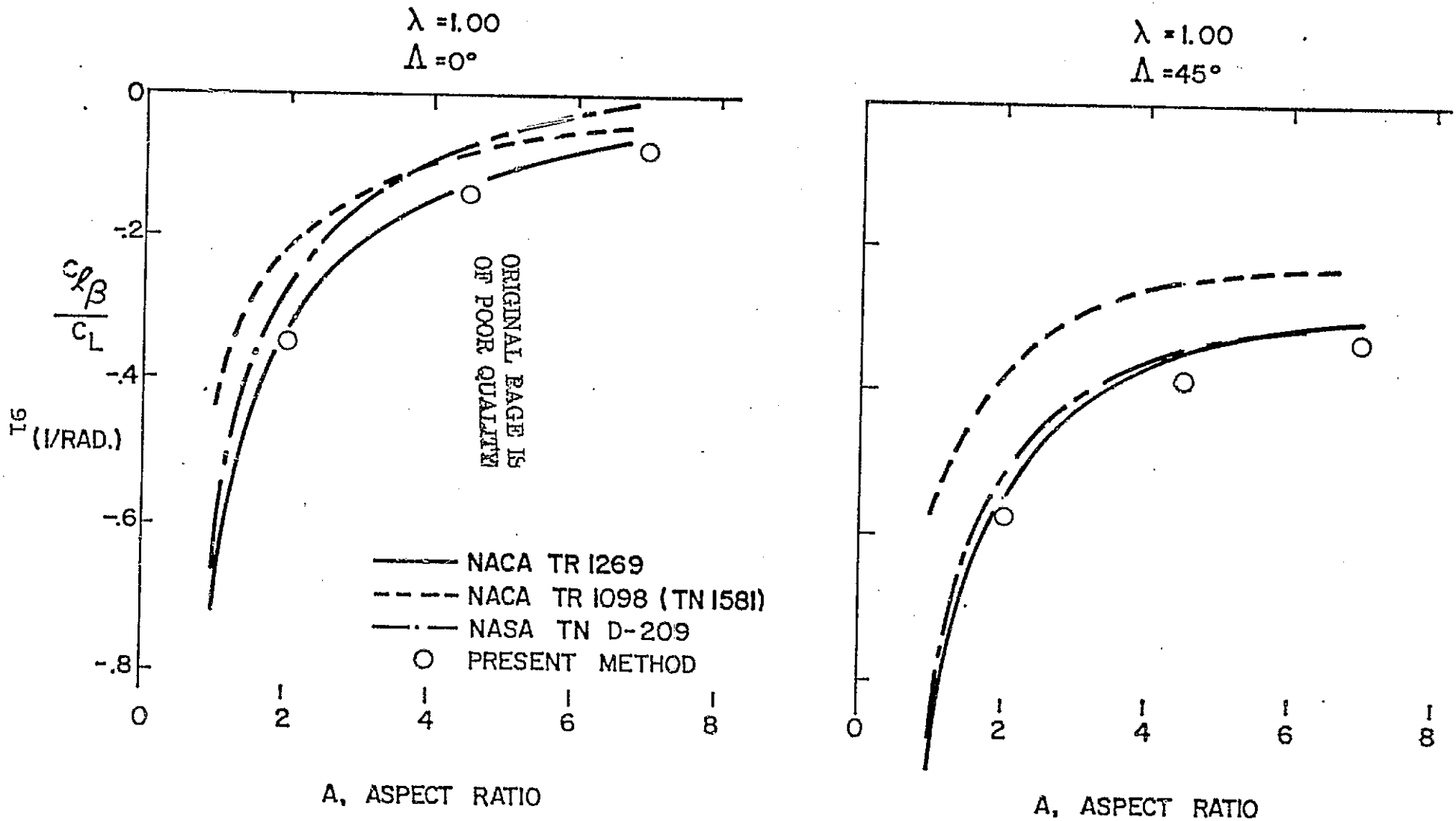

FIG. 14 a COMPARISON OF PRESENT METHOD WITH RESULTS OF VARIOUS REFERENCES FOR ESTIMATING C_{ℓ_β}/C_L : UNTAPERED WINGS

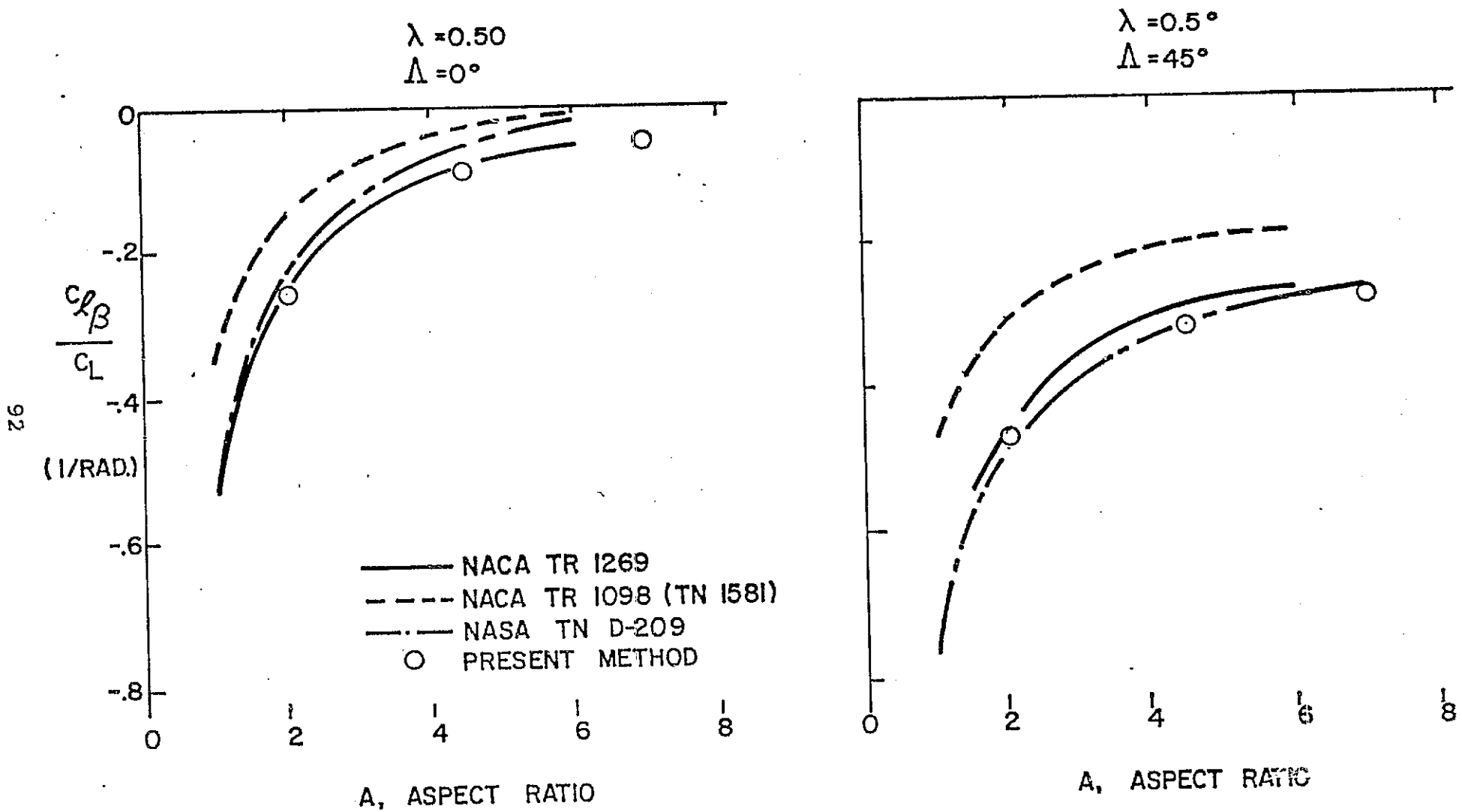

FIG. 14b CONTINUED : TAPERED WINGS

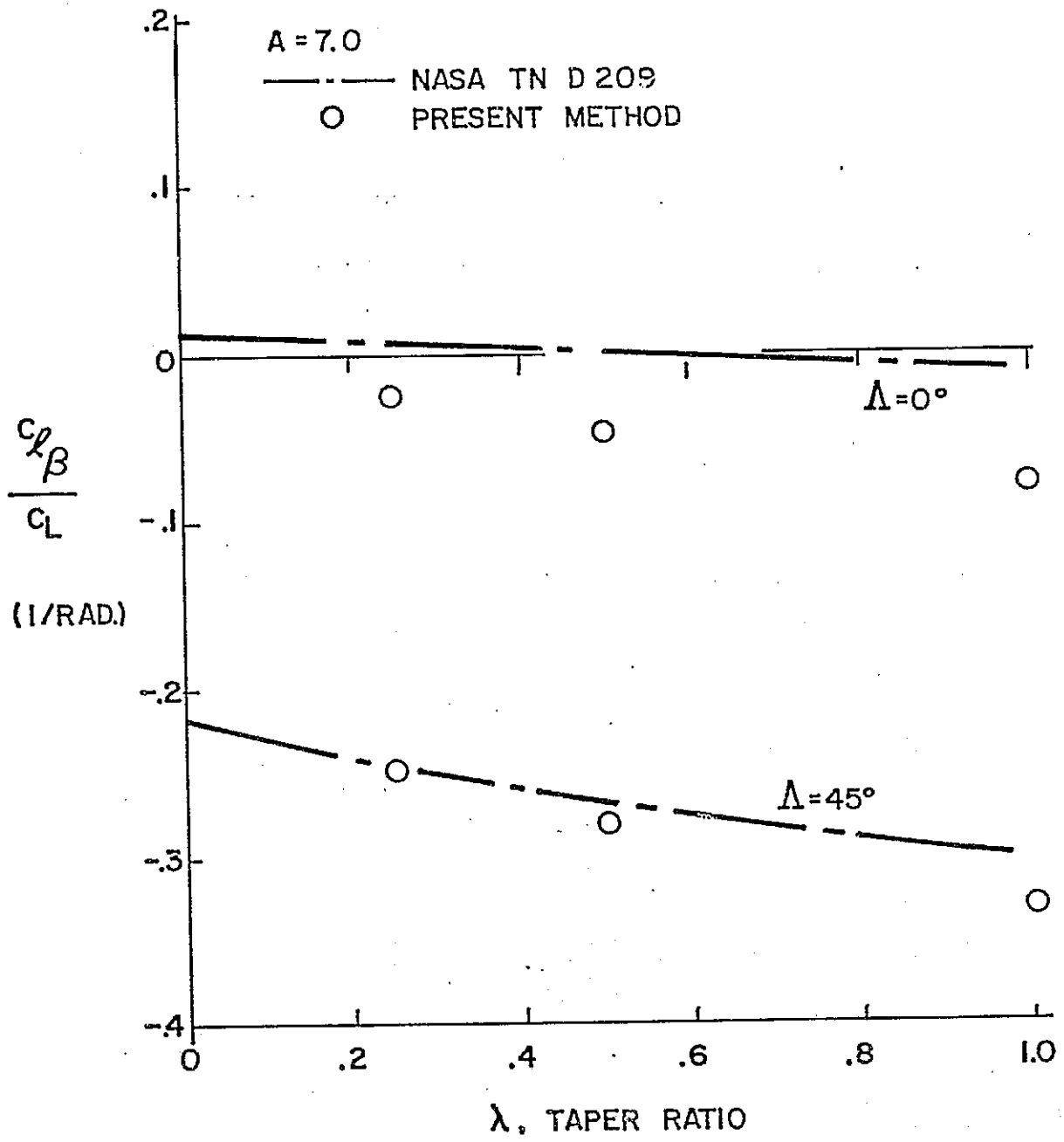

C-8

FIG. 14c CONTINUED: EFFECT OF TAPER ON A = 7 WINGS

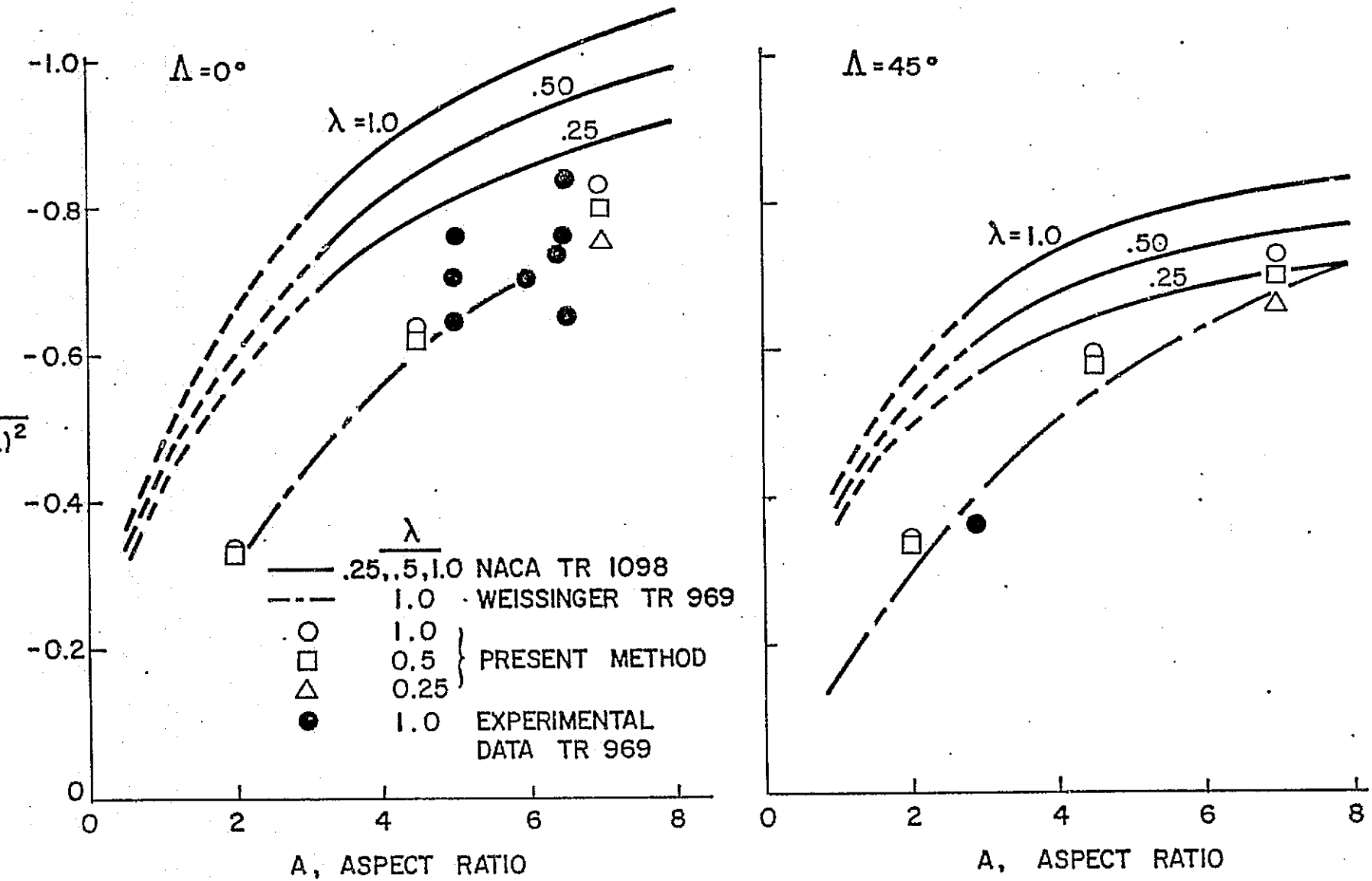

FIG. 15 COMPARISON OF VARIOUS METHODS FOR ESTIMATING THE EFFECT OF WING DIHEDRAL ON C_{ℓ_β}

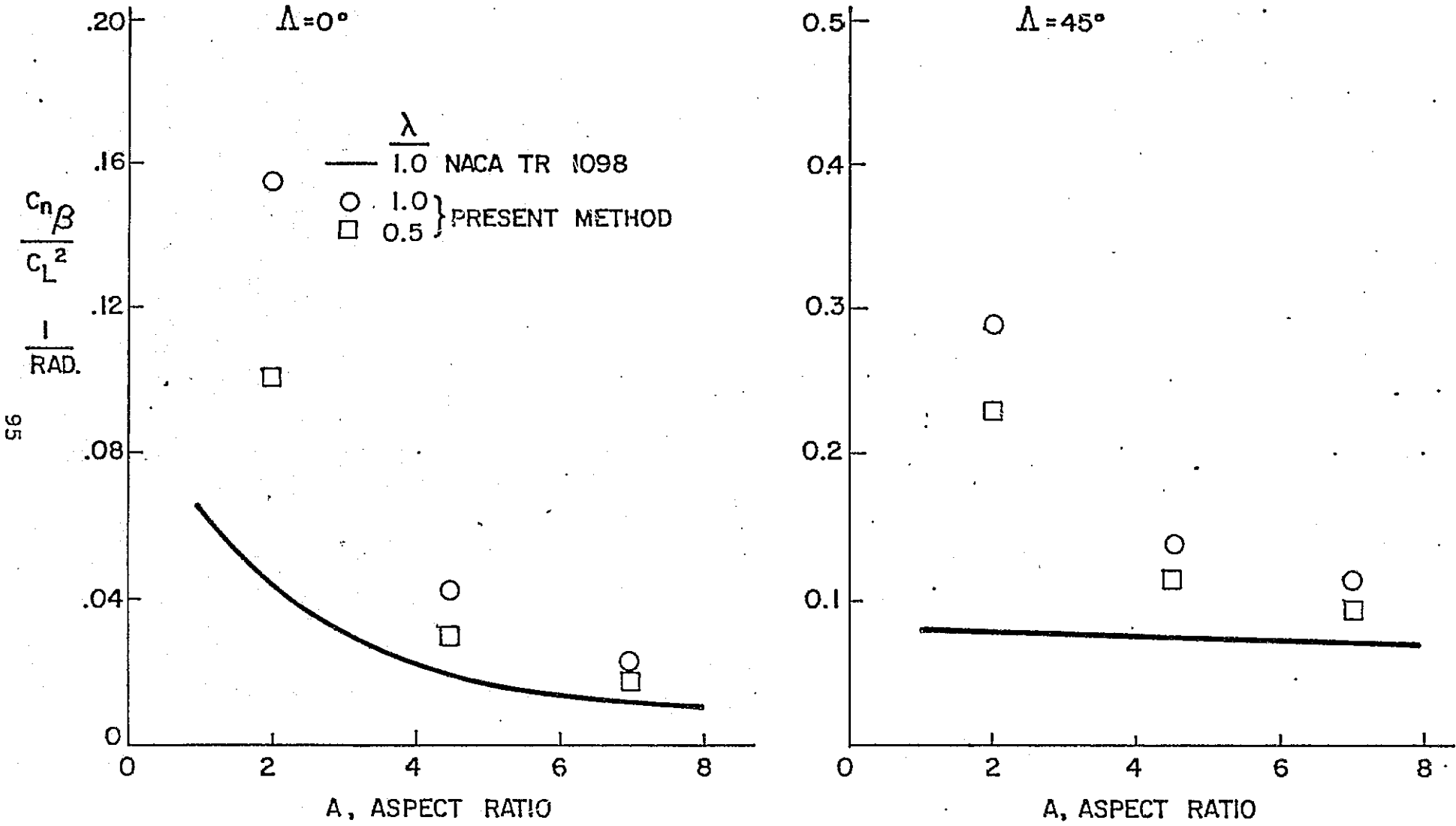

FIG. 16 DIRECTIONAL STABILITY DERIVATIVE C_{n_β}/C_L^2

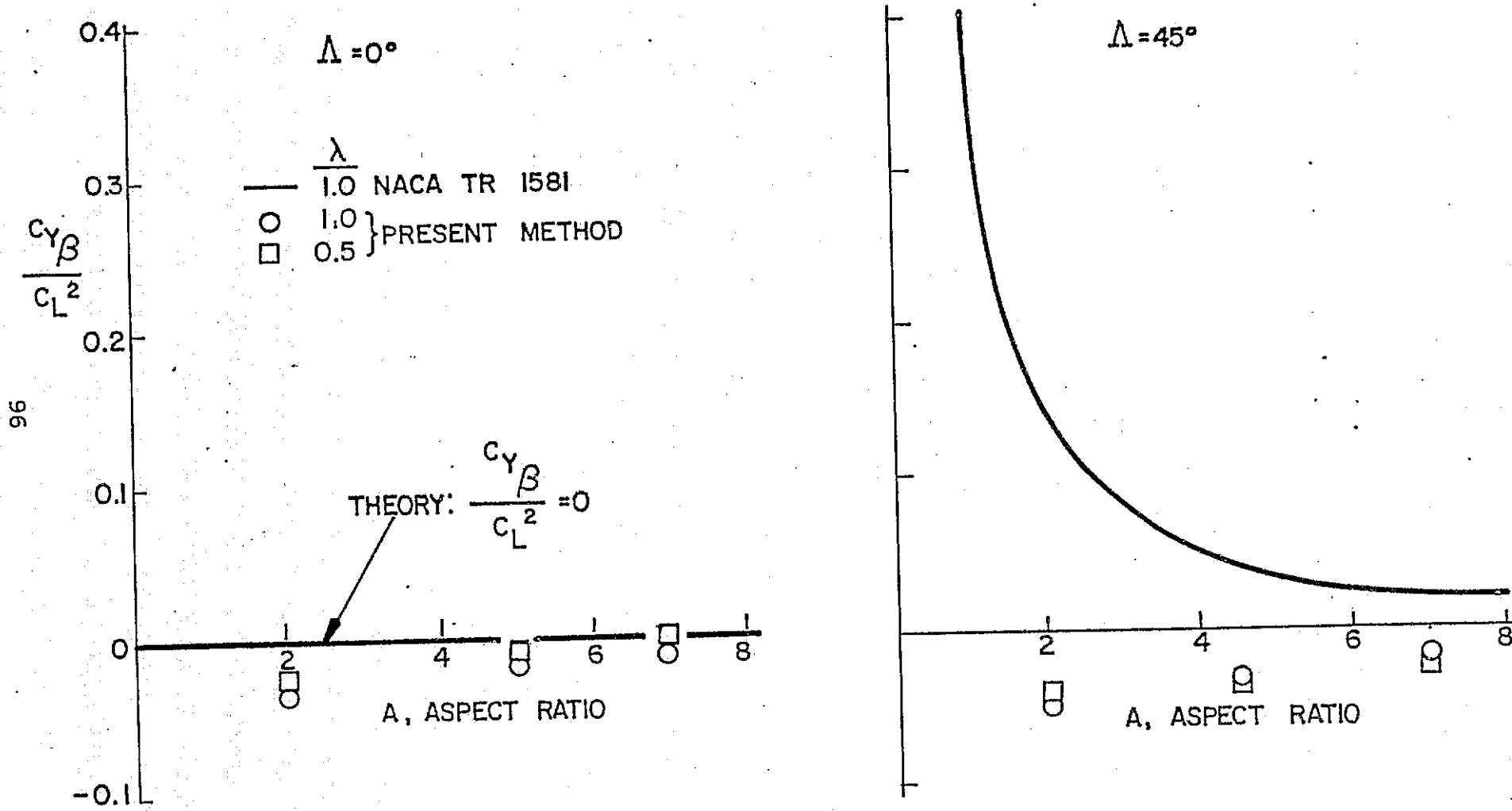

FIG. 17 SIDE FORCE - DUE - TO - SIDE SLIP DERIVATIVE

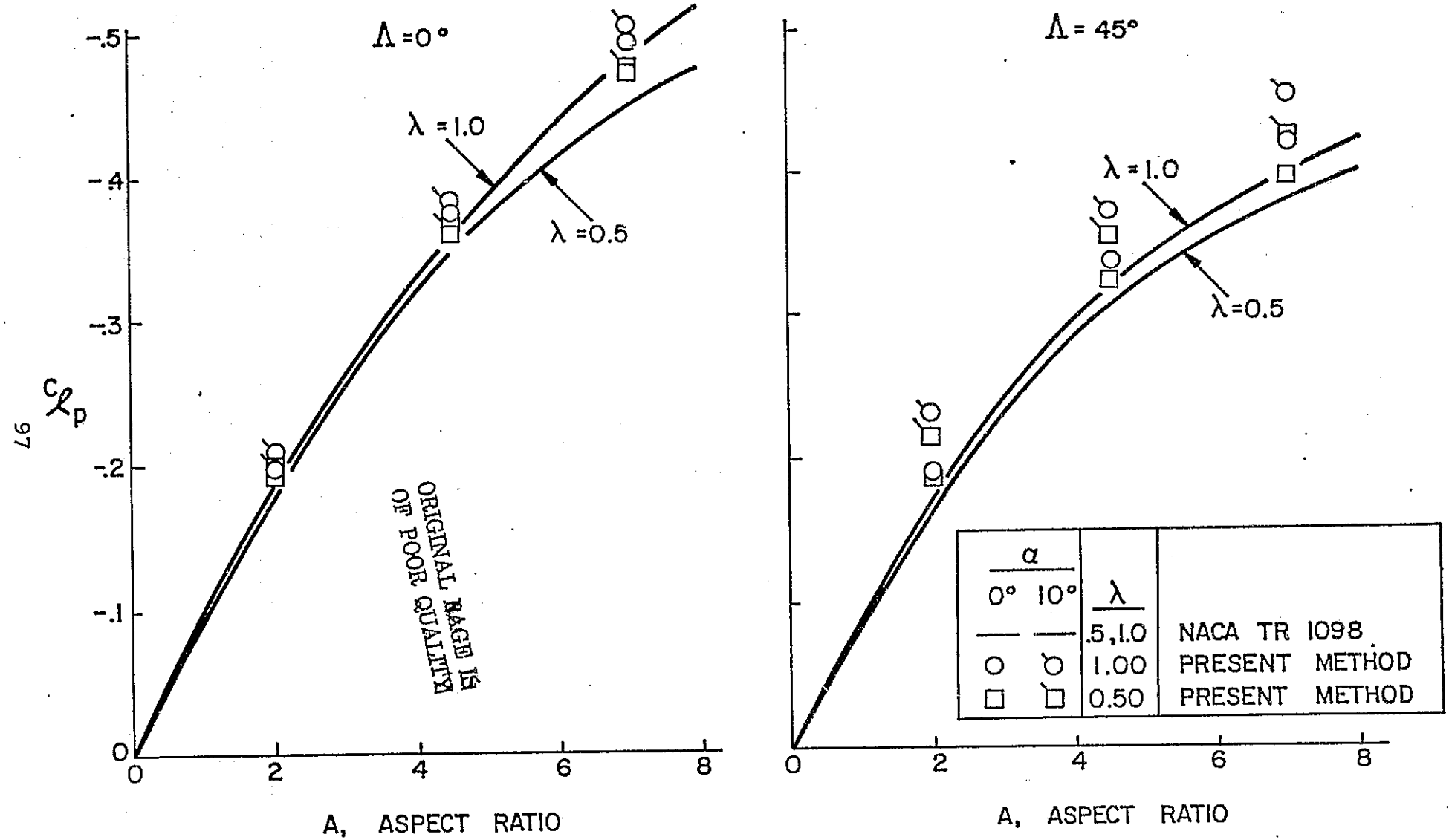

97

FIG. 18 COMPARISON OF PRESENT METHOD WITH METHOD OF NACA TR 1098 FOR ESTIMATING DAMPING-IN-ROLL C_{ℓ_p}

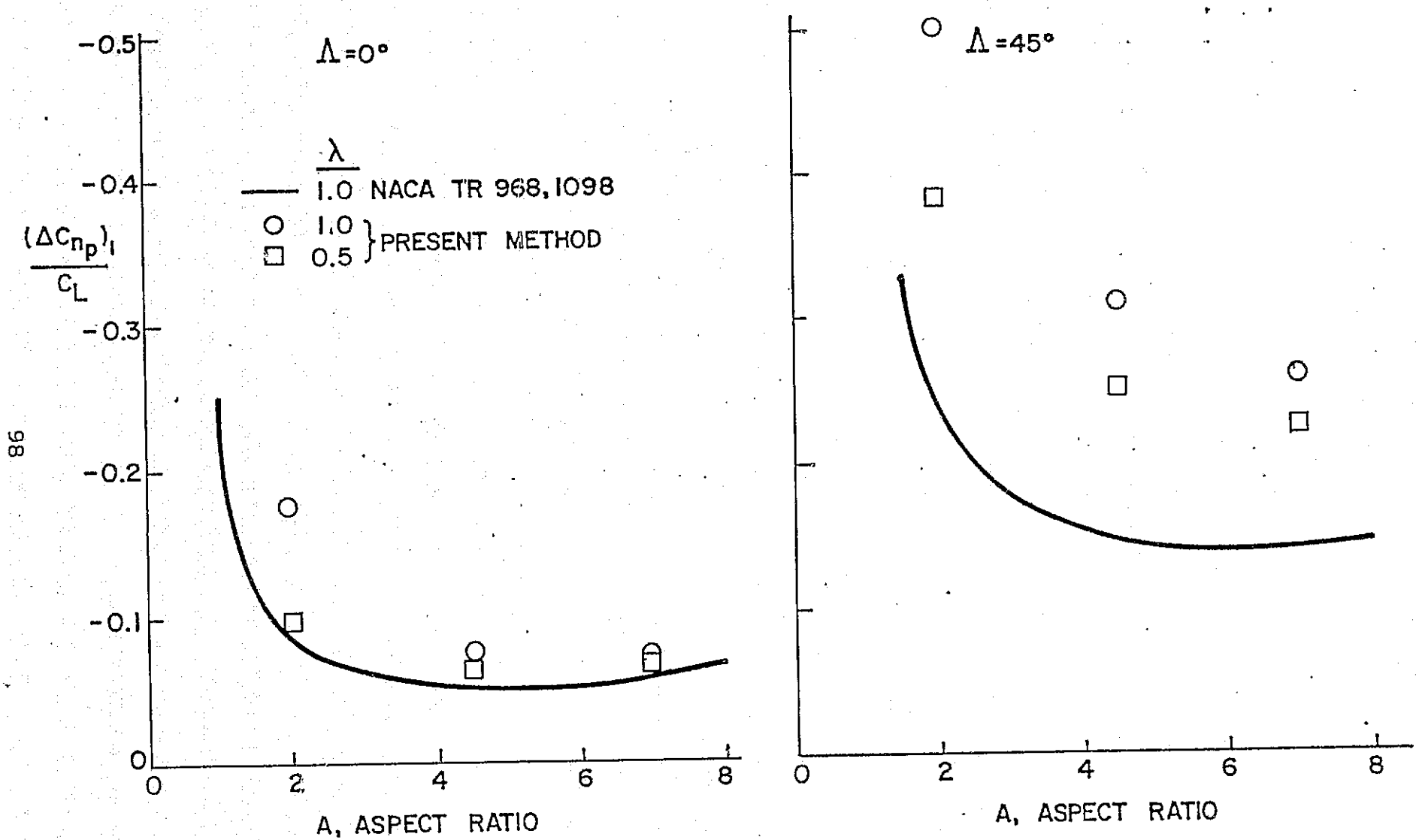

FIG. 19 YAW-DUE-TO ROLL DERIVATIVE, $(\Delta C_{n_p})_l / C_L$ DUE TO LIFT AND INDUCED-DRAG FORCES ONLY, c.g. AT a.c.

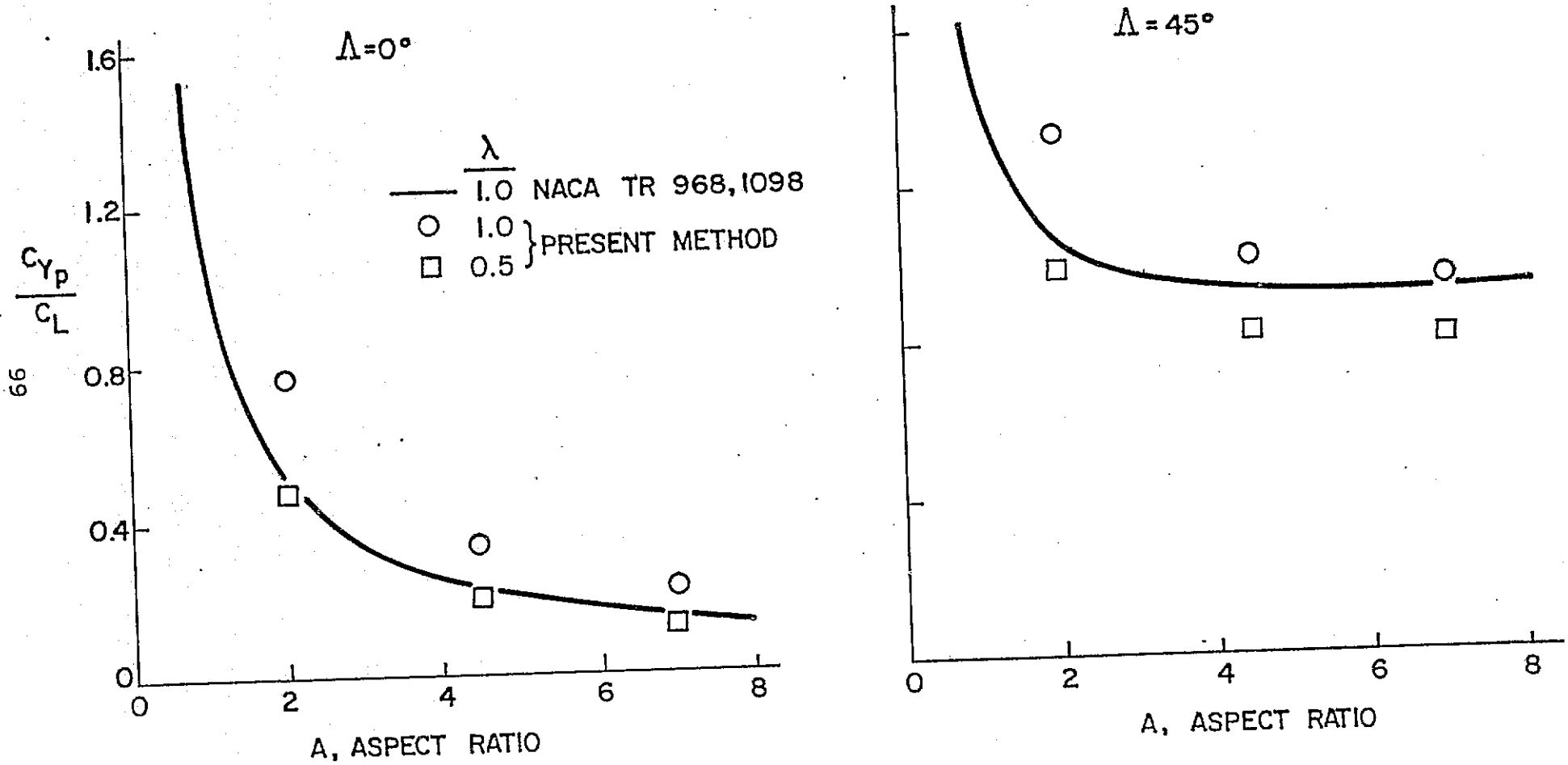

FIG. 20 SIDE FORCE - DUE - TO - ROLLING DERIVATIVE C_{Y_p}/C_L

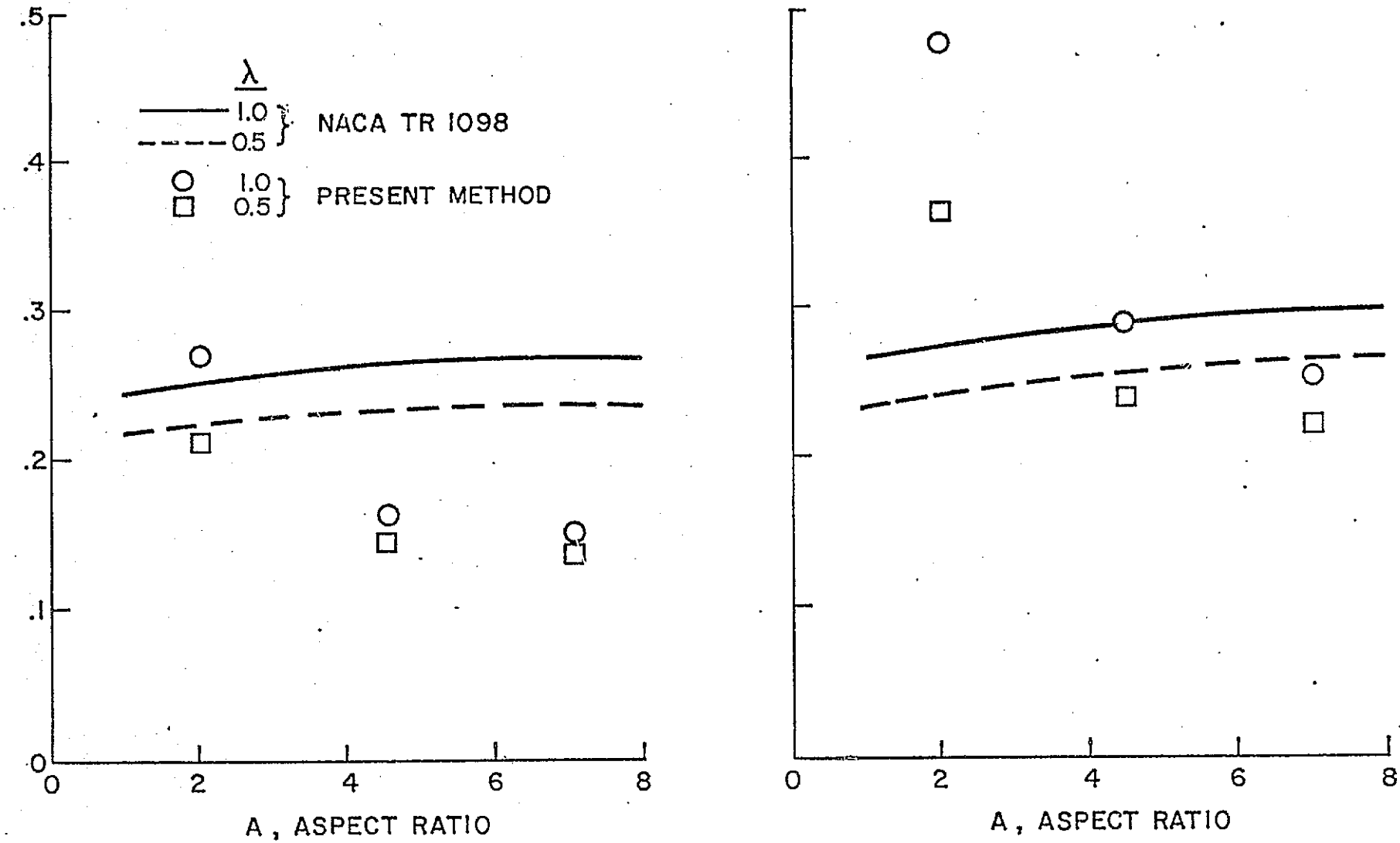

FIG. 21 ROLL—DUE—TO YAW DERIVATIVE $\frac{C_{\ell_r}}{C_L}$

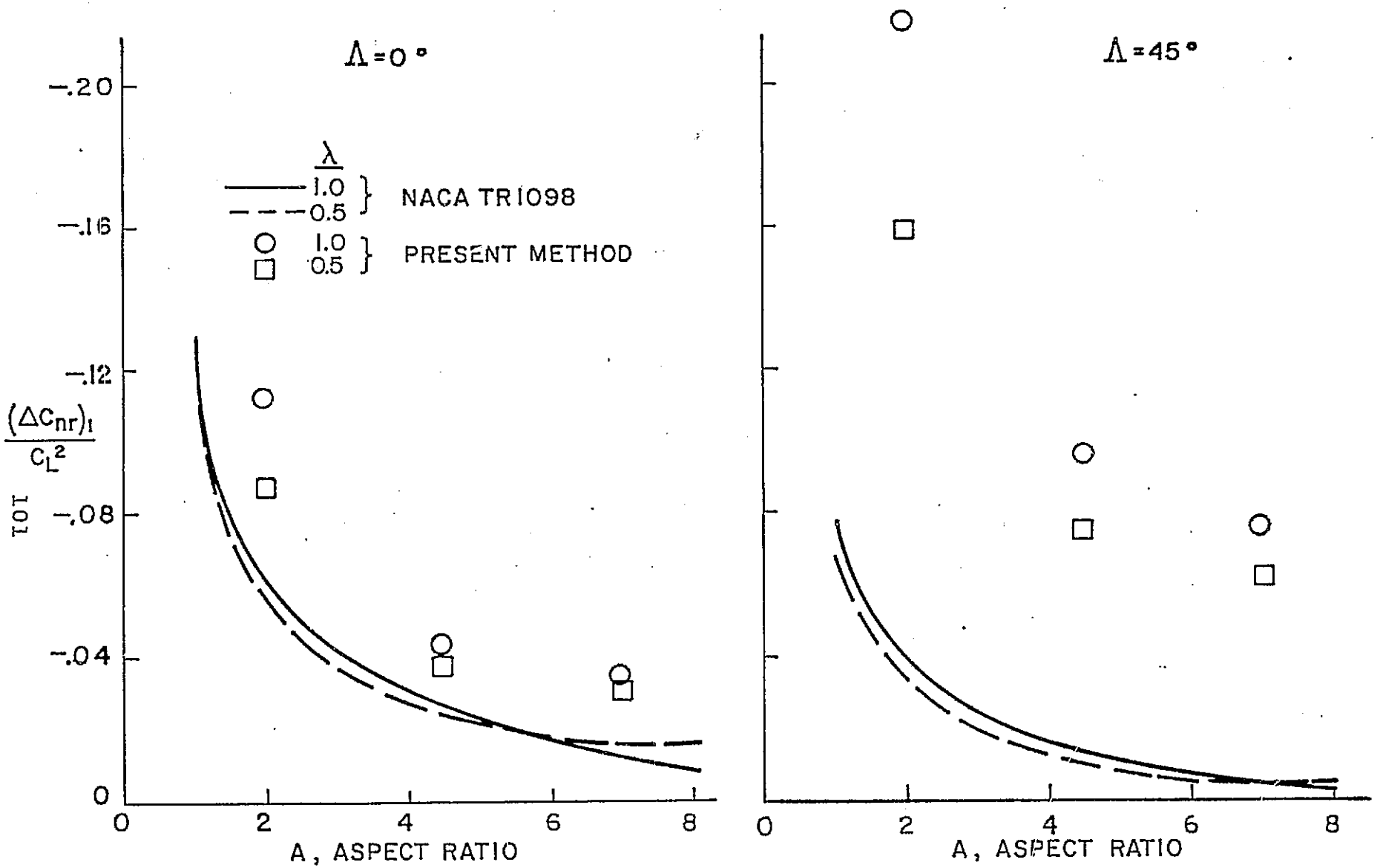

FIG. 22 DAMPING IN YAW DERIVATIVE, (ΔC_{n_r}) DUE TO LIFT AND INDUCED DRAG FORCES ONLY, c.g. AT a.c.

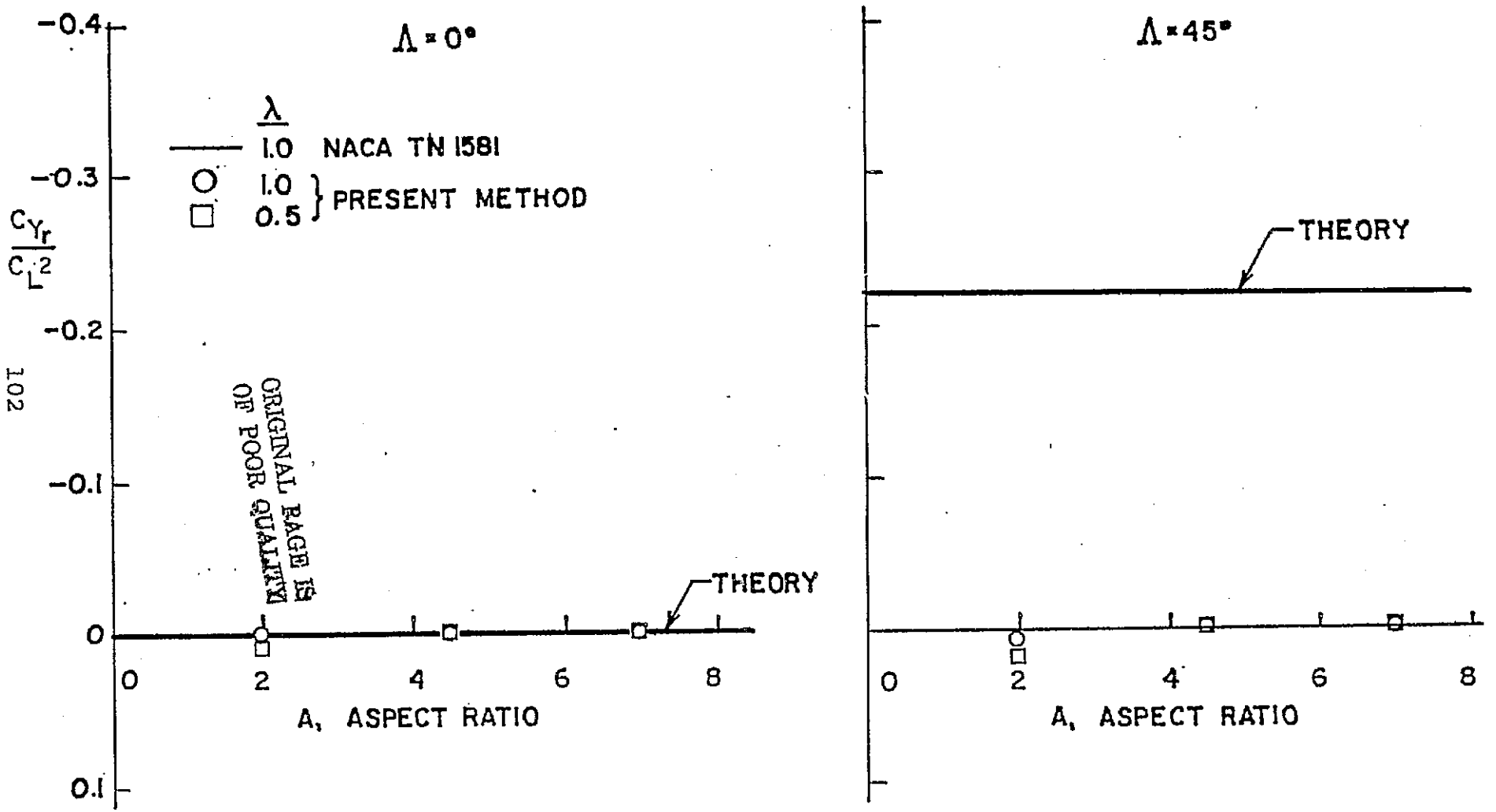

FIG. 23 SIDE FORCE DUE TO YAW RATE DERIVATIVE, C_{Y_r}/C_L^2